

**AUTOMATED 3D VISUALIZATION
OF BRAIN CANCER**

AUTOMATED 3D VISUALIZATION
OF BRAIN CANCER

By

MONA AL-REI, MSc.

A Thesis Submitted to the School of Graduate Studies
In Partial Fulfillment of the Requirements for the Degree
Master of eHealth Program

McMaster University @ Copyright by Mona Al-Rei, June 2017

McMaster University Master of eHealth (2017) Hamilton, Ontario

TITLE: 3D Brain Cancer Visualization. **AUTHOR:** Mona Al-Rei.
SUPERVISOR: Dr. Thomas Doyle. **SUPERVISORY**
COMMITTEE: Dr. Reza Samavi, Dr. David Koff.
NUMBER OF PAGES: xvii, 119.

To my beloved and wounded country Yemen

Abstract

Three-dimensional (3D) visualization in cancer control has seen recent progress due to the benefits it offers to the treatment, education, and understanding of the disease. This work identifies the need for an application that directly processes two-dimensional (2D) DICOM images for the segmentation of a brain tumor and the generation of an interactive 3D model suitable for enabling multisensory learning and visualization. A new software application (M-3Ds) was developed to meet these objectives with three modes of segmentation (manual, automatic, and hybrid) for evaluation. M-3Ds software was designed to mitigate the cognitive load and empower health care professionals in their decision making for improved patient outcomes and safety. Comparison of mode accuracy was evaluated. Industrial standard software programs were employed to verify and validate the results of M-3Ds using quantitative volumetric comparison. The study determined that M-3Ds' hybrid mode was the highest accuracy with least user intervention for brain tumor segmentation and suitable for the clinical workflow. This paper presents a novel approach to improve medical education, diagnosis, treatment for either surgical planning or radiotherapy of brain cancer.

Table of Contents

Chapter 1	1
1. Introduction.....	1
1.1. Problem statement	1
1.2. Research objective.....	2
1.3. Proposed System (M-3Ds Brain Cancer Visualization).....	2
1.4. Thesis contribution	3
1.5. Survey among simulating 3D visualization software of medical images	4
1.5.1. 3D Slicer	5
1.5.2. ParaVeiw.....	7
1.5.3. ImageJ	8
1.5.4. Synapse 3D	10
1.5.5. 3D- DOCTOR.....	10
1.5.6. OsiriX.....	11
1.6. Connection to eHealth	12
1.7. Organization of the thesis.....	14
Chapter 2.....	15
2. Theoretical background	15
2.1. Types of tumors.....	15

2.2.	Main types of imaging modalities	16
2.2.1.	Computed Tomography (CT)	16
2.2.2.	Magnetic Resonance Imaging (MRI).....	17
2.2.3.	Single Photon Emission Computed Tomography (SPECT)	18
2.2.4.	Positron Emission Tomography (PET).....	19
2.3.	Main types of algorithms for 3D segmentation.....	19
2.3.1.	Main segmentation algorithms.....	19
2.3.2.	Marching cube algorithms (surface extraction and volume rendering)	23
Chapter 3	27
3.	Literature review	27
3.1.	Perception of healthcare professionals for 3D visualization	27
3.2.	Liminality and threshold concepts in 3D visualization	29
3.3.	Different algorithms related to image processing and 3D reconstruction.....	31
3.4.	Modes of segmentation	33
3.5.	Overview of some existing 3D visualization platforms	35
3.6.	Volumetric measurements of isolated tumor	37
Chapter 4	39
4.	Design and implementation of the software	39
4.1.	Different empirical methodologies for brain tumor segmentation.....	39

4.1.1.	Method A	41
4.1.2.	Method B	46
4.1.3.	Method C (M-3Ds)	53
4.2.	3D reconstruction of three methods	61
4.3.	Visualization via modern graphical user interface (GUI) of method C	61
4.4.	Modes of segmentation	67
4.5.	Extension of method C: Identification and visualization of both gray and white matter	69
	<u>9</u>	
Chapter 5	70
5.	Discussion and experimental results.....	70
5.1.	Validation by checking the completeness and accuracy of each approach.....	70
5.1.1.	Accuracy tests	70
5.1.2.	Sensitivity and specificity tests for each method with the both cases (case1 and case2).....	72
5.2.1.	Volume calculation of the segmented tumor by the three methods for the three modes of segmentation (manual, automatic and hybrid) of method C.....	73
5.2.2.	Volume calculation of the actual tumor	80
Chapter 6	82

6. Conclusion and future work.....	82
6.1. Limitations	82
6.2. Challenges	82
6.2.1. Challenges related to the researcher’s background.....	82
6.2.2. Challenges during developing M3Ds software.....	83
6.3. Future directions.....	87
Appendices.....	90
Appendix 1: Distortion.....	90
Appendix 2: Volume calculation software programs.....	95
Appendix 3: Texts file for area and perimeter of each segmentation mode.....	103
Bibliography	109

List of Figures

Figure 1-1 M-3Ds converts series of brain tumor of MRI from 2D into 3D model of tumor, skull and both of them	3
Figure 1-2 Both images demonstrated different planes of brain and its 3D reconstruction offered transparent function	6
Figure 1-3 (a) Segmentation and 3D reconstruction of tumor. (b) role of accuracy during coloring ROI, where lateral ventricle was involved as well	7
Figure 1-4 Example of interactive 3D surface plot of breast tissue [1]	9
Figure 1-5 (a) Image acquisition of brain tumor of Case1, (b) 3D reconstruction of skull and (c) transparent function	9
Figure 1-6 See-through (transparency) technique for tumor in (a) 3D-DOCTOR[33] and (b) M-3Ds.....	10
Figure 1-7 Both(a) 3D-Doctor [2] and (b) M-3Ds have similar features about segmentation and 3D reconstruction.....	11
Figure 1-8 Both (a) Osirix [3] and (b) M-3Ds show the similarity in 2D images acquisition	12
Figure 4-1 Flowchart of method A image processing.....	44
Figure 4-2 (a) case1 and (b) case2, demonstrate colorful segmentation of tumor and its edema	45
Figure 4-3 Upper row: case 2 (a) segmentation of lateral ventricle (FPR), (b) Portion of lateral ventricle is segmented due to similar pixel values with tumor. Lower row: case1	

(c) tumor without segmentation (FNR), (d) segmentation of white matter as a part of edema	46
Figure 4-4 Flowchart of method B image processing.....	49
Figure 4-5 (a) case1, (b) case2, from left to right: original image, watershed segmentation into different areas including the tumor, extracting the tumor, and output image of segmented tumor	50
Figure 4-6 Case2: brain tumor segmentation with portion of lateral ventricle	51
Figure 4-7 Pre-processing: (a) image acquisition,(b) image enhancing; processing (c) binary thresholding, (d) morphological operation;post-processing (e) image filtering,(f) hole filling.	56
Figure 4-8 Flowchart of method C image processing.....	57
Figure 4-9 (a) small portion of lateral ventricle was segmented with the tumor, (b) segmented tumor without lateral ventricle. Both (a) and (b) have irregular boundaries ...	59
Figure 4-10 Shape changing of the segmented tumor depends on the selected seed points;(a) SP (64,78), area 19.40 square cm , peimeter = 19.37cm; (b) SP (88,73), area = 21.14 square cm, perimeter = 20.34 cm; (c) SP (91,68), area + 22.27 square cm, perimeter=20.76 cm	59
Figure 4-11 Graphical User Interface (GUI).....	633
Figure 4-12 View Image Tab: downloads images and displays brain dataset	64
Figure 4-13 2D Segmentation Tab displays the segmented tumor	655
Figure 4-14 (a) 3D reconstruction of the segmented tumor with volumetric calculation, (b) 3D reconstruction of the skull, (c) see through technique.....	66

Figure 4-15 Morphological distortion of gray and white matter for (a) case 1 & (b) case 2	69
Figure 5-1 MeshLab converts non-watertight object into watertight.(a) non-watertight object, (b) watertight object.	744
Figure 5-2 Similarity of volume measuring results of different approaches.(a) M-3Ds, (b) MeshLab and (c) Autodesk Inventor.	75
Figure 5-3 Outline and isolate the tumor by 3D Slicer through using Editing and GrowthCutEffect.	800
Figure 5-4 Volume calculation of the actual tumor for both cases by Inventor Autodesk	81
Figure 6-1 Initial work related to Augmented Reality	88
Figure 1: (Appendix 1) Distortion tab differentiates the grey and white matter (black region: tumor, white region: edema, green area: grey matter and blue area: white matter)	93
Figure 2: (Appendix 1) Flowchart processing of white and grey matter distortion.....	944
Figure 3: (Appendix 2.1) Open STL. file	955
Figure 4: (Appendix 2.1) Visibility	955
Figure 5: (Appendix 2.1) converts to base feature.....	966
Figure 6: (Appendix 2.1) Press composite to start stitching.....	966
Figure 7: (Appendix 2.1) Apply stitching.....	97
Figure 8: (Appendix 2.1) No open edges.....	97
Figure 9: (Appendix 2.1) stitching is done	98

Figure 10: (Appendix 2.1) from iProperties --> Physical--> Update--> the volume is calculated	98
Figure 11: (Appendix 2.2) Import mesh	99
Figure 12: (Appendix 2.2) Filters--> Quality measure and computation--> Compute Geometric measures	99
Figure 13: (Appendix 2.2) shows it is not watertight	1000
Figure 14:(Appendix 2.2) In order to convert it into watertight: Filter-->Remeshing ...	100
Figure 15: (Appendix 2.2) Apply.....	101
Figure 16: (Appendix 2.2) watertight object.....	1011
Figure 17: (Appendix 2.2) Now the tumor is watertight and it can be measured by MeshLab. Filters--> Quality measure and computation--> Compute Geometric measures.	102

List of Tables

TABLE I: FEATURE COMPARISON OF M-3Ds SOFTWARE AND SOME POPULARE SOFTWARE PROGRAMS IN LITERATURE AND MARKET	5
TABLE II: CURRENT FORMS OF ACTIVE LEARNING[83]	30
TABLE III: ACCURACY OF EDECTION RESULTS OF METHOD A AND B	71
TABLE IV: ACCURACY OF DETECTION RESULTS OF METHOD C (MANUAL, AUTOMATIC AND HYBRID)	72
TABLE V: VALIDATION OF ACCURACY AND COMPLETENESS OF SEGMENTATION IN ALL THREE METHODS AND THREE MODES OF SEGMENTATION.....	72
TABLE VI: VERIFICATION BY VOLUME MEASURMENTS OF 3D RECONSTRUCTED TUMOR OF THE THREE METHODS AND THREE MODES OF METHOD C (THE UNIT IS CUBIC CENTIMETER).....	79
TABLE VII: VOLUME CALCULATION OF SEGMENTED TUMOR BY M-3Ds AND ACTUAL TUMOR BY 3D SLICER.....	81

Acknowledgement

First and foremost, I would like to thank my supervisor Dr. Thomas Doyle for his priceless suggestions and guidance. He encourages and motivates me every step of the way throughout this process as well as inspires me to continue this work in the future. Furthermore, he gave me a lot of freedom to explore different areas that would support my work. I have not only continued my studies after a gap of nine years but also worked on a project that was different from my medical background. Dr. Doyle was patient with me and helped me to catch up with new techniques and resources.

Also, I would like to express my appreciation to Dr. Reza Samavi for his encouragement, support and invaluable comments during my study at McMaster University. At the same time, I am deeply grateful to Dr. David Koff for being member of my supervisory committee despite of all of his concerns. I also appreciate Dr. Colm Boylan Chief of Diagnostic Imaging, St. Joseph's Hospital for his time and support.

I would also like to express my appreciation to my colleagues Qian Shan and Jennifer Wong for their support. I would also like to acknowledge the administrative support of Iris Kehler from the eHealth program.

List of Abbreviations and symbols

3D	Three-dimensional
2D	Two –dimensional
MRI	Magnetic Resonance Image
CT	Computed Tomography
SPECT	Single Photon Emission Computed Tomography
PET	Positron Emission Tomography
DICOM	Digital Imaging and Communications in Medicine
ROI	Region of Interest
VTK	Visualization Toolkit
ITK	Insight Segmentation and Registration Toolkit
STL	Stereo Lithography
AR	Augmented Reality
VR	Virtual Reality
PACS	Picture Archiving and Communication System
JPEG	Joint Photographic Experts Group" or "Image file format"
OS	Operating System
CAD	Computer-Aided Diagnosis/ Computer-Assessed Diagnosis
CAD	Computer-Aided Design
CDSS	Clinical Decision Support System
GUI	Graphical User Interface
ICD-O	International Classification of Diseases—Oncology
T1WI	Relaxation Time1 Weighted image
T2WI	Relaxation Time 2 Weighted image

FLAIR	Fluid Attenuation Inversion Recovery
PDWI	Proton Density-Weighted Image
RANO	Response Assessment in Neuro-Oncology
CSF	Cerebrospinal Fluid
RGB	Red, green and blue
RGBA	Red, green, blue and opacity
TPR	True Positive Result
TNR	True Negative Result
FPR	False Positive Result
FNR	False Negative Result
GDCM	Grassroots DICOM
Qt	“Quicktime Computing” Software
LSM	Level Set Method
Σ	Summation

Declaration of Academic Achievement

The researcher was rewarded because of her project (M-3Ds project) and got Outstanding Achievement Award since this project has a great contribution in the field of cancer control.

Chapter 1

1. Introduction

1.1. Problem statement

The 3D structure of organs make it difficult for clinicians to read 2D images from MRI's, CT scans, SPECT and PET scans [4]. Therefore, 3D modelling of the cancer tumor from a set of 2D Digital Imaging and Communications in Medicine (DICOM) images can provide a more direct and realistic visualization for the clinicians. Such a model offers to play a vital role in the medical education, clinical diagnosis and treatment [5] as it improves cancer visualization, detection, and monitoring. Our 3D visualization of DICOM images is a process that uses a large set of 2D images to produce a 3D image model that can be analyzed quantitatively [5]. Accurate segmentation of pathological structures as tumor is a challenging process because tumors have a large diversity in shape and appearance with overlapping intensities with the normal tissues. An expanding tumor can defect/ deform adjacent tissue in the body giving healthy tissue an abnormal shape [3,4]. In addition, the heterogeneous density of the brain tissue with a tumor can result in inaccurate location identification [7]. Commonly available 3D visualization programs only provide manual and/or automated segmentation. However, the proposed method (M-3Ds) in this paper is a software prototype that provides three types of segmentation modes: manual, automated, and hybrid.

1.2. Research objective

Developing an automated method by which 2D DICOM images could be converted into 3D model for brain cancer segmentation and visualization.

1.3. Proposed System (M-3Ds Brain Cancer Visualization)

M-3Ds Brain Cancer Visualization is specified software for meningiomas and homogenous hypo-intensity gliomas. Automated cancer visualization through image processing, segmentation to extract the region of interest (ROI) and 3D reconstruction improves cancer diagnosis by determining the size and location of the tumor. In this 3D cancer visualization prototype, cancer is going to be extracted by using one of the three modes of segmentations (manual, automated and hybrid) followed by 3D reconstruction for both the tumor and the skull. The orientation of the reconstructed skull and tumor can be manipulated along three axes (x, y, and z) through an interactive screen. Furthermore, these two objects (the tumor and skull) are developed in different colors to enhance visualization of both of them as shown in Fig.1.1. The generated skull can change its opacity and make it translucent to preserve sufficient details for visualization and depth cueing by control of the pixel transparency of the skull; this visualization option allows intuitive depth perception[8].

Development of this prototype requires installing several open source libraries, such as VTK (Visualization Toolkit), SimpleITK (Insight Segmentation and Registration Toolkit) and numpy-STL, Skimage, WXpython, and Py.DICOM. Tumor segmentation and extraction were performed by using the region growing and binary thresholding algorithms. For 3D reconstruction, the marching cube algorithm was used to create STL-

file (Stereo Lithography). Seeds of 3D reconstruction of skull and tumor are stored in STL- file and enable it to be printed by 3D printing. This system is designed to work on MRI of localized intracranial tumors particularly the meningiomas and hypo-intensity, homogenous gliomas by using FLAIR saggital images.

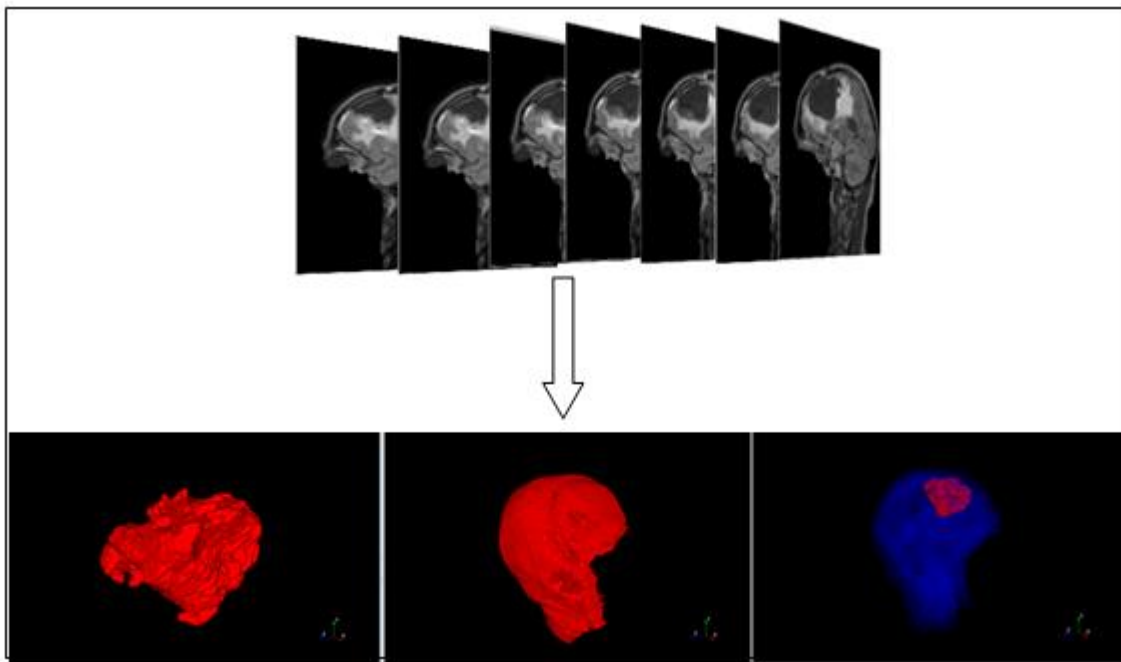


Figure 1-1 M-3Ds converts series of brain tumor of MRI from 2D into 3D model of tumor, skull and both of them

1.4. Thesis contribution

In the medical field, 2D images represent the 3D anatomical structure that must be mentally reconstructed by physicians to make the decision for specific steps of treatment. M-3Ds Brain Cancer Visualization software is specialized for localized brain tumor extraction and strongly contributes to clinical decision support by providing computational assistance. The focus of this thesis was to develop a prototype that segments/isolates the brain tumor while the classification of the brain tumors[9] is beyond

the scope of this work. That leads the researcher to develop a framework for accurate brain tumor isolation algorithm and quantify the accuracy of different 3D tumor segmentation by comparing the proposed software with some of the existing 3D visualization software and different approaches of segmentation algorithms.

The main contribution of M-3Ds software is being a brain tumor extraction tool that offers three modes of segmentations (manual, automated and hybrid). These modes of segmentation were assessed on their performance and accuracy which are required for computer assisted diagnosis, tumor monitoring, and therapy planning [10]. Additionally, it can be considered as a prognostic tool[11] and would offer an important step forward for better understanding of tumor dynamics, temporal growth, and response to treatments (radiotherapy and surgery) [12,13] by providing an automatic 3D volumetric assessment of the tumor.

1.5. Survey among simulating 3D visualization software of medical images

Various software packages for image processing and visualization of medical images are commonly used for this type of work. Several of these applications exist as off-the-shelf applications and available for research and diagnosis purposes like 3D Slicer, imageJ, Osirix, ParaView, 3D-Doctor and Synapse 3D. Most of the previously mentioned programs are open sources. Open source programs are considered a public collaboration and made available for use, modification, and redistribution. Recently, the largest commercial companies in medical imaging started to contribute to this field and developed flexible and robust systems [14]. Comparing between these software and M-3Ds is illustrated in Table I.

TABLE I: FEATURE COMPARISON OF M-3Ds SOFTWARE AND SOME POPULARE SOFTWARE PROGRAMS IN LITERATURE AND MARKET

Product name	Type of segmentation mode			Imaging modalities	Online source	Operating system (OS)			Segmentation platform	Measurement of ROI	Visualization
	Automated	Semi-automated (Hybrid)	Manual			Mobile setting (smart applications)	Portable workstation (Mac/Windows/Linux)	PACS workstation			
M3D	✓	✓	✓	MRI	Free/ Open source	✓	✓	✓ if supports python	Skull & tumor only	Volume, 2D area, perimeter	3D
3D slicer [15], [18-20]	X	✓	✓	MRI/CT & Biomedical images	Free/ Open source	X	✓	✓	Multiple	Volume, surface area, distance	3D
Paraview [16],[18][21]	Segmentation / extraction is exit but the mode is not determined.			Medical imaging & others	Free/ Open source	X	✓	✓	Multiple	--	3D
Image J (Fiji) [28-31]	X	✓	X	MRI/CT & Biomedical images	Free/ Open source	X	✓	--	Multiple	Volume, surface area, distance	3D
Synapse 3D [32]	✓	X	X	MRI/CT/ PET	Not online, not open source	X	X	✓	Multiple	Distance/ volume	3D
3D-DOCTOR [15],[33]	✓	X	X	MRI/CT/ PET & Biomedical images	Online but Not open source	X	✓	✓	Multiple	Volume, surface area, distance	3D
OsiriX [34-36]	✓	X	X	MRI/CT/ PET/ PET-CT	Free/ Open source	✓(iOS)	✓(onlyMac)	✓	Multiple	Distance, estimate ROI volume	3D, 4D, 5D

Each of the software packaged compared in Table I will be described below:

1.5.1. 3D Slicer

It is an open source software application developed to enable flexible radiological and biomedical imaging research[14],[15],[20]. 3D Slicer runs on modern Windows, Mac and a variety of Linux distributions. It considered as one tool of interactive brain tumor segmentation and 3D reconstruction [16]as in Fig.1.2, 1.3. It is a portable workstation that supports visualizations and provides advanced functionality such as automated segmentation and registration for a variety of applications. It provides abstractions for the data communication, visualization and user interface development[15]. 3D Slicer is unique as it is open source and the user can add new

processing routines to it. This feature has made this software more practical and appropriate for academic and research applications[10]. For a better understanding of 3D Slicer, a comparison of its performance with M-3Ds, and DICOM images of case 1 and case 2 were evaluated. It was found that 3D Slicer has manual and semi-automated segmentations requiring several user interventions; for example, each region of interest (ROI) requires a specific color and the user must determine the appropriate color of ROI then highlighting the ROI with that color as illustrated in Fig.1.3. Notably, if segmentation is not performed carefully inaccuracy will occur due to pixel value similarity in adjacent structures. Moreover, 3D Slicer segmentation method is based on GrowCut algorithm which is an interactive region growing segmentation method. The algorithm uses a competitive region growing approach and is considered as having good accuracy and speed for the 2D and 3D image segmentation. [17].

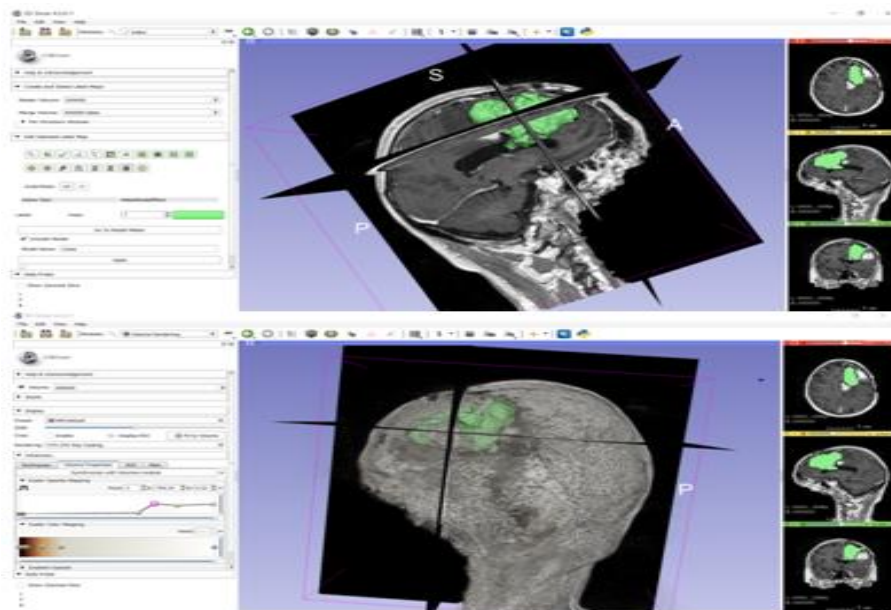


Figure 1-2 both images demonstrated different planes of brain and its 3D reconstruction offered transparent function

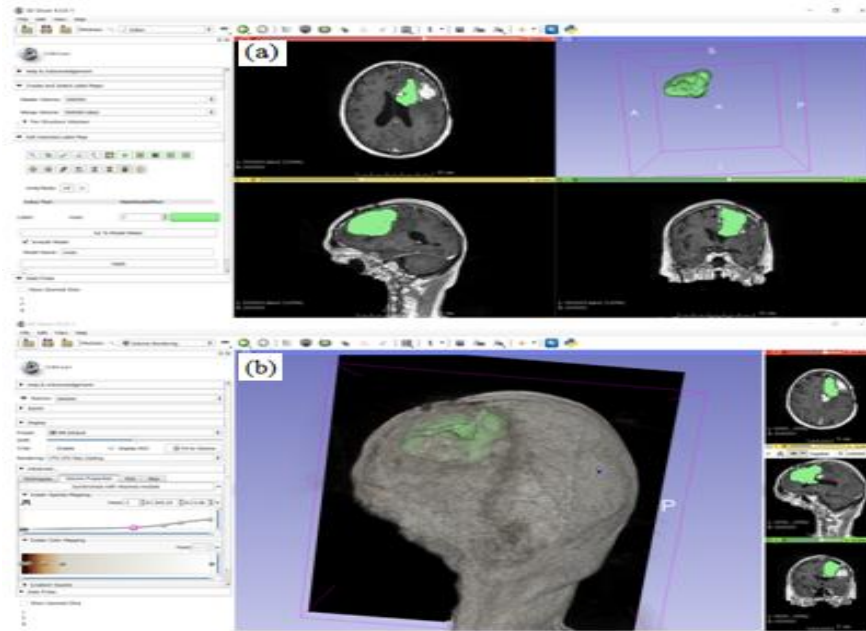


Figure 1-3 (a) Segmentation and 3D reconstruction of tumor. (b) Role of accuracy during coloring ROI, where lateral ventricle was involved as well

1.5.2. ParaView

ParaView is a free, open-source, multi-platform data analysis and visualization software[14],[18]. The data exploration can be done interactively in 3D or programmatically using ParaView batch processing capabilities. ParaView provided with memory computing resources that support analyzing extremely large datasets [18]. ParaView enhanced by Computational Anatomy Works (CAWorks) for medical imaging[19]. Computational Anatomy defined as the mathematical and computational analysis of human shape and form. Computational: anatomy has three components:

- Anatomical manifold generation via segmentation of known structures
- Anatomical manifold quantification via morphometric comparison
- Disease detection and diagnosis.

Kitware (an open-source software research and development company)[20]in corporation with The National Alliance for Medical Image Computing (NA-MIC), which is a collaborative community for the researchers, who share the same goals and objectives that modern health care demands improved technologies[21]. They launched a visualization platform project that considered as a combination of three platforms [22]; MIDAS[23], 3D Slicer[16], ParaView[18].This is made possible by loading the data from a MIDAS data storage[24], [25] then processing the data using 3D Slicer modules. Finally, by providing surface modelling and volume rendering using the ParaView. However, similar results were conducted by M-3Ds per sue.

1.5.3. ImageJ

ImageJ (or Fiji) is open source image processing software that provides 3D rendering of 2D images slices[26],[27]. It can be installed on any platform that supports Java such as Linux (32 bit), Linux (64 bit), Windows (32 bit), and Windows (64 bit) [26]. ImageJ is not only for radiological images, but also for other biomedical images. Its role is to import an image stack from the file, getting image information, selecting the image portions with a rectangle and processing the selected portion only, removing selected portion of the image, subtracting a particular intensity value from each pixel in the image, multiplying each pixel intensity value by a particular number, applying the image processing procedures to a single image or to the whole image stack[28]. ImageJ does not offer automated segmentations, but is provided with a plugin that creates interactive surface plots from all image types. This plugin has "Perspective" and "Scale" sliders allow the 3D-projection and the size of the surface plot to be changed [28]. Furthermore,

manipulation of these sliders could help in isolation of the specified portion as illustrated in Fig.1.4. ImageJ is a combination of powerful libraries with a broad range of scripting languages to provide rapid prototyping of image-processing algorithms[29]. The methodology of image segmentation of imageJ is summarized in the following steps: 1) pre-processing steps, which decrease the spatial variation of the image, 2) thresholding, which produces one or more binary masks, 3) masking or Region of interest (ROI) selection, 4) post-processing steps, for example including second thresholding or parametric fitting and 5) final measurement of volume, area, angles, etc[30]. At the beginning of this project ImageJ was installed to learn and understand the ways of segmentation and 3D reconstruction as demonstrated inFig.1.5.

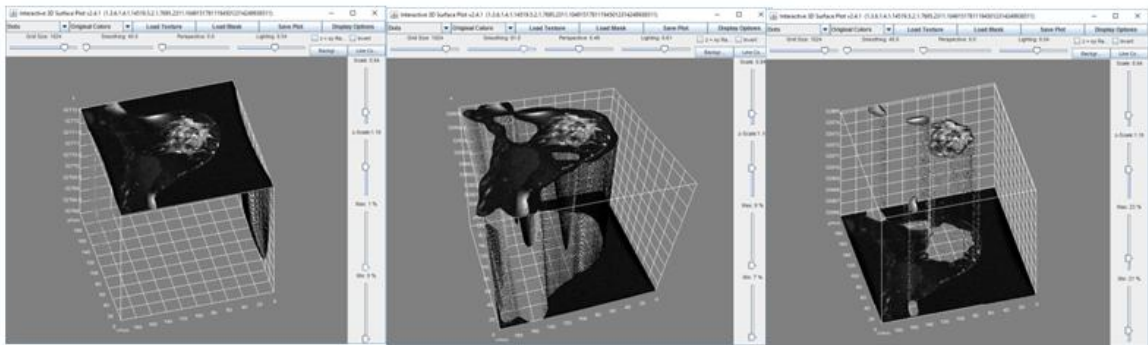


Figure 1-4 Example of interactive 3D surface plot of breast tissue [1]

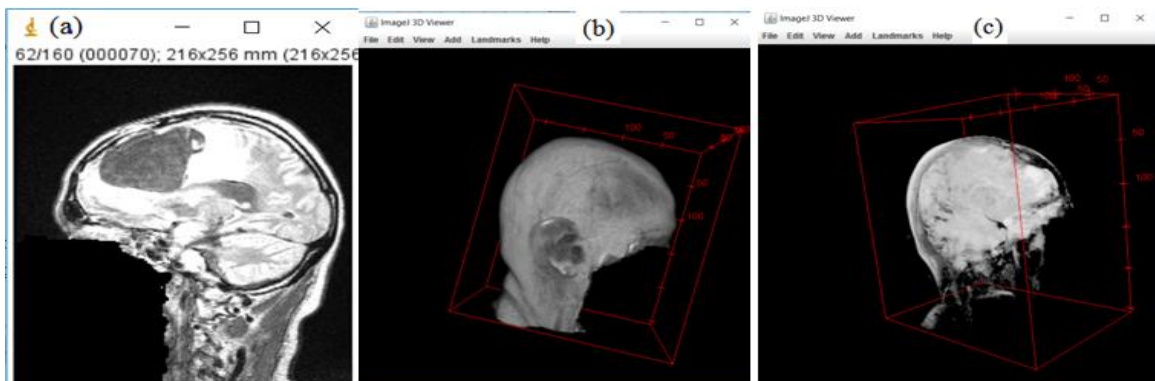


Figure 1-5 (a) Image acquisition of brain tumor of Case1, (b) 3D reconstruction of skull and (c) transparent function

1.5.4. Synapse 3D

Advanced visualization workflow just by a one-click user can access to 3D images [31]. Synapse 3D is integrated with Synapse PACS and can be a supportive tool for doctors and surgeons. Designed and developed by Fujifilm. It can support DICOM storage for CT, MR, and PET. Synapse 3D provides clinicians with a streamlined, rapid, and efficient workflow. The patient database was synchronized with Synapse PACS because of SYNAPSELink that used in Synapse 3D to save time during retrieving and saving images. Fujifilm Image Intelligence technology provides volume rendering through a 3D viewer, automatic extraction of ROI and accurate volumetric measurements. Also, users can easily scroll through orthogonal images and take snapchat that can be saved directly to Synapse PACS[31].

1.5.5. 3D- DOCTOR

It is an advanced 3D modeling, image processing and measurement software for MRI, CT, PET, and other biomedical images[10],[2]. It supports both grayscale and color images stored in DICOM, JPEG and other image file formats. It exports the mesh models to STL and other formats for surgical planning, simulation, rapid prototyping applications and quantitative analysis. 3D volume can be calculated and make other 3D measurements for quantitative analysis. 3D CT/MRI images can be re-sliced easily along an arbitrary axis. Some degree of similarity between 3D- Doctors and M-3Ds in segmentation and 3D modeling is displayed in Fig.1.6 and 1.7.

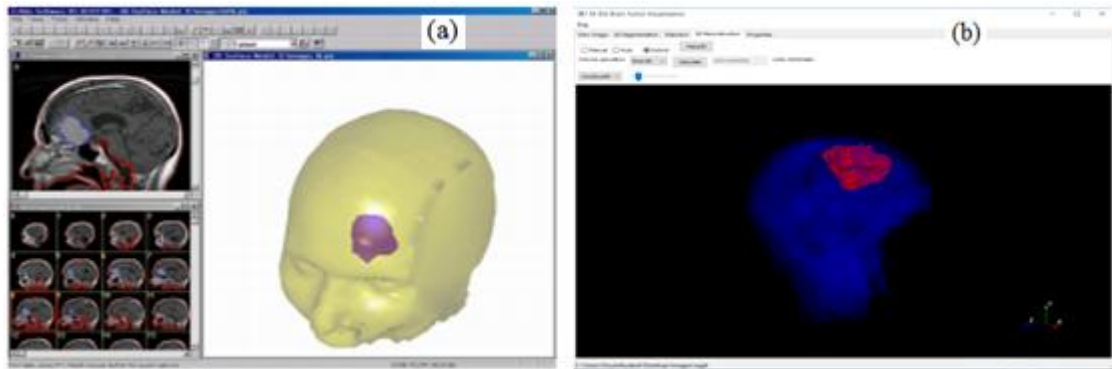


Figure 1-6 See-through (transparency) technique for tumor in (a) 3D-DOCTOR[2] and (b) M-3Ds

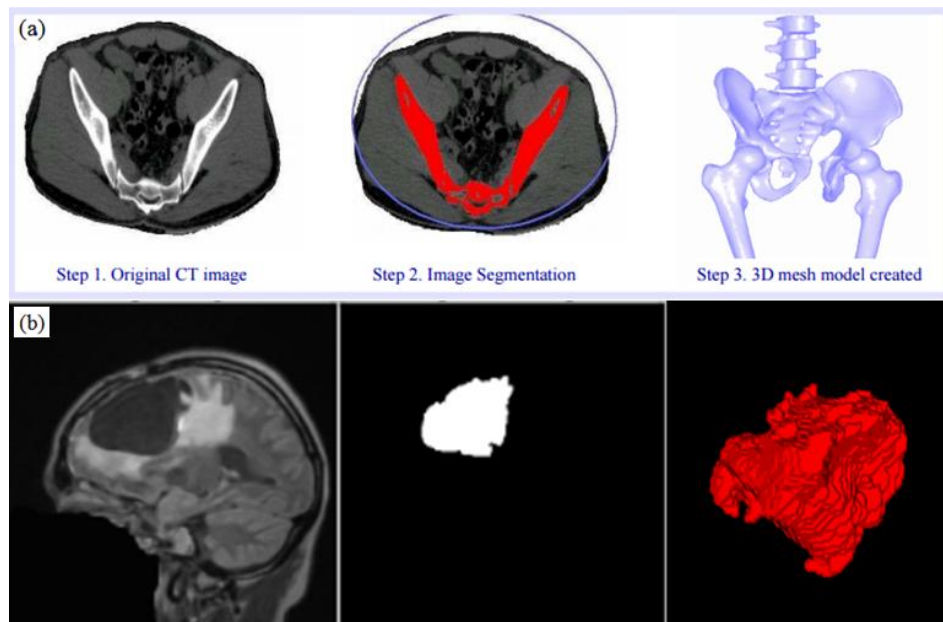


Figure 1-7 Both(a) 3D-Doctor[2] and (b) M-3Ds have similar features about segmentation and 3D reconstruction

1.5.6. OsiriX

It is an open source software that stands alone on a Mac OS X operating system [3]. The first iPhone (iOS) version of OsiriX was released in November 2008, and in December 2010, OsiriX developed a new version of for iOS that supports iPad devices[32].Image processing and rendering based on open source libraries as ITK and

VTK [3]; and ROI is segmented semi-automatically. The aim of OsiriX is to deliver the best possible viewer for images produced by radiology equipment, such as MRI, CT, PET, PET-CT, SPECT-CT, Ultrasounds, etc.[32], [33]. The program displayed the images directly without pre-loading of images from the disk to memory before a review. As series of 2D images is selected the images are displayed automatically [3]. The similarity between OsiriX and M-3Ds in this feature is demonstrated in Fig.1.8.

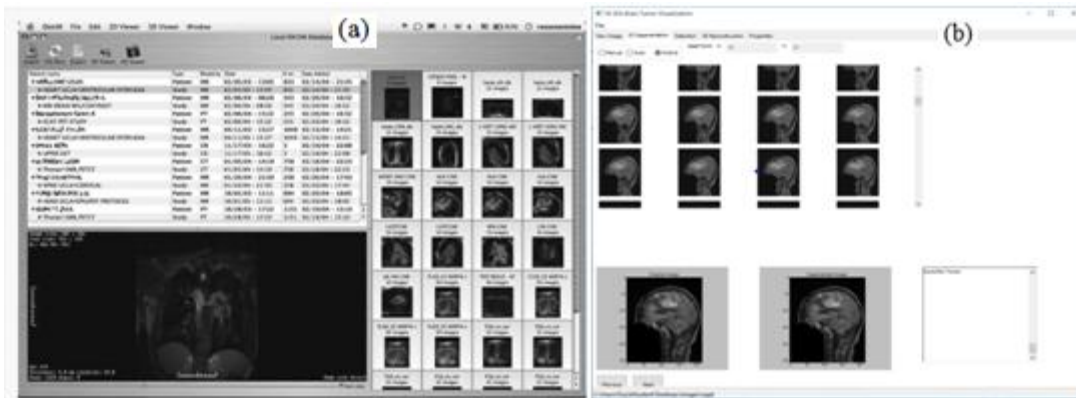


Figure 1-8 Both (a) OsiriX [3] and (b) M-3Ds show the similarity in 2D images acquisition

1.6. Connection to eHealth

3D visualization of cancer grants clinicians the ability to observe lesions more intuitively and precisely during the diagnosis process where they found it a helpful tool particularly when it used as a computer-aided diagnosis (CAD) and computer-assisted therapy and surgery with 3D images in healthcare services. 3D visualization of cancer plays an important role in the quantitative analysis of imaging data. From these concepts M-3Ds could be considered as a part of a clinical decision support system (CDSS) especially if machine learning technique is used.

As demonstrated in Table I, some commercial visualization systems are available in the market for decision support and providing solutions for visualization design in both 2D and 3D design. One of these examples is the 3D Slicer that could be considered as a portable workstation provided with additional functionalities that empower clinicians' performance[15].

3D Cancer visualization would be helpful in telediagnostic imaging support system particularly if the 3D object is bandwidth optimized. In turn, it will impact positively in the field of eHealth when it is connected to network and mobile technologies[34]. M-3Ds Brain Cancer Visualization could be applied in a mobile setting, thus allowing it to be accessed anywhere, because the algorithm is designed to be less processing power. Also, it is intended to be free and open source software that could be installed on any operating system or web client that supports Python. Thus, it could be considered as a portable tool for diagnosing gliomas that enables physicians to access patient's data easily from any computer station to support their decision. The importance of this structure is particularly evident in emergency conditions where quick decisions should be made in locations where resources are limited, such as outside of the hospital or in the field. Physicians can access and process the patient's medical data quickly and easily using this kind of medical imaging software[10]. Mobile technology facilitates remote visualization and remote diagnosis[19]. As a result, M-3Ds prototype bridges some gaps and provides a future success for various eHealth applications in the medical domain. The concept of 3D visualization makes clinically vital tools more easily accessible, and help clinicians to

save time, improve patient safety and enhance confidence about the treatment plan[31], [35].

1.7. Organization of the thesis

This thesis is divided into seven chapters that are explained below.

The first chapter addresses the problem statement, the proposed system, thesis contribution, objectives and connection to eHealth. In the second chapter, the theoretical background is covered. It involves types of tumors, types of imaging modalities, types of main using algorithms and the imaging of the tumor. While in chapter three, the literature review and related work are presented. And in chapter four, an architecture overview of the proposed system including segmentation process of 2D DICOM images (Input), feature extraction, 3D reconstruction (system output) and visualization via modern Graphical User Interface (GUI) are discussed. Furthermore, chapter five is going to explain the design and implementation of software and the study. Next, in chapter six experimental results are presented. Then in the last chapter, discussion and conclusion are presented with consideration for future directions. Finally, appendices are going to terminate the paper by showing all associated work.

Chapter 2

2. Theoretical background

2.1. Types of tumors

There are three types of tumors: Benign; Pre-Malignant; Malignant. A) Benign tumor: Is a tumor that does not grow suddenly; it doesn't affect its neighboring healthy tissues and also does not extend to non-adjacent tissues. The common examples of benign tumors are moles. B) Pre-Malignant tumor: It is a precancerous stage, considered as a disease, if not properly treated it may lead to cancer. C) Malignant tumor: Is the type of tumor that worsens over time and leads to death. Malignant is a medical term used to describe a severe progressing disease and typically used for the description of cancer[36]. Brain tumor classification according to World Health Organization(WHO) are: Diffuse astrocytic and oligodendroglial tumors; Other Astrocytic tumors; Ependymal tumors; Other gliomas; Choroid plexus tumor; Meningioma; Other mesenchymal non-meningeal tumor; Tumor of pineal region; Ependymal tumor; Tumors of cranial and paranasal sinus; Melanocytic tumors; Lymphoma; Histiocytic tumors, Germ cell tumors; Tumors of the sellar regions; Metastatic tumors. Moreover, International Classification of Diseases—Oncology (ICD-O) provides coding for the histopathological nature of the tumor[37].

M-3Ds software prototype and research scope are limited to meningiomas and low intensity, homogenous gliomas. Gliomas represent 70% of adult primary intra-axial,

intracranial tumors. Morphological changes due to the tumor and its surrounding oedema called mass-effect [13] it impacts adjacent anatomical structures causing pressure, displacement and sometimes herniation of certain structures. On the other hand, meningiomas are the most common extra-axial, intracranial tumors. They represent 20-43% of intracranial neoplasm. Treatment is usually performed by radiotherapy or surgery or both [13],[38].

2.2. Main types of imaging modalities

The two most important and generally used tumor imaging modalities are CT and MRI. Once a brain tumor is clinically suspected, radiologic determination of the location, the extent of the tumor and its spatial relationship to the surrounding structures are required. The technical improvement of CT and MRI, the introduction of contrast agents in brain imaging and the innovations of new imaging techniques all improve the evaluation and cancer detection [39].

2.2.1. Computed Tomography (CT)

CT of the brain is considered the procedure of choice for evaluation and diagnosis of brain tumors. In the past, invasive procedures such as pneumoencephalography or cerebral angiography were performed but currently it is replaced by CT. A CT-guided stereotactic biopsy is a reliable and valuable method for histological diagnosis of brain tumors, in addition to the planning of appropriate treatment and intervention for each patient. Although MR is the main diagnostic tool for diseases of the central nervous system, CT is still an essential modality in the imaging of brain tumors. CT is superior in

detecting calcification, hemorrhage, and in evaluating bone changes related to a tumor. Also, patients with pacemakers or metallic devices and those who are critically ill, children or unstable patients represent as comatose patients; CT is the diagnostic modality of choice[40].

2.2.2. Magnetic Resonance Imaging (MRI)

Magnetic resonance imaging (MRI) stills the modality of choice for the brain tumor. It plays a valuable role in assessing tumor location, size, and extent, in directing biopsies, in therapy planning, in the disease prognosis and in evaluating the therapeutic results. The standard protocols are; spin-echo T1-weighted image (T1WI), T1WI after the administration of a paramagnetic agent, T2-weighted image (T2WI), T2-weighted MRI with fluid-attenuated inversion recovery (T2 FLAIR) and proton density-weighted image (PDWI)[13], [40].

Most homogenous brain tumors have prolonged T1 and T2 relaxation times and appear hypointense relative to the normal brain on T1WI and hyperintense on T2WI. While on PDWI the tumors show intermediate hyperintensity. However, some of the tumors are heterogenous due to the presence of fat, hemorrhage, necrosis, and calcification[40]. Acquisition parameters of these sequences are not standardized for different types of tumors where the patient undergoes to MRI protocols according to the response assessment in neuro-oncology (RANO) guidelines with a slice thickness of ≤ 5 mm without a gap between the slices [13],[38]. T1-weighting is the most commonly used sequence for the structural analysis; it also allows for an easy explanation of the healthy

tissues. In T1WI with contrast(paramagnetic agent), the contrast agent accumulates at the tumor borders and makes them brighter; this happens due to disruption of the blood-brain barrier in the proliferative region[13],[38]. In T2WI and FLAIR the edema appears bright; however, FLAIR is superior on T2WI via suppressing the free water signal of the cerebrospinal fluid (CSF)[13] and easily differentiates between edema and CSF. This explains the reason behind choosing FLAIR sequence in this research.

Defining the tumor margins in radiology is performed manually and based on T2WI and T1WI with contrast images by thresholding boundaries between the hyperintensity of tumor in T2 /T1 with contrast and the surrounding tissue[13], [38].

2.2.3. Single Photon Emission Computed Tomography (SPECT)

It is one of metabolic imaging of brain tumors with radiolabeled amino acids that improves the diagnostic accuracy in combination with anatomic radiologic method[39], this technique using gamma rays and it can make 3D images[41]. It is a useful measure of brain function as recurrence of brain tumor and non-neoplastic brain abnormalities following treatment[42], [43], [44]. SPECT plays an important role in differentiation between brain tumor recurrence and radionecrosis while MRI and CT cannot always distinguish between both of them. The main advantages of SPECT are represented by increased specificity and accurate localization of disease and a possible involvement of adjacent tissues[45], [46].

2.2.4. Positron Emission Tomography (PET)

It is a nuclear medical imaging technique that is a useful tool in the staging, treatment monitoring, detection and identification of recurrent disease in a large number of malignancies[47]. It uses glucose as a form of radioactive agent to create a three-dimensional image that represents the functional processes inside the body. It aims to evaluate normal and abnormal biological function of the structure. The PET scanner is made up of detectors arranged in a circular shape. The role of these detectors to pick up on the pattern of radioactivity from the scanned area in the body then 3D color images of the area are created by computer. Different colors on a PET image represent different levels of tissue or organ function [47]. PET scanning can provide information about the diagnosis, degree of malignancy, recurrence, response to treatment, and differentiation between recurrence and post- radiation injury, all with low risk to the patient. The PET scan is an important tool in the diagnosis of patients with brain tumors [48], [49].

2.3. Main types of algorithms for 3D segmentation

2.3.1. Main segmentation algorithms

Visually it is easy to recognize and pickup the region of interest (ROI); however, doing the same task by using a computer algorithm is difficult. For example, how does the computer define a region? What kind of features can identify one region from another? How many regions of interest in a given image? Similarity/homogeneity and discontinuity properties of the pixels in relation to their local neighbourhood are the two basic properties that used in different segmentation methods[50]. Furthermore,

segmentation algorithms classified into supervised and unsupervised algorithms[12], M-3Ds segmentation algorithms belong to the supervised category. The following algorithms are the background theory behind each of the segmentation algorithm, where each method A, B and C combined two types of these algorithms as displayed in the flowcharts of each method in Chapter 4. For example, in method B, the following steps were applied 1) watershed algorithm applied first (alone); followed by 2) region growing algorithm applied in the next step in assistance with connected component algorithm (together).

2.3.1.1. Region growing algorithm

Region-based segmentation is an approach to recognize the region of interest directly[50]. It is a simple region-based image segmentation technique. Initially, seed points should be selected, and image segmentation is based on pixel classification[50]. The procedure starts with a set of seed points and then groups neighbouring pixels that provide similar properties [51],[52]. The pixels of the same region are labelled by the same symbol while the pixels of other regions are labelled by another symbol [53]. Through this approach it examines the neighbouring pixels of initial “seed points” and decided whether the pixel neighbours should be added to that region or not. These pixels are called allocated pixels which lead to its growth while the rest of pixels called unallocated pixels. The process is iterated several times, in the same manner as general data clustering algorithms [50],[53].

The selected criteria could be, for example, gray level texture, color, or pixel intensity. Regions that are disjoint must be assigned because a single seed point" cannot

be held in two different regions. The regions must cross the entire image because each point has to be belonged to one region or another. If these criteria are met, the image is accurately segmented into regions [51].

2.3.1.2. Binary thresholding algorithm

It is a simple and popular approach for image segmentation and processing. This technique classified into global and local thresholding [54], [55]. Global if the same critical value is used all over the image; however, if the critical values are different is known as local thresholding. Thresholding algorithm converts the gray scale image into binary one (black and white). Pixels whose value exceeds a critical value are assigned to one group and the rest to another. Consequently, the image consists of only object and background[56], [57]. In local thresholding, the original image is partitioned into smaller sub-images, and a threshold is determined for each of the sub-images. This leads to a thresholded image with gray level discontinuities at the boundaries of two different sub-images. After that, smoothing technique is applied to remove the discontinuities [54].

The output of the thresholding operation is a binary image whose one state will indicate the foreground objects (white) and background (black) [58]. Thresholding is extensively used in many image processing applications and as optical character recognition [59], automatic target recognition [60], detection of video changes [61], and medical image applications [62].

2.3.1.3. Watershed algorithm

The term watershed means that the area of land where all of the water that is under it or drains off of it goes into the same place, this meaning is used in image processing as a method of solving problems[63]. Watershed segmentation is the best method to group pixels of an image according to their intensities. Pixels of the same intensities are grouped together. It is a good segmentation method for dividing an image and separates a tumor from the image[64],[65]. Watershed segmentation is the best method for image segmentation in the field of mathematical morphology [64],[65],[66]. It segments the image as a dam and each segmented regions are called catchment basins [65]. In order to understand the watershed transform a hole in each local minimum is imagined and that the topographic surface is immersed in water. Water begins filling all catchment basins at a uniform rate. If two catchment basins would merge consequently a dam is built all the way to the highest surface altitude and the dam represents the watershed lines. Final dam represents the continuous boundaries extracted by watershed segmentation algorithm [66].

2.3.1.4. Connected component algorithm

One of the purposes of image processing is to identify and recognize the shape of an object on a digital image [67]. Connected component labelling (CCL) is widely used in image processing. In computer vision most objects have surfaces and the points in a connected component form a candidate region to represent an object. The image object, which is the component, is separated from the background image on binary image. Then each component is labelled and displayed as output images. Points belonging to a surface

project to spatially closed points. The CCL algorithm works by scanning the image from top to bottom and left to right and assigns labels to each pixel and the iteration process continues until the labels for the pixels no longer changes[6].

2.3.2. Marching cube algorithms (surface extraction and volume rendering)

Marching Cube algorithm relies on three algorithms; interpolation, approximation and rendering. Marching cubes are also known as polygonising a scalar field, 3D Contouring, Marching Cubes and Surface Reconstruction. It is used in reconstruction of a surface from medical volumetric datasets. For example, MRI scans result in a 3D volume of samples at the vertices of a regular 3D mesh [68], [69]. It creates triangle models of constant density surfaces from 3D medical data and uses a divide-and-conquer approach to generate inter-slices connectivity[70]. Marching cube algorithm is used for rendering isosurfaces into volumetric data. Voxel (cube) can be defined as the pixel values; each voxel has eight corners. If one or more pixels have values less than or greater the user-specified isovalue that means the voxel must provide some component of the isosurface. The intersected edges of the cube with the isosurface lead to creating triangular patches. In turn, these patches will divide the cube between regions within the isosurface and regions outside. Then these patches from all cubes are going to be connected on the isosurface boundary to get a surface representation[68], [69], [70].

2.3.2.1. Approximation (Tessellation)

Datasets of polygons are managed by tessellation where the objects are presented in a scene or break them up into suitable structures for rendering. Data is tessellated into

triangles for real-time rendering as in OpenGL and Direct3D 11[71]. “Tessellation is a process that reads a patch primitive and generates new primitives used by subsequent pipeline stages. The generated primitives are formed by subdividing a single triangle or quad primitive according to fixed or shader-computed levels of detail and transforming each of the vertices produced during this subdivision. Tessellation functionality is controlled by two types of tessellation shaders: tessellation control shaders and tessellation evaluation shaders. Tessellation is considered active if and only if there is an active tessellation control or tessellation evaluation program object”[71]. The aim of approximation (Tessellation) is to make the pieces of the 3D volume are easy-to-analyze [71], [72].

2.3.2.2. Interpolation

The idea of linear interpolation could be summarized in estimating a new value by joining two adjacent known values with a straight line in as sequence value. If these two known values are (x_1, y_1) and (x_2, y_2) , then y value for some point x is: Linear interpolation is a straight line that falls between two data points [73].

2.3.2.3. Rendering

It is defined as volume visualization that is considered as a collection of techniques for visualizing 3D functions [74].The earliest methods extracted conventional computer graphics primitives such as surfaces, curves, or points, and then displayed them. More recent methods render the volume directly, without this intermediate conversion. This involves forming an RGBA (color and opacity) volume and projecting it from the desired point of view [75], [76]. RGBA volumes can represent both interiors and the surfaces

representing the boundaries between different regions. If just surfaces are shown, the pictures look quite similar to those generated by first extracting the surfaces and then rendering those[75].

Isosurfaces can be determined by mapping the similar data values to opaque and transparent. The appearance of surfaces can be improved by using shading techniques to form the RGB mapping [77]. However, if interiors are also shown, they appear as clouds with varying density and color. The main advantage of volume rendering is keeping interior information so 3D data set can be seen as a whole; a disadvantage is that cloudy interiors are hard to interpret and the long time, compared to surface rendering, needed to perform volume rendering [77], [78]. Volume rendering includes these steps: the discrete data set forming of an RGBA, then reconstruction of a continuous function from these data set, followed by projecting it onto the 2D viewing plane which is considered as an output image, from the desired point of view. An RGBA volume is a 3D four-vector data set, where RGB represent Red, Green, and Blue color elements and the last element, A, represents opacity. An opacity value of 0 means completely transparent, and a value of 1 means completely opaque. An opaque background is placed behind the RGBA volume. The mapping of the data to opacity values acts as a classification of the data one is interested in[77]. Also, three-dimensional arrays of digital data representing spatial volumes arise in many scientific applications. Computed tomography (CT) and magnetic resonance (MR) scanners can be used to create a volume by imaging a series of cross sections. These techniques have found wide use in medicine [79]. Despite of considering

the volume rendering as a flexible technique for visualizing scalar field but high quality images take tens of seconds or minutes to generate a 3D model[79].

Chapter 3

3. Literature review

3.1. Perception of healthcare professionals for 3D visualization

Perception of 3D modeling enhances spatial information about the relationship of structure and its pathology. Automated segmentation (identifying the required structure) leads to signification time reduction and increases the effectiveness of this practice [80]. The spatial anatomical relationship is not an easy task where it is used to be processed in the radiologist's mind. 2D images only tell the clinician the size and location of the structure. Therefore, an image-processing tool is required to display an interactive image for clinicians. 3D interactive visual information can be similar to that of a surgeon's view during surgery, and is a more accurate representation of the anatomy of interest, whereas, mentally reconstructing the image may not align with planes of image acquisition [80].

E. Vegra and A. Freudenthal[81] defined computationally supported images as a technical solution replacing the cognitive process. Interventional radiology procedures require the physician to read 2D radiology images as CT, MRI to make a plan and treatment evaluation. The 3D anatomy of the patient represented by 2D images should be mentally reconstructed and manipulated to make decisions. 3D reconstructions may provide a general 3D understanding of the scanned body part; however, 2D images do not provide detailed anatomical information for the planned treatment. Furthermore, 3D reconstruction provides interaction with the 3D images such as rotation and zooming.

3D visualization influences the communication process in multidisciplinary projects. It provides better understanding clinicians to communicate ideas with the rest of multi-disciplinary team about spatial images. These spatial images are related to human anatomy, and their manipulation is required to perform successful procedures [82]. 3D visualization and image processing provide the surgeons with information similar to what they see during the surgery, which provides them with better comprehension of the whole anatomy. Particularly, some structures, such as the vascular tree are extremely difficult to manipulate mentally if it is based on 2D images alone [80]. B.M. Hemminger et al. [84] developed an interactive combination 3D and 2D visualization system. Radiologists and surgeons recorded their impressions with and without the use of the interactive visualization system. The cardiothoracic surgeons reported positive results from using a 3D visualization tool. It changed the surgical plan, increased the surgeon's confidence, and correlated well with the anatomy found at surgery. However, the radiologists reported fewer major changes compared with other surgeons in their understanding of the case due to the 3D visualization, and this result due to their accumulated experience in using 2D images. This study concluded that is helpful in communication and understanding for radiologists and surgeons. It impacts on surgeons more than radiologists especially in their planning for the surgery. Also, M. Tory and T. Mo'ller [84] believed that visualization could provide valuable assistance for data analysis and decision-making tasks. J. Vuchkova et al. [85] investigated the effect of 3D visualization software on students' learning of oral radiographic interpretation from 2D radiographic images. The intervention was assessed by quantitative means, using a radiographic

interpretation test, and by qualitative means, using a structured Likert-scale survey. They concluded that training with the interactive 3D visualization software would provide additional depth cues, which enables students to develop spatial-mental models of anatomy that facilitate their understanding of the 2D radiographic interpretation of oral pathoses. Although the results of quantitative assessment did not support this, the questionnaire showed a positive outcome of the 3D visualization by enhancing students' learning about radiographic interpretation.

3.2. Liminality and threshold concepts in 3D visualization

Studies showed that clinicians are going to pass through what is called by liminal space to understand and interact with advanced technology, which will immerse them into a new spatial space and enable them to take advantage of it by introducing 3D reconstruction modeling onto virtual reality field. Therefore, how does this kind of advanced technology affect the spatial cognitive ability? Threshold concept is defined as a transition through a gateway or a portal that could be counted as a barrier or source of engagement to the creativity[86], [87]. A threshold concept is stated as a core or centre of any discipline. The learner is considered in a state of liminality right before he/she finally grasps the concept then passing through the threshold[87]. It is characterized as liquid space, and the aim of teaching threshold concepts is to be critical, creative and flexible learners [86]. Learning leaps are described as cognitive transformation where new concepts change the learner's role and is characterized by enhancing fluidity, creativity, and knowledge capturing of the learner[86]. Recently, teaching threshold concepts are required to support virtual reality(VR)[88]. First of all role of the threshold concept in

creativity should be clarified then the role of virtual reality in learning and education[86].
 Molka-Danielsen et al.[86]worked to develop a 3D- recording VR system in education,
 the learning possibilities offered by this design are summarized in Table II.

TABLE II: CURRENT FORMS OF ACTIVE LEARNING[86]

Approach to Learning	Organization of Knowledge	Forms of Knowledge	Related theory	Theorist	Role of Student	Role of tutor
Problem based learning	Open ended situation and problem	Contingent and constructed	Critical pedagogy and social action	Freire (1972, 1974) hooks (1994)	Active participant and independent critical inquirer who owns their own learning experiences	Enabler of opportunities for learning
Project based learning	Tutor-set, structured tasks	Performative and practical	Cognitive learning theory	Vygotsky (1978) Ausubel et al (1978)	Completer of project or member of project team who develops a solution or strategy	Task setter and project supervisor
Problem-solving learning	Step-by-step logical problem solving through knowledge supplied by lecturer	Largely propositional but may also be practical	Cognitive learning theory	Vygotsky (1978) Ausubel et al (1978)	Problem-solver who acquires knowledge through bounded problem-solving	Guide to right knowledge and solution
Action Learning	Group-led discussion and reflection on action	Personal and performative	Change management	Revans (1983)	Self-advisor who seeks to achieve own goals and others to achieve these via reflection and action	Facilitator of reflection and action

Adopted from J. Molka- Danielsen et al. 2013

Characters and conceptual role of threshold concepts[86], [87]:

- Transformative - shifting in subject perception. It is necessary for the learner to grasp concepts in any specific discipline.
- Bounded – any conceptual space has boundaries and yields to new conceptual space. Irreversible – unforgettable, once learn will not be forgotten.
- Integrative – introducing new ontology and a new way of understanding.

- Troublesome knowledge –
- Discursive - overcoming the threshold will lead to deep understanding of knowledge.
- Liminality – state of mind during which the learner encounters troubles in the learning process. The notion of liminal space is relatively ill-defined [87].

3.3. Different algorithms related to image processing and 3D reconstruction

When experts work on tumor images, they can use three different types of algorithms. Some techniques that are pixel based, those based on the texture of images, or those based on the structure of images[64]. H. Dong et al. [5] proposed a new method for medical image reconstruction platform which is developed based on ITK (Insight Segmentation and Registration Toolkit) and VTK. The `itkBinaryMask3DMeshSource` class is used to extract the surface of DICOM series, and then transform the mesh to the polygon data by the class of `itkMeshToVtkPolyData`. Finally, the 3D visualization outcome will be visually displayed by the VTK. M. M. Hossam et al. [6] proposed an image segmentation scheme to segment 3D brain tumors from MRI images by the clustering process. They used K-mean algorithm and the connected component labelling algorithm to link the similar clustered objects in all 2D slices and then the 3D segmented tissue is obtained by using the patch object rendering process.

A. Mustaqem et al.[64] an efficient algorithm is proposed in this paper for tumor detection based on segmentation and morphological operators. First, enhance the quality of the scanned image, and then apply the morphological operators to detect the tumor in the scanned image. S. Mengmeng and W. Shuicai[89]suggested that to display and

process images in different DICOM formats, they introduce a new method of integrating ITK, VTK, and QT to process the images in DICOM format, and software was designed based on the three tools. The results indicate that this software can read and display DICOM images with different suffixes and can process medical images simply. N.N. Gopal & M. Karnan[90] proposed an algorithm that used multi-scale image segmentation. They used a fuzzy c-mean algorithm for brain tumor detection. D.M. Joshi & et al.[91]used neuro-fuzzy algorithm for the segmentation of to improve the tumor detection. M.N. Wu et al.[92] suggested clustering technique (k-means algorithm) to detect the brain tumor in MRI by converting the gray scale images into color images and then using k means clustering and histogram clustering. P. Vasuda and S. Satheesh[93] suggested fuzzy clustering technique for detection of a brain tumor in MRI. This algorithm uses fuzzy C-means (FCM), but the major drawback of this algorithm is the computational time required.

P. G. Cavalcanti et al. [94] introduced a new technique to estimate the background of nodules in chest CTs and displayed the role of the simple thresholding-based algorithm in the extraction of these lung nodules with accurate nodule segmentation results. A higher percentage of true positive results (TPR) levels indicate the accuracy of segmentation that greater portions of the nodules are accurately segmented, and this feature will impact positively on a computer-assisted diagnosis (CAD) system. They believed that this approach can be adapted and may be also useful for other medical applications and diseases.

3.4. Modes of segmentation

M.R. Kaus et al.[80] compared the automated brain tumor segmentation and manual segmentation with 3D MRI in 20 patients with brain gliomas and meningiomas. They found the run time for automated segmentation was 5-10 min. while for manual segmentation was 3-5 hours. Automated segmentation allowed rapid identification of tumors with high accuracy and reproducibility. In manual segmentation, The structures were outlined slice-by-slice by human operators by pointing and clicking with a mouse; then the program connects consecutive points with lines. A closed contour is used to identify an anatomical object, and every voxel of the enclosed volume is labeled by the program. They suggested manual segmentation as the gold standard for interactive computer segmentation despite its human error and inter-observer variability.

J. Liu et al. [95] provided a comprehensive overview of MRI-based brain tumor segmentation methods (manual, automated and semi-automated). They elaborated in these three methods where and evaluate them. Manual, automated and semi-automated segmentation based on the degree of human interaction. For example, in manual segmentation, the experts or users must master the information in the brain tumor images including the anatomy of the brain because in this type of segmentation the tumor is drawn manually with its boundaries and paint the regions of anatomic structures with different labels[96]. Because of time-consuming and error –prone of the manual method; therefore, hybrid (or semi-automated) and fully automated methods are required to bridge the gaps of the manual method. The semi-automated method is a combination of user interaction and software computing where the user needs to input parameters and is

responsible for analyzing the visual information and providing feedback response for the software computing. The interaction is in charge of adjusting segmentation information between the user and the software computing. Although brain tumor semi-automatic segmentation methods can obtain better results than manual segmentation, it shows some inter-observer variability between the experts. Hence, the fully automated segmentation method is highly required. In fully automated, the computer determines the segmentation of brain tumor without any human interaction. As a result, machine learning and artificial intelligence are combined with segmentation algorithm. Semi-automated and fully automated segmentation methods still facing some challenges like irregular boundaries with discontinuities and partial-volume effects for brain tumor images.

Computational segmentation time over a few minutes is unacceptable in clinical routine. Also, the robustness of automatic segmentation technique is needed, if it fails in some cases, clinicians will lose trust and not use this technique. Therefore, the robustness is also one of the major assessment criteria for each new method applied in clinical practice. N. Idrissi and F. E. Ajmi[97] presented a new approach called hybrid segmentation, combining the mathematical morphology operators and morphological watershed segmentation. They had also compared manual and automatic segmentation methods. For instance, manual segmentation is usually accurate but is impractical for large datasets because of time-consuming that impact on clinical workflow. Automatic segmentation techniques can be useful because of its reasonable processing speed for large datasets; however, if they have: ability to segment like an expert, excellent performance for variable datasets will be resulted [98].

S. Bauer [38] commented on reasons behind continuity of using the manual method by clinician despite the huge amount of work involved in automatic field and referred these reasons to a lack of communication between researchers and clinicians. Also, these pure research programs are not easy to handle for clinicians. Therefore, a huge effort should be spent on embedding the developed tools into more user-friendly environments in the future. A. Mikheev et al. [99] developed and validated new fully automatic algorithm based on Bridge Burner which is a new segmentation algorithm relied on thresholding, connectivity, surface detection, and a new operator of constrained growing. They found this new fully automatic algorithm provide accurate brain segmentation from high-resolution T1-weighted MR images. Additionally, they discussed how these programs have considerably reduced the amount of segmented time in comparison to manual extraction. Some flaws accompanied this algorithm as including ventricular and subarachnoid cerebrospinal fluid (CSF). Moreover; current tools force the user to compromise either processing speed or accuracy. B. Fischl[100], they launched a technique for automatically determining a neuroanatomical label to each voxel in an MRI volume and validating these automatic segmentation results comparing them with those of manually labeling the same datasets. They concluded that there is no significant bias in the automated volume measurements, which are statistically indistinguishable from the manually computed volumes.

3.5. Overview of some existing 3D visualization platforms

S.J. Taka et al. [101] reported that medical image visualization platforms work with either image space or mesh space. Image space refers to the manipulation of image data

such as Digital Imaging and Communications in Medicine (DICOM); Tiff; Jpeg formats. Some examples of image space software are 3D Slicer, VR Render, and OsiriX. Mesh space refers to manipulation of mesh data and corresponding solutions in formats such as Vtk, nod/ element files, Stl, Abacus and Ansys formats. Before any software development was done, the software libraries had to be downloaded and built into binaries. In particular, these versions of the libraries were downloaded: VTK version 5.2.1; ITK version 3.10.2; GDCM version 2.0.12; C Make version 2.6.2; Qt version 4.5.0. In another study conducted by J.M. Yu et al. [102] they differentiated the commercial free mesh creation tools as follows:

- MeshLab: It is an open-source tool designed for 3D triangular meshes creation. It has some flaws such as; no semi-automated segmentation routines and is also lacking some workflow features such as the ability to undo the last action.
- Mimics: It is the most popular commercial packages that designed for medical image processing. Its disadvantage demonstrated in a great deal of manual input for mesh creation. Also, some difficulties with multiple-region problems.
- Netgen: It is a freely available 3-D tetrahedral mesh generator, but has limitations with multiple-region problems.

Z. Li et al.[4] developed 3D image display element called MedViewCtrl which is simply plugin a PACS (Picture Archiving and Communication System) workstation. The MedViewCtrl not only has 3D visualization functions such as maximum intensity projection (MIP), multi-planar reformation (MPR), direct volume rendering (DVR), and

surface shaded display (SSD).But also with multi-modal medical image fusion as well as a computer-assisted diagnosis (CAD).

3.6. Volumetric measurements of isolated tumor

Some of 3D visualization platforms provide volumetric information which is clinically significant for tumor diagnosis and grading, radio therapy dose determination, surgery and patient follow-up. Therefore, tumor volume segmentation is required [103].

K.P. Kirana[28] established a methodology to reconstruct 3D biological organs from image sequences and use the organs (3D solids) for finite element analysis. This methodology deals with the conversion of a segmented organ to polygonal surface meshes, and finally conversion of these meshes to 3D solids to figure out its volume. The research discussed the impact of volumetric information on brain tumor surgical intervention. Anatomical dimensions, measurements and geometry of body organs vary from person to person due to several factors such as weight, body size, age and presence of any cysts or masses as cancer which could cause mass-effect [104]. CT and MRI provide clinicians with specific details including measurements; however, 3D modelling will not only provides surgeons with better visualization of the organ only but also with accurate surgery planning and surgery simulations because of its accurate object geometry.

B. Preim et al. [105], described the design and implementation of measurement tools to measure distances, angles and volumes in 3d visualizations. They mentioned that accurate geometry of ROI (tumor) is necessary for many tasks in diagnosis and surgical

planning, as in the preoperative planning of oncologic surgery. Currently, in radiology, 2D measurements tool is used to define the distances, areas, and diameters of radiological data. However, the rough estimation for spatial measurements such as the extent of a 3D object is not achieved by 2D measurements and the volume of an object is only be estimated roughly.

S. Bauer et al. [38] they aimed to provide a comprehensive overview on brain tumor segmentation and highlighted on a volumetric aspect of a segmented brain tumor. They found that volumetric measurement of segmented tumor assess its temporal behavioural growth which is an essential step in monitoring tumor growth or shrinkage in patients during therapy, for tumor volume measurements and it also crucial in surgical planning or radiotherapy planning. Automatic 3D volumetric assessment of gliomas would offer the next important step forward for better understand tumor dynamics and responding to treatment.

G. Iliadis et al. [11], they elaborated on The Importance of Tumor Volume in the Prognosis of Patients with Glioblastoma. They suggested that tumor volume could be admitted as one of the prognostic factors. In order to eliminate subjectivity, computerized image processing has been developed. Despite controversy about the correlation between brain tumor volume and survival of patients, however, one study [106] showed the correlation between them.

Chapter 4

4. Design and implementation of the software

4.1. Different empirical methodologies for brain tumor segmentation

Different methods have been developed to perform tumor segmentation. These methods are classified into; Conventional methods, classification and clustering methods, and deformable model methods. In this thesis, conventional brain tumor segmentation methods were used such as region growing, threshold methods, whereas the other two methods are beyond the scope of this work. Classification and clustering methods based on machine learning that provides an effective and fully automated segmentation[107], [108]. Since MRI data segmentation is challenging, the deformable model methods would solve this problem because of including parametric and geometric deformable models and its ability to accommodate the variability of biological structures over time and across different individuals[95], [109].

For more clarification, the segmentation algorithm had a broader concept than detection algorithms. Detection algorithms only try to decide if the tumor is present and output the approximate tumor location instead of providing a complete segmentation. Saha et al. [110] described the detection segmentation that it is only located the tumor and drew a bounding box, instead of extracting it. However, extraction of the region of interest from the rest of imaging data is called segmentation [12],[38].

MRI images acquisition either multimodal as it combines several acquisitions under different contrast; or unimodal where only use one type of acquisition as T1 or T2[97]. In

this work, FLAIR was selected to be the acquisition model. A publicly available dataset of DICOM images for brain tumors was obtained from online source called Cancer Image Archive (TCIA) [111], [112]. The Cancer Imaging Archive (TCIA): Maintaining and Operating a Public Information Repository [113]. Two cases were downloaded as examples (Case 1 and Case 2).

In this paper, three empirical methods were conducted to find out the most efficient way in brain tumor segmentation (Method A, B and C). The computer script that was used to segment brain tumor from the MRI image and the reconstruction in 3D was written in Python Language because most image processing and manipulation techniques can be carried out effectively with Python and with the Skimage Library. Python is preferable more because of its speed in image processing. The Skimage provides a lot of functions that can help in brain tumor segmentation from the DICOM image also the skimage have a DICOM reader which will allow reading DICOM images which are later converted to numpy array.

The first step in this program is to read the image that tried to be segmented with python. Therefore, each slice of MR image is read to python then picks the required image to the segment after that covert the selected image to numpy array. After the image has been read successfully, the next step to do is to smooth/de-noise the image. Later on, according to each method, different algorithms were applied. These steps are going to be elaborated in image processing section of each segmentation method.

4.1.1. Method A

In method A segmentation method was based on [114], it was performed to isolate the tumor and the surrounding oedema from the remaining brain tissue. The main using algorithms for tumor segmentation were region growing and connecting component algorithms. Image processing passed through different phases; pre-processing, processing and post-processing. The flowchart is displayed in Fig.4.1

4.1.1.1. Image processing

i. Pre-processing:

(a) Image acquisition:

1. Loading DICOM file: A SimpleITK uses Grassroots DICOM library (GDCM) to load DICOM files that leads pesky JPEG compressed DICOM files.
2. Reading the entirety of the DICOM file series
3. Labelling tumor and surrounding oedema:

High intensity surrounding oedema = 1 Low intensity surrounding tumor = 2

4. Image displayed in size of 220 x 255

(b) Smoothing/ denoising:

Image-smoothing is a required step for the majority of segmentation algorithms. CurvatureFlowImageFilter that implements a curvature driven image denoising algorithm was used. The math behind this filter is based on a finite-differences algorithm.

ii. Processing:

(c) Applying segmentation algorithms:

From this step image segmentation of tumor and oedema are going to be processed separately, then they are going to be recombined at the end of processing.

The aim of this method is to extract the tumor and the surrounding edema from the rest of brain tissue by applying region growing algorithm in assistance of ConnectedThresholdImageFilter. This filter labels pixels that are connected to a seed and fall within a range of pixel values. This filter operates on the input image starting from a series of given 'seed points.' After that, it starts 'growing' a region around those points and keeps adding the neighbouring points of those which their values fall within given thresholds. The main criteria for seed point selection is based on determining a seed point that most of neighbouring pixels falls in the same value of this specific seed point, in turn it will get into the largest area of segmented tumor. In this condition, this seed point which involves the large number of pixels considered as the best seed point for segmentation.

For oedema: Lower threshold = 150

Upper threshold = 270

For tumor: Lower threshold = 50

Upper threshold = 100

iii. Post-processing:

(d) Rescaling image:

Denoising and image smoothening comprises pixels with float values while the results of segmentation should be on integer type. Mixing both of them will not work properly.

Therefore, rescaling the image is required by applying the `RescaleIntensityImageFilter` and its default values ranges between 0 and 255.

(e) Colour depiction:

Then overlay the image through the `SimpleITK.LabelOverlayImageFilter` which creates a nice basic-color RGB depiction of the otherwise monochrome second image.

(f) Hole-Filling:

Hole-filling is a very standard procedure in image segmentation, especially when employing region-growing algorithms. Often, enough regions of the tissue exhibit pixel values outside the defined thresholds either due to excessive noise in the image or the nature of the tissue itself in the given region. SimpleITK provides as the `VotingBinaryHoleFillingImageFilter` which in a nutshell that fills in holes and cavities by applying a voting operation on each pixel. This filter checks every ‘off’ pixel, i.e., a pixel with a `backgroundValue`, and sets it to a `foregroundValue` if the majority of the pixels around it also have a `foregroundValue`.

(G) Combination of the two label fields:

Since the `SimpleITK.Image` class overloads and supports all binary and arithmetic operators. The two label-fields should be combined, i.e., the tumor and oedema.

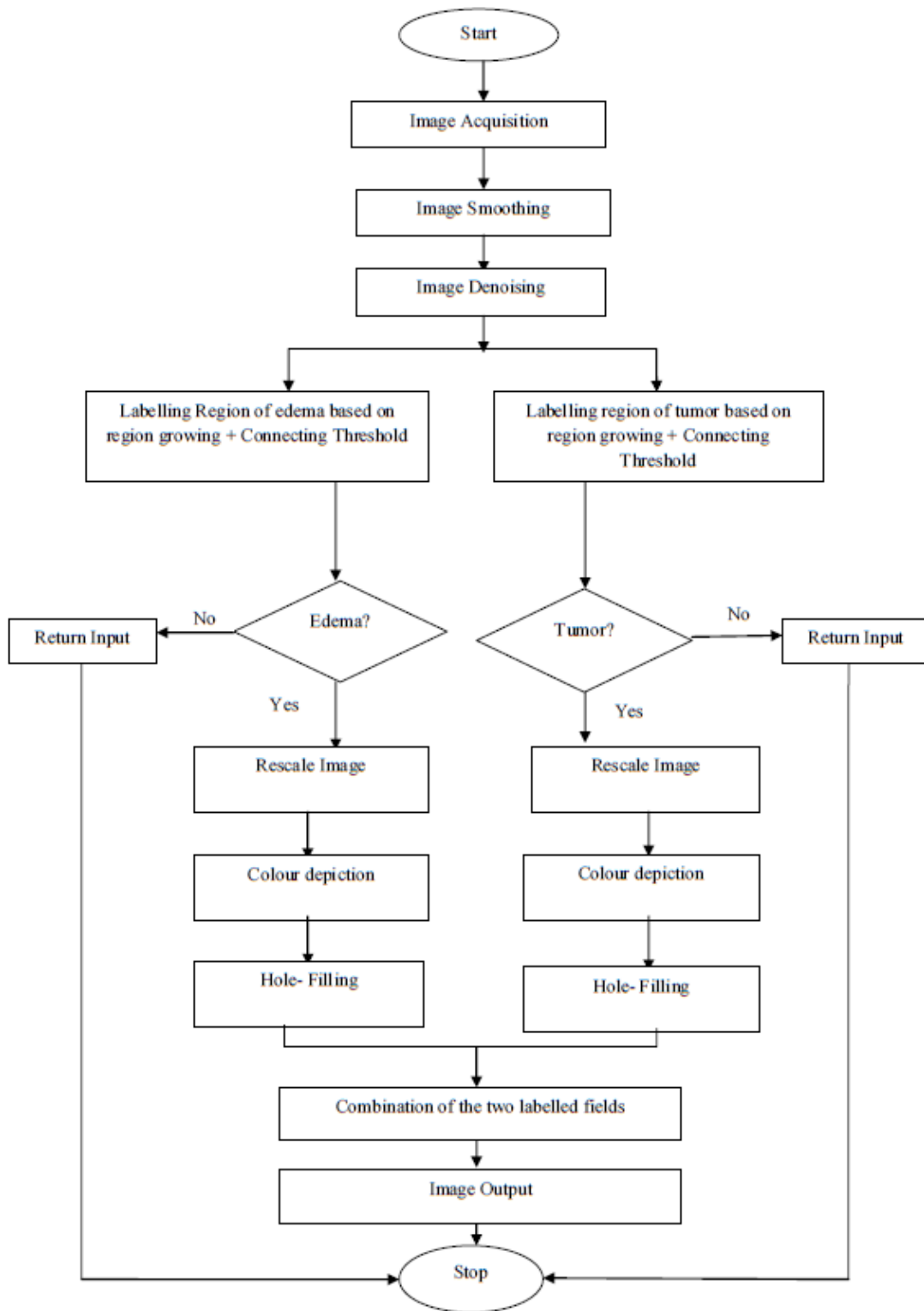


Figure 4-1 Flowchart of method A image processing

4.1.1.2. Advantages and disadvantages

Advantages:

1. Provides segmentation and differentiation for both the tumor and the surrounding oedema as shown in Fig.4.2.
2. Colourful segmentation.

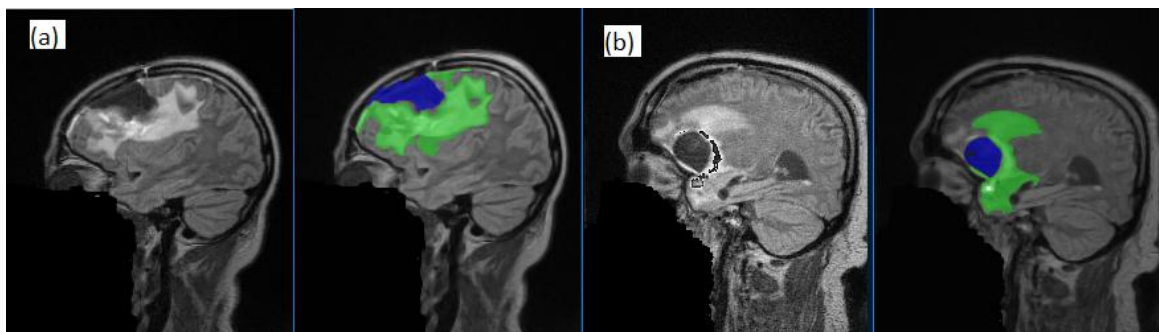


Figure 4-2 (a) case1 and (b) case2; demonstrate colourful segmentation of tumor and its edema

Disadvantages:

1. Segmentation process is not applicable for all 2D images slices and it is associated with segmentation errors as false positive (FPR) and false negative results (FNR) especially with case 2, Fig.4.3.demonstrates these flaws.
2. Lateral ventricle is isolated as well with the segmented tumor in certain slices as displayed in Fig.4.3.

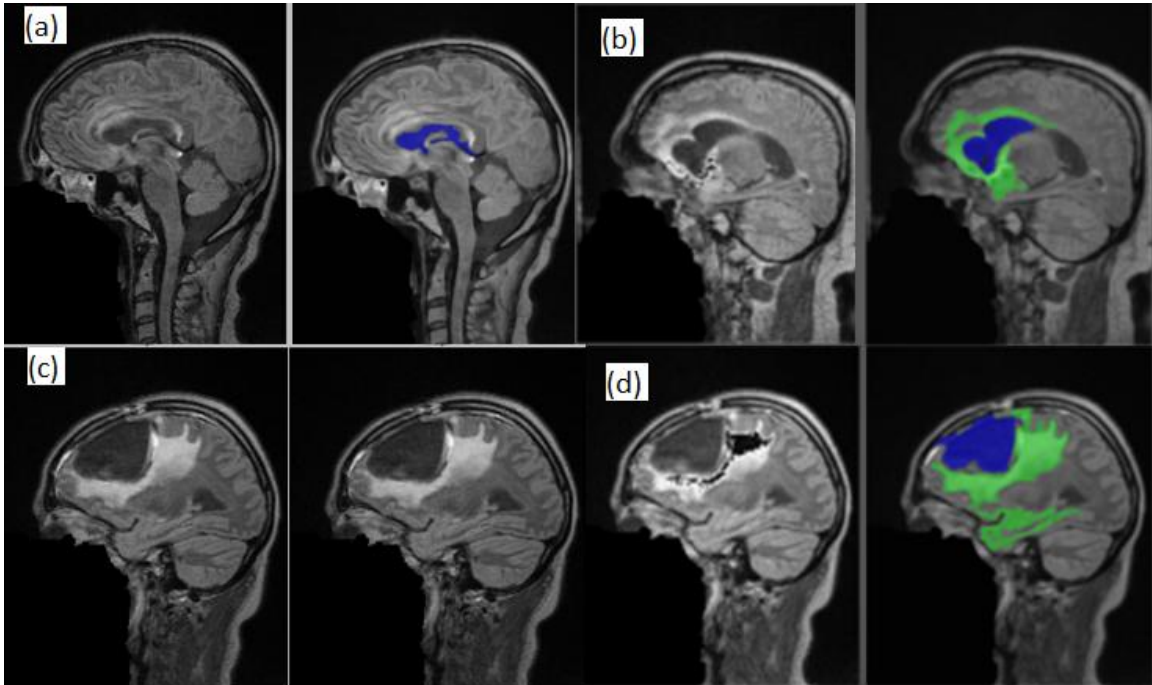


Figure 4-3 Upper row: case 2 (a) segmentation of lateral ventricle (FPR), (b) Portion of lateral ventricle is segmented due to similar pixel values with tumor. Lower row: case 1 (c) tumor without segmentation (FNR), (d) segmentation of white matter as a part of edema

4.1.1.3. Feature extraction

Since features extraction for method A and method B are similar and for sake of brevity the author is going to be elaborated this point in section 4.1.2.3.

4.1.2. Method B

In method B, it based on method A[114] with some modifications to improve the outcomes of segmented images. In this method, only the tumor has been segmented, and new scripts were built on top the previous work and added a new algorithm that based on two studies the first one was done by S. Z. Oo and A.S. Khaing[115] and the second one was conducted by M.M. Hossam et al. [6]. The main using algorithms for this method are

the watershed, region growing, and connecting component algorithms. Image processing passed through different phases; pre-processing, processing and post-processing. The flowchart is illustrated in Fig.4.4.

4.1.2.1. Image processing

i. Pre-processing:

(a) Image acquisition and (b) Smoothing/ denoising: are similar steps as in method A.

(c) Applying Otsu method:

Otsu method is used to automatically perform clustering-based image thresholding or, the reduction of a gray level image to a binary image. This algorithm considers that the image contains two groups of pixels foreground pixels and background pixels[116].

ii. Processing:

(d) Watershed algorithm:

Watershed segmentation is a gradient-based segmentation technique; it segments the image as a dam and the segmented regions are called catchment basins. Some of its advantages that it is suitable for the images that have higher intensity value also it solves a variety of image segmentation problem. It is helpful in contour extraction and detection where it divides the brain into different areas including the tumor [110], [117].

(e) Region growing algorithm with connecting component labelling process:

The aim of this method is to extract the tumor from the rest of brain tissue by applying region growing algorithm in assistance of ConnectedThresholdImageFilter. This filter labels pixels that are connected to the seed point that falls within a range of pixel values. This filter operates on the input image starting from a series of given 'seed points.' After that, it starts 'growing' a region around those points and keeps adding the neighbouring points of those which their values fall within given threshold value of the tumor:

Lower threshold= 50

Upper threshold= 100

iii. Post-processing:

(f) Rescaling image and Hole-Filling are similar as in method A.

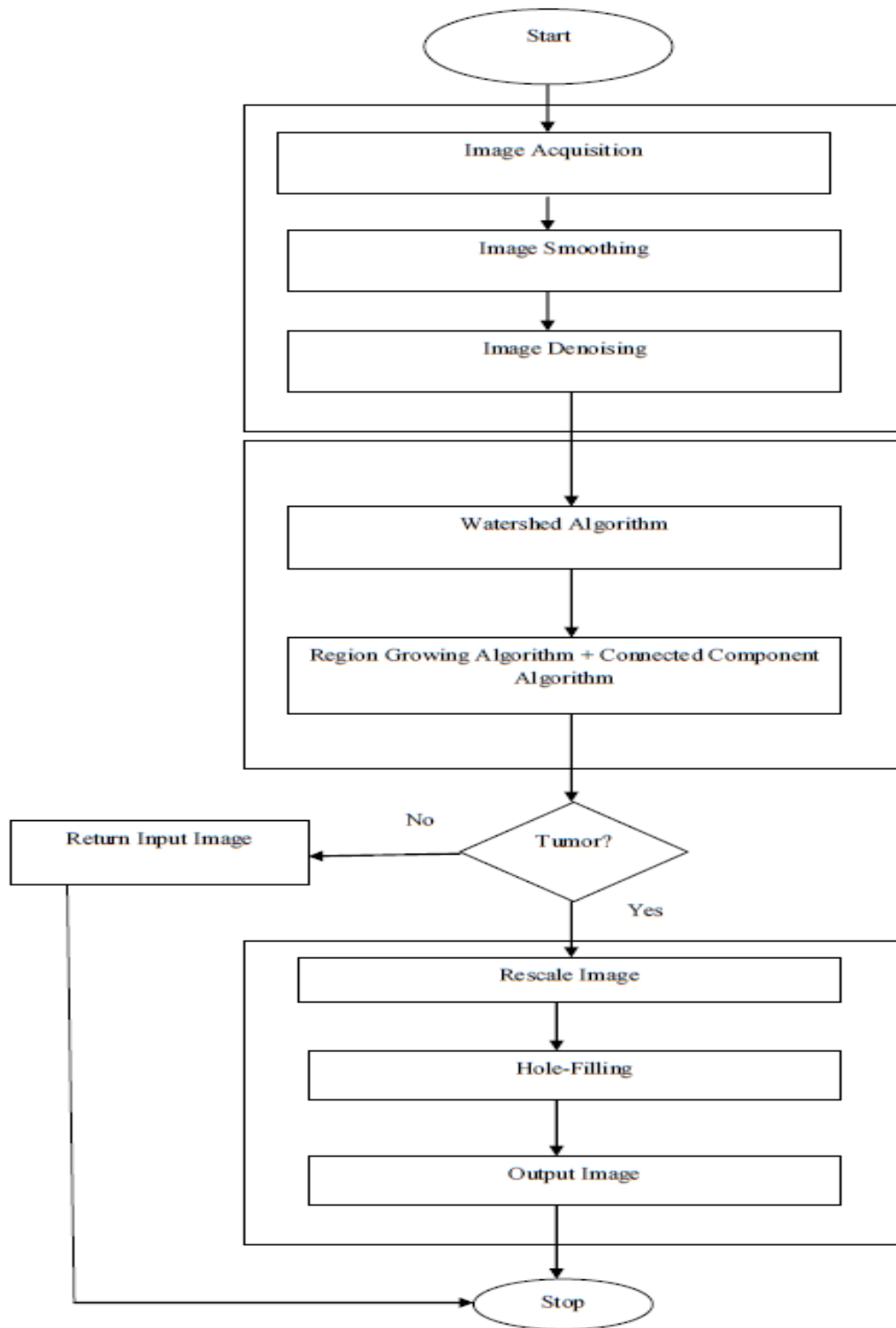


Figure 4-4 Flowchart of method B image processing

4.1.2.2. Advantages and disadvantages

Advantages:

1. Providing colourful segmentation of different areas of brain including the tumor.
2. Method B is more efficient in tumor segmentation than method A (as it is going to be explained in chapter five), Fig.4.5 displays the efficiency of this method.

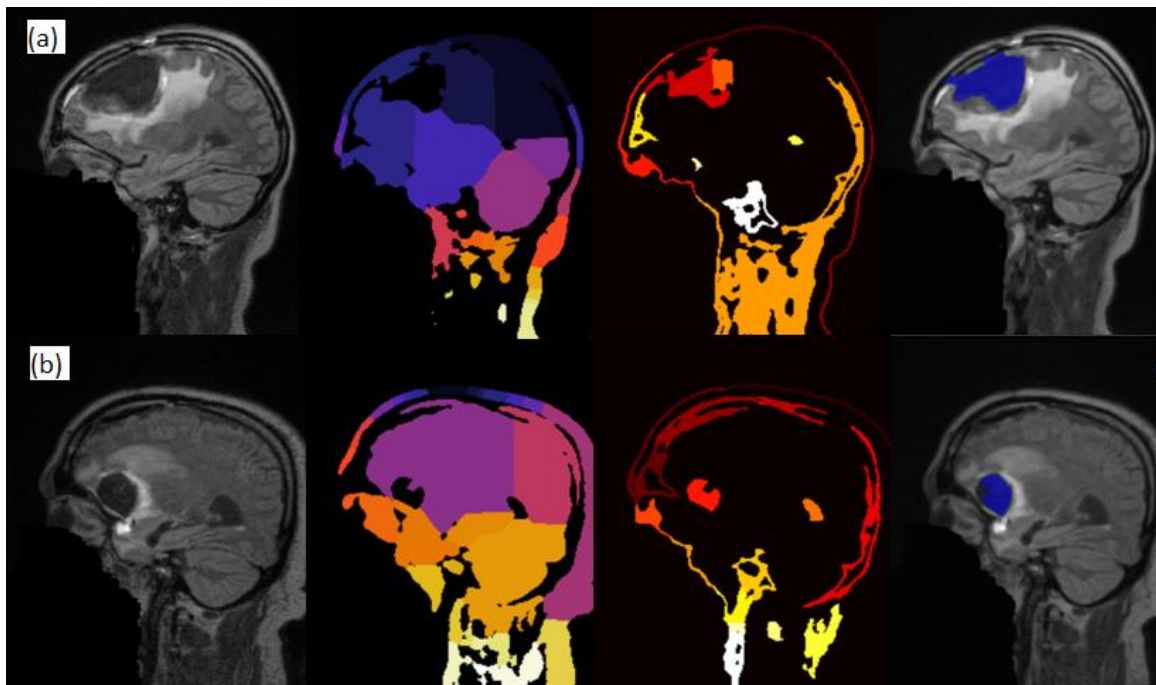


Figure 4-5 (a) case1, (b) case2, from left to right: original image, watershed segmentation into different areas including the tumor, extracting the tumor, and output image of segmented tumor

Disadvantages:

1. Segmentation process is not applicable for all 2D images slices, where there are some missing slices are not including in the segmentation method.

2. Lateral ventricle is isolated as well with the segmented tumor in certain slices

Fig.4.6.shows this defect.

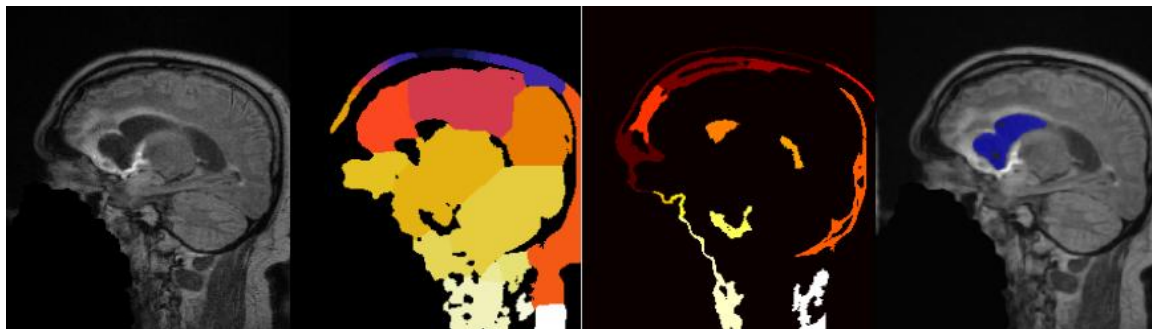


Figure 4-6 Case2: brain tumor segmentation with portion of lateral ventricle

4.1.2.3. Feature extraction

Main reasons of low segmentation accuracy of method A and B were referred to the feature extraction: In image segmentation analysis, feature extraction is what making segmentation possible. The feature of extraction in method A and B are: area, eccentricity and mean intensity. The effectiveness of the tumor segmentation is based on the three features (Area, Eccentricity and mean Intensity) and these features should be used carefully. Since DICOM image are produced either through MR scan or CT scan, the setting of these imaging are not the same hence a specific value should not be sat and will lead to errors. However, assigning maximum or minimum value for area or maximum and minimum value for eccentricity is more efficient in tumor determination.

Area of tumor: Area of a tumor is calculated by the summation of all the pixels within the tumor, and each pixel's intensity is not the same with all type of image so setting a particular area value for a condition to determine if it's a tumor or not, is a

mistake. For example, the tumor in case 2 is too small where its area is below 50 cm^2 . However, in this script set a condition that any area less than 2500 cm^2 should not be considered as a tumor. While in the method C code the setting parameters for the area were if any area less than 6 cm^2 should not be considered as tumor. 2500 is too large a lot of small tumors will not be segmented.

Eccentricity is also used to determine the roundness of tumor, its known that tumor does not have a specific shape and the shape is irregular only a regular shape as an eccentricity as 1, for irregular object like tumor should be lesser or greater than 1 depending on the shape and size [118]. Again the mistake was that only this was used as the criteria to judge if its tumor or not (it is supposed to be part of the criteria). Finally, the mean intensity [9] which is a function of pixel intensity is the most common feature used for brain tumor segmentation is the image intensities. This is based on the assumption that different tissues have different gray levels. The intensity is a function of the settings in the scanner it should not suppose to be a single.

The main point improper segmentation is that once one feature fails to make segmentation it automatically declares there is no tumor. However, the segmentations should be based on the three features altogether, and at the end of the segmentations a small script should be written to confirm if it's a tumor or not by combining the three features and certain percentage should be considered.

Other reasons could be due to missing applying certain operators, for example, morphological operator to separate lateral ventricle from tumor. As long as the lateral

ventricle is attached to the tumor this script will identify it as tumor because the script didn't have any line of code that separates them because the tumor and the lateral ventricle have similar pixel values.

4.1.3. Method C (M-3Ds)

Also, it based on method A[114] and alterations relied on [9], [64] studies. Finally, came up with a new approach. The main algorithms for tumor segmentation were 1) binary threshold and 2) region growing. Image processing, as demonstrated in Fig.4.7 and Fig.4.8 passed through different phases: pre-processing, processing, and post-processing.

4.1.3.1. Image processing

i. Pre-processing

(a)Image acquisition

In this approach, the MRI scan images of a given patient are gray-scale or intensity images which are displayed with a size of 255×220 pixel. A gray-scale converted image is defined by using a large matrix whose entries are numerical values between 0 and 255, where 0 corresponds to black and 255 to white for instance.

(b)Image smoothing/enhancing

There are different types of noise found by several techniques, depending on noise nature and characteristics namely Gaussian noise and impulse noise [119], [120]. These are very typical of MRI datasets. However, region-growing and thresholding segmentation algorithms lead to some irregularities and defects. Therefore, smoothing and

homogeneous pixel distributions were achieved by applying filters to perform the required smoothing and edge-preserving. The filter uses a level set formation where the image has a low-intensity contours (brain tumor) in an image are viewed as level sets, and pixels of a particular intensity form one level set. The level set function is then evolved under the control of a diffusion equation [121]. Level set function (level set method (LSM)) are a conceptual framework for using level sets as a tool for numerical analysis of surfaces and shapes. The advantage of the level set model is that one can perform numerical computations involving curves and surfaces on a fixed Cartesian grid without having to parameterize these objects [122].

ii. Processing

(c) Binary threshold and region growing algorithms

After the image has been pre-processed and noise has been removed, threshold algorithm in assistance of region growing algorithm will be applied to the image. Threshold methods are a simple replacement of each pixel in an image with a black pixel if the pixel intensity is less than a fixed constant T , and white if the pixel intensity is greater or equal to that constant. Binary Threshold produces an output image whose pixels are either one of two values (Outside Value or Inside Value), depending on whether the corresponding input image pixels that equal to T value or lie between the two thresholds (Lower Threshold and Upper Threshold).

More precisely

$$\text{Output}(x_i) = \begin{cases} \text{InsideValue} & \text{if } \text{LowerThreshold} \leq x_i \leq \text{UpperThreshold} \\ \text{OutsideValue} & \text{otherwise} \end{cases}$$

(d) Morphological operation

The goal of this morphological operator is to isolate the lateral ventricle from the tumor part of the image. After the image has been thresholded, the output image is called the *binary image*. They are both derived from the fundamental operations of erosion and dilation (they are mathematical models). The morphological operator is normally applied to binary images. The basic effect of an opening is somewhat like erosion in that it tends to remove some of the un-required foreground (bright) pixels from the edges of regions of foreground pixels.

iii. Post- processing

(e) Image filtering

The goal of edge detection is to identify a region of interest (ROI) while preserving the structural features to be used for additional image processing. After the brain tumor has been detected, the output image can appear to be incomplete (having unnecessary holes) as a result of image processing. To retrieve the lost information, a method called Sobel operator, or Sobel filter, is applied [123]. The Sobel, or Sobel–Feldman, operator is used in image processing and is especially useful for image edge detection. The Sobel operator is based on convolving the image into a small, separable, and integer-valued array filters

in both the vertical and horizontal directions and is therefore relatively inexpensive regarding computation.

(f) Hole filling

After the edge of the brain tumor has been defined. The detected area is filled with flood fill. Flood fill, or seed fill, is an algorithm that determines the area connected to a given node in a multi-dimensional array. It is also called boundary fill when it is applied to a specific bounded area with color [124].

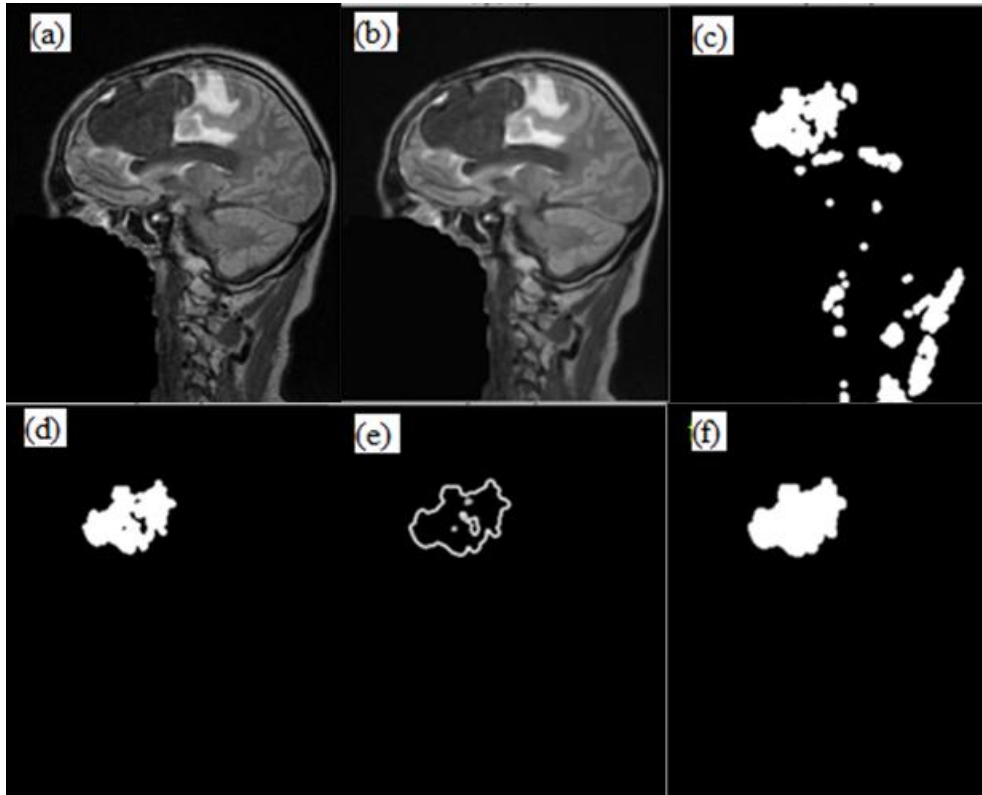


Figure 4-7 Pre-processing: (a) image acquisition,(b) image enhancing; processing (c) binary thresholding, (d) morphological operation;post-processing (e) image filtering,(f) hole filling.

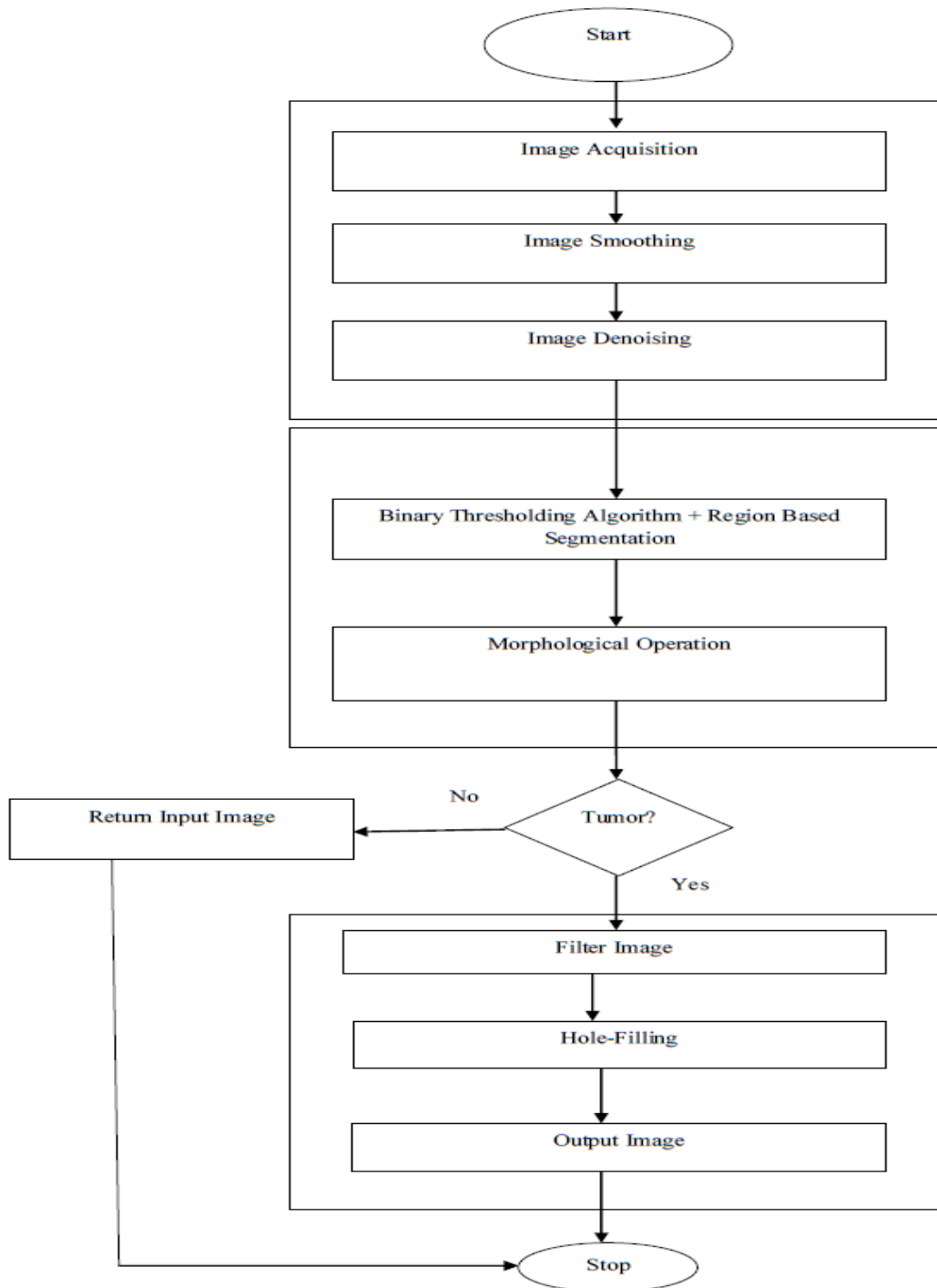


Figure 4-8 Flowchart of method C image processing

4.1.3.2. Advantages and disadvantages

Advantages

1. Method C demonstrates high accuracy level of segmentation for both cases in comparison to method A and B as it is going to be explained in chapter five.
2. It shows good results regarding separation of the tumor from lateral ventricle comparing to method A and B.
3. It develops with Graphical User Interface software to make it easy for users without the knowledge of computer programming and for easy communication and visualization.
4. It provides different mode of segmentation (manual, automated and hybrid).

Disadvantage

1. Automated mode of segmentation has low accuracy comparing with manual and hybrid which shows high accuracy as will be shown in chapter five.
2. Small portion of lateral ventricle could exist with certain segmented images as in Fig.4.9.
3. Some irregularities in the boundaries of the tumor Fig.4.9.
4. It is highly relied on seed points' determination and with each different seed point selection, the output segmented result would show little bit different selection of the tumor, Fig.4.10 demonstrates this point.

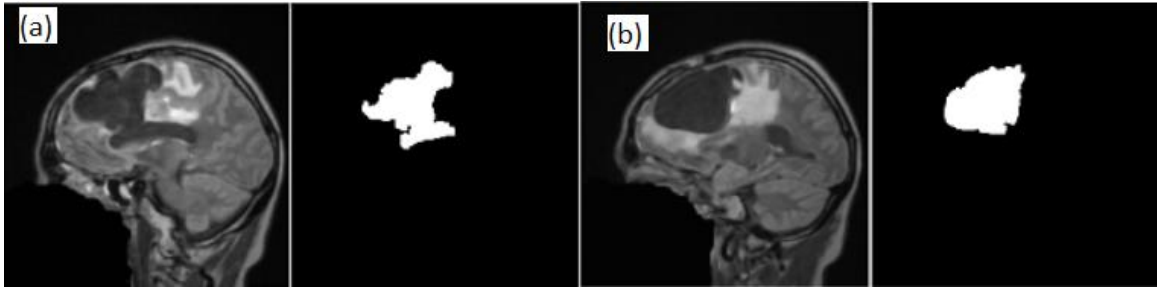


Figure 4-9 (a) small portion of lateral ventricle was segmented with the tumor, (b) segmented tumor without lateral ventricle. Both (a) and (b) have irregular boundaries

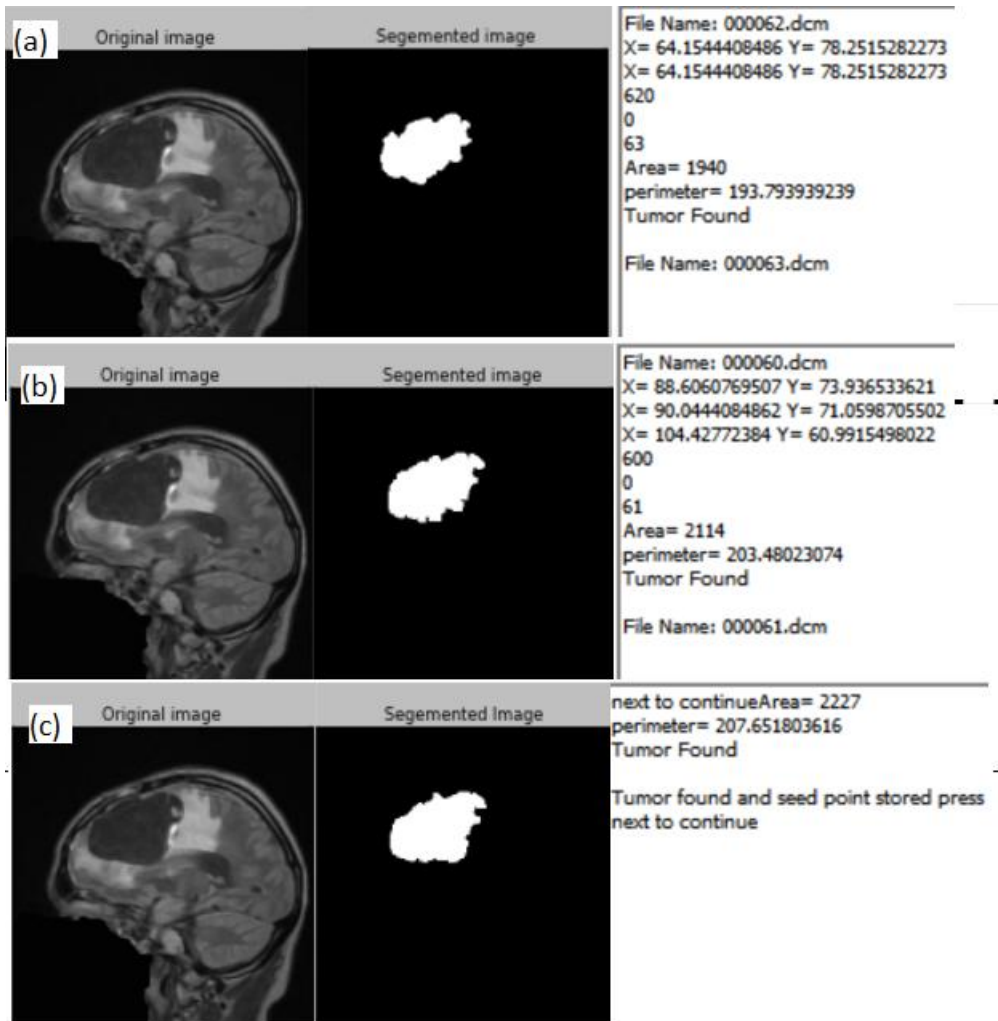


Figure 4-10 Shape changing of the segmented tumor depends on the selected seed points;(a) SP (64,78), area 19.40 square cm , peimeter = 19.37cm; (b) SP (88,73), area = 21.14 square cm, perimeter = 20.34 cm; (c) SP (91,68), area + 22.27 square cm, perimeter=20.76 cm

4.1.3.3. Features extraction

Feature extraction in image processing is a special form of dimensionality reduction. Feature extraction is helpful in identifying brain tumor where is exactly located and helps in segmentation process. Features are the characteristics of the objects of interest, if selected carefully are representative of the maximum relevant information that the image has to offer for a complete characterization of a lesion. Feature extraction methodologies analyse objects and images to extract the most prominent features that are representative of the various classes of objects. Features are used as inputs to classifiers that assign them to the class that they represent. The purpose of feature extraction is to reduce the original data by measuring certain properties, or features, that distinguish one input pattern from another pattern[125].

The following features are used:

1. The shape: The term shape is commonly used to be referred to the geometric properties of an object.
 - a. Area: The area of the object is calculated using the actual total number of pixels which are present inside the object, which describes the area of that region.
 - b. Solidity: the concavity of the particle can be measured by Solidity. the particle becomes more solid if the image area and convex hull area approach each other
 - c. Circularity: Circularity represents the degree of similarity in the particles to the circular shape. It takes into consideration the degree of smoothness

surroundings. This means that the circularity is a measure of particle shape and roughness.

2. Contrast: it calculates strength of the contrast between a pixel and neighbour pixel for the entire image. Contrast is zero for contrast image.
3. Intensity: Intensity is a purity or strength of colour.

4.2. 3D reconstruction of three methods

The marching cube algorithm has been applied to the segmented brain tumor. After the brain tumour has been detected and confirmed the extracted brain tumor will be passing to marching cube function as “data” where the vertices and the faces will be generated to form the 3D. After the 3D has been formed it will be stored as a Stl (Stereo Lithography) file which contains the vertices and faces information.

4.3. Visualization via modern graphical user interface (GUI) of method C

Graphics user interface (GUI) overview: the graphics user interface (GUI) allows user to interact easily with the brain-tumor software, that it will speed up the user time also it will make it easy and comfortable for user. The GUI is written in python and it has a window size of 900 by 900 pixels as shown in Fig.4.11. The GUI was created with the python module named “WxPython”. Wxpython is a GUI toolkit for python programming that allow us to create a highly functional graphics user interface, easily and simply. Wxpython is Open Source and the reason for choosing it over other GUI modules, such as “tkinter,” is because wxpython provided powerful capability with extensive flexibility.

The wxwidgets that are used in the brain tumor segmentation and 3D reconstruction software includes:

1. Panels: This is used as containers, and in this software it is also used as container to hold other wxwidget such as our matplotlib figure that shows our images.
2. Scroll Window: The scroll window is also used as a container but the properties it has over panel is that it has a scroll bar but vertical and horizontal, the scroll bar is used to scroll down if the scroll window is over sized (i.e. the wxwidget is holding is more than its size).
3. Menu bar: The menu bar create an extra menu for the software, this menu includes file, which has a submenu “select folder” and “exit” the select folder submenu is used to select the folder containing the DICOM images and the exit submenu is to exit or close the software.
4. Status bar: The status bar is below the program the status bar hold the current folder location containing the DICOM images.
5. Static Bitmap: this is used to view all the DICOM images and added to the scroll window. The number of the static bitmap depends on the number of the DICOM images.
6. Radio button: The radio button is used to switch between mode of segmentation (automatic, manual and hybrid). This mode of segmentation has different advantages, efficiency and speed.
7. Textbox: This is used as an output window to display results and information about the segmentation also the text box is used to display the seed point.

8. Choicebox: This is used to select the type of 3D model to display the choicebox contain tumor, brain and combine (the combine shows both the tumor and brain together).
9. The slider: this is used to change the threshold properties of the brain (to reduce the opacity). The slider is only activated when the combine mode is choosing.
10. Button: when users want to move to the next image or previous images a button is pressed
11. Render Window: this is used as our 3D viewer, it displays our 3D tumour and brain, the 3D tumor and brain are both in STL format (Stereo Lithography file.)

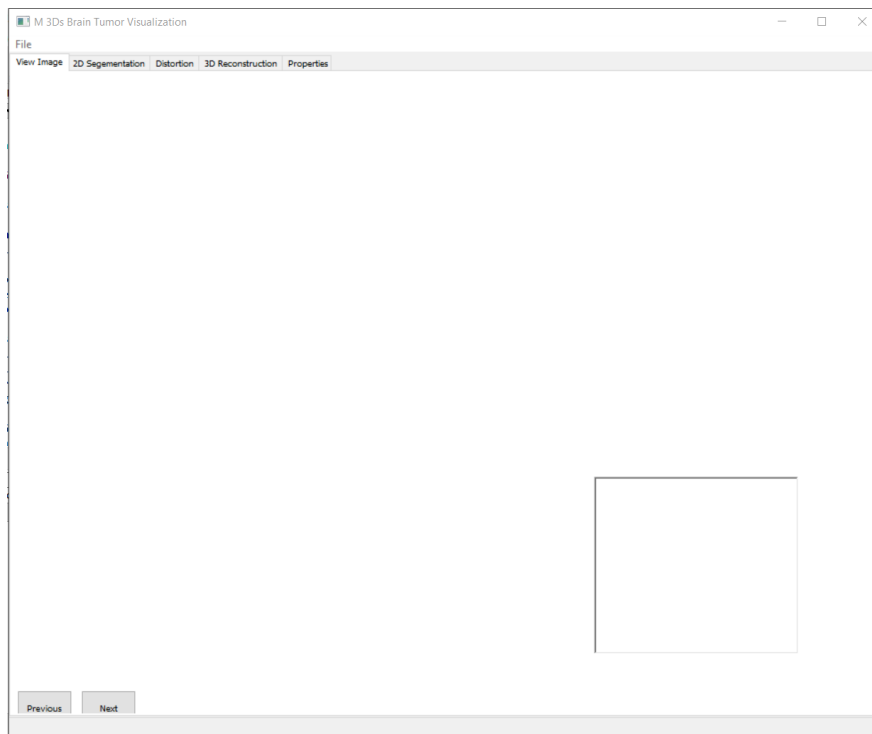


Figure 4-11 Graphical User Interface (GUI)

GUI section:

Tab 1 (View image): This section contains a scroll window that contains all the images in the DICOM folder, two matplotlib figure that contain the current selected DICOM image and the smoothed version of the image. It also contains a “next” and “previous” button to show the next and previous image. And finally the textbox which provide the information about the current or chosen DICOM image, and also it has a mouse event attached to it (the mouse event means the figure will display the current location of the cursor on the figure this location is further used as the seed point). All of these functions are demonstrated in Fig.4.12.

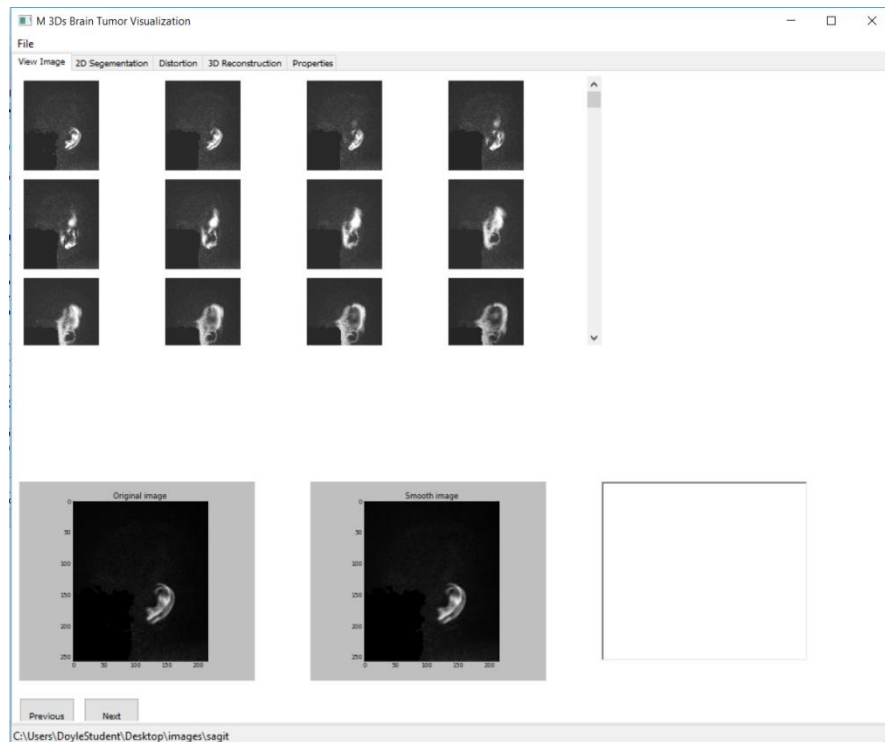


Figure 4-12 View Image Tab: downloads images and displays brain dataset

Tab 2 (2D segmentation): this section is used to segments (isolates) the brain tumor from each slice of the image as shown in Fig.4.13. The segmentation is accomplished by using three different methods with different efficiency of segmentation

and frequency of user intervention. These methods include the automatic segmentation; the manual segmentation and the hybrid segmentation (see section 4.4). In the 2D segmentation also have the scroll window that views the entire image slices of all the DICOM and it also contain two figure which display the original image and the segmented image (if no tumor found the smoothed image is been showed). Finally, it contains three textboxes two of them display the seed point and the remaining textbox display the information of the selected image and also result of the segmentation.

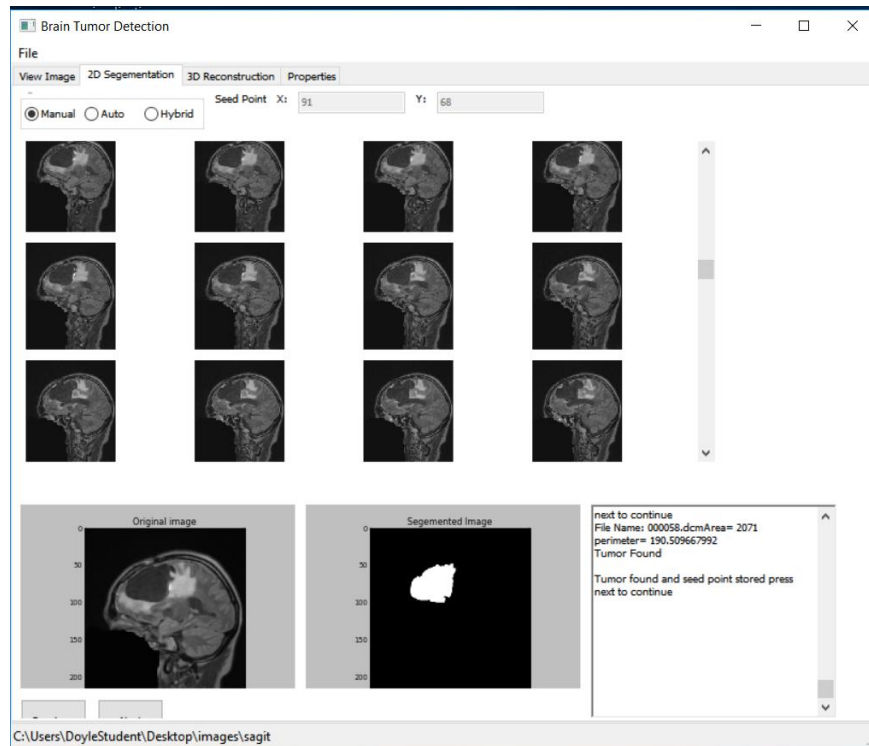


Figure 4-13 2D Segmentation Tab displays the segmented tumor

Tab3 (3D reconstruction): the last tab is known as the 3D reconstruction Tab. This Tab serves as a 3D viewer which was done with the “vtk” library, also with the 3D viewer. It has a slider that changes the opacity of the brain for us to see the tumor. This

slider is only activated if only showing the tumor and the 3D at the same time. The function behind the slider is to make the brain transparent is and done by changing the property of the skull to reduce the opacity while making the tumor constant (not changing the property of the window). In this tab 3D reconstruction is perused by selecting the mode of segmentation. Lastly, a volumetric measurement tab was added to assess the volume of the segmented tumor and the skull. All of these descriptions are illustrated in Fig.4.14.

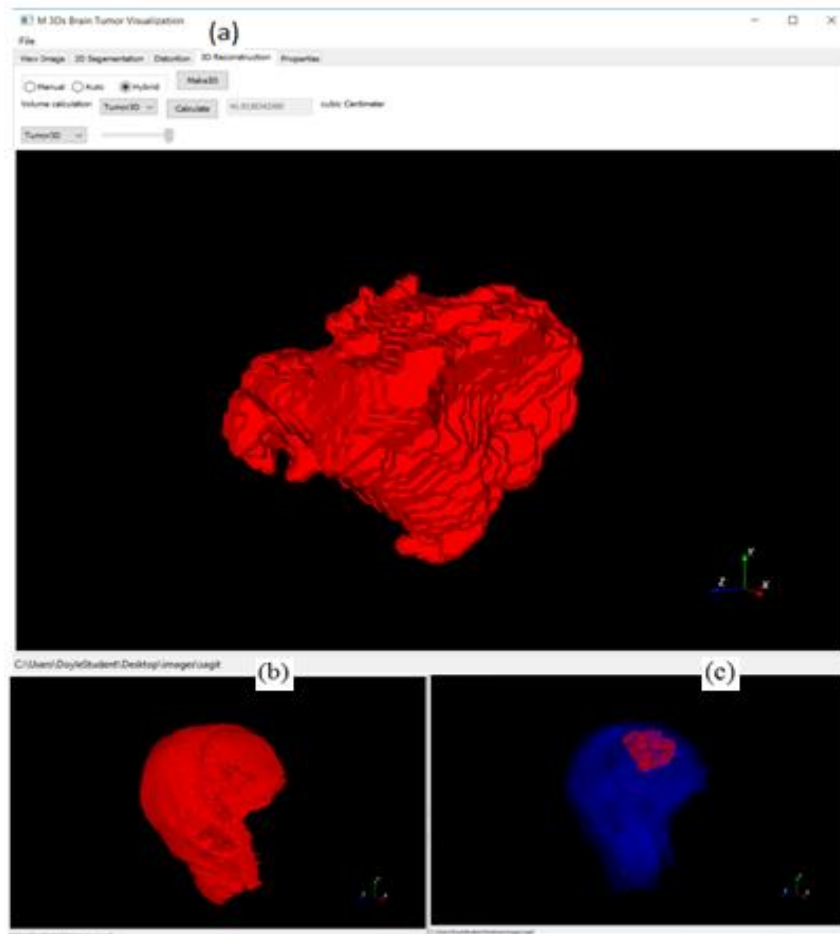


Figure 4-14 (a) 3D reconstruction of the segmented tumor with volumetric calculation, (b) 3D reconstruction of the skull, (c) See through technique

4.4. Modes of segmentation

2D segmentation tab of M-3Ds: this section is used to segment (isolate/separate) the brain tumor from each slice of the image. The segmentation is accomplished by using three different methods with different efficiency of segmentation and speed. These methods include the manual segmentation, automatic segmentation, and hybrid segmentation.

Manual segmentation: this mode is highly accurate because the user identifies the brain tumor from the background of each slice separately. Manual mode is programmed to identify the tumor by requiring the user to select the proper seed point manually for each slice. But this method has multiple user interaction because the user has to separate the tumor on each slice from the beginning to the end of the complete set of images. Each image will be segmented manually by M-3Ds to store the location of tumor in the database. The time required for segmentation depends on the number of slice of the DICOM dataset. Therefore, is this method is considered very accurate, but requires significant user interaction and long duration.

Automatic method: this method is fast because only a single seed point is needed to be selected by the user to segment the entire series of images. This method is less accurate because the intensity of the tumor pixel may cause the algorithm to fail to detect the tumor due the particular user selected seed point. Automatic mode requires the user to select a single seed point after which the program will proceed to identify the entire tumor, even if it fails causing some missing slices in the result. The seed point is determined by using the mouse to click on any tumor observed in the DICOM image

slice. The selected seed point is used to detect the tumor in all other slices. This mode has minimal user interaction with less accurate segmentation.

Hybrid (*semi-automated*) method: it was given that the manual method has high accurate and the automatic method has minimal user interaction, while this method attempts to combine these strengths. However, it was recognizing the shortcoming of both fully automated and fully manual. The hybrid mode is programmed in a way that if it fails to identify the tumor in a slice then it stops at that point (even if there is tumor, as long as the program fails to detect tumor it stops) and user intervention is required. The main reason behind failing in tumor identification is that the seed point shift and because we use 3D medical scanner as MRI that may change the seed point from slice to slice during the rotation (360 degree) of its detectors around the patient. If the tumor shifts away from the seed point that used initially the program will fail to detect the tumor because it has shifted away from the seed point. This mode has both the properties of manual and automatic method because it uses the mouse to detect tumor and also register the seed point to be used for the next slice and if the next slice fails to detect a tumor, the user is prompted to input a new seed point (manual method) and this process continues to the end of the DICOM dataset. This mode is considered best because it has high accuracy and requires less interaction.

4.5. Extension of method C: Identification and visualization of both gray and white matter

This portion is demonstrated by adding a new tab to M-3Ds called distortion, the aim of this section is to display the morphological changes of gray and white matter because of tumor and its oedema as illustrated in Fig4.15. The methodology of image processing is greatly similar to method A. More details in are displayed in Appendix 1.

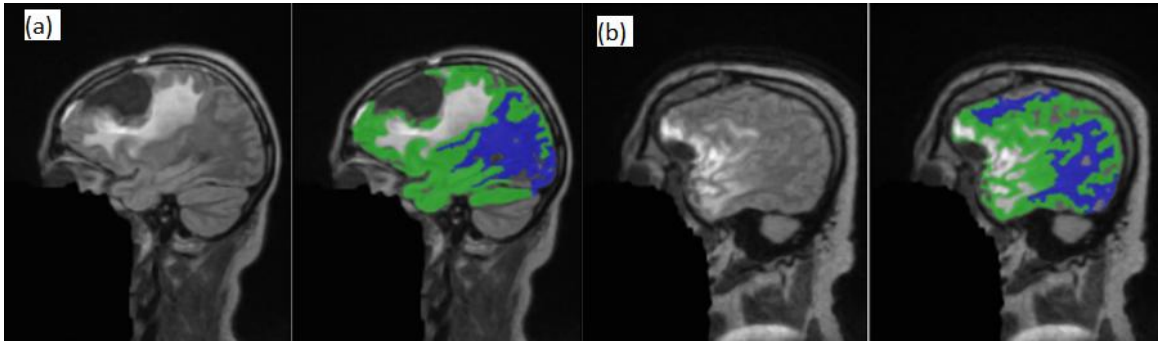


Figure 4-15 Morphological distortion of gray and white matter for (a) case 1 & (b) case 2

Chapter 5

5. Discussion and experimental results

As observed from the previous chapter each of those three methods have different ways of segmentation. Subsequently, that leads to different segmentation and 3D reconstruction results. These three methods are quantitatively evaluated.

5.1. Validation by checking the completeness and accuracy of each approach

5.1.1. Accuracy tests

For brain tumor segmentation several different gold standards may be used to validation. Our work considered the following: 1) T1WI with contrast, 2) manual/visual segmentation by an expert, and 3) comparing the symmetry of both sides of the cerebral hemi-sphere (since in our cases, the tumor did not cross the midline). In this study, T1WI with contrast was not chosen because contrast uptake and image acquisition time after contrast injection can vary, which changes tumor appearance significantly and it is debatable if and how the non-imageable component of the tumor should be handled by segmentation algorithm [38]. On the other hand, expert localization of tumor structure came with “ground truth” information [104]. Therefore, symmetrical comparisons between both sides of cerebral hemispheres with expert segmentation of tumor were used as a gold standard for assessing the accuracy of segmentation.

The following Tables III and IV guided us to find out which method and which mode is the most accurate. In method A, case 1 its true positive result(TPR) 15.7%,false

positive result(FPR) 21.4% and the accuracy 63%, while in case 2 TPR 9%,FPR 45.2 and accuracy 45.2%. However, in method B, Case-1 its TPR 26.3%, FPR 10.7% and accuracy 74.2% and in case 2 TPR 15.1%, FPR 23% and accuracy 64.1%. Hence method B has better results than method A. But method C proved to have highest accuracy compared to method A and B. For Case-1, the results of manual mode were (True Positive Result) TPR 97.3%, (False Negative Result) FPR 0% and accuracy 99.3% while in hybrid mode the TPR 92.1%, FPR 0% and accuracy 98.1% and finally, automatic mode yielded TPR 89.4%, FPR 0% and accuracy 97.4%. For Case-2; the manual mode results, TPR 90.9%, FPR 0% and accuracy 98.1% and for hybrid TPR 84.8%, FPR 0% and accuracy 96.8%. However, the automatic has these results TPR 78.7%, FPR 0% and accuracy 95.5%. Manual mode had the best results in terms of accuracy; however, its significant user interaction makes it slow to use and much less practical.

TABLE III: ACCURACY OF EDECTION RESULTS OF METHOD A AND B

Method A	Case 1			Case 2		
	Tumor	No tumor	Total	Tumor	No tumor	Total
Segmentation	6 (TP)	26(FP)	32	3(TP)	57(FP)	60
No segmentation	32 (FN)	95 (TN)	127	30 (FN)	69 (TN)	99
Total	38	121	159	33	126	159
Method B	Case 1			Case 2		
	Tumor	No tumor	Total	Tumor	No tumor	Total
Segmentation	10 (TP)	13(FP)	23	5(TP)	29(FP)	34
No segmentation	28 (FN)	108 (TN)	136	28 (FN)	97 (TN)	125
Total	38	121	159	33	126	159

TABLE IV: ACCURACY OF DETECTION RESULTS OF METHOD C (MANUAL, AUTOMATIC AND HYBRID)

Method C	Case 1			Case 2		
	Tumor	No tumor	Total	Tumor	No tumor	Total
Manual						
Segmentation	37 (TP)	0 (FP)	37	30 (TP)	0 (FP)	30
No segmentation	1 (FN)	121(TN)	122	3 (FN)	126 (TN)	129
Total	38	121	159	33	126	159
Automatic	Case 1			Case 2		
	Tumor	No tumor	Total	Tumor	No tumor	Total
Segmentation	34 (TP)	0 (FP)	34	26 (TP)	0 (FP)	26
No segmentation	4 (FN)	121(TN)	125	7 (FN)	126 (TN)	133
Total	38	121	159	33	126	159
Hybrid	Case 1			Case 2		
	Tumor	No tumor	Total	Tumor	No tumor	Total
Segmentation	35(TP)	0 (FP)	35	28 (TP)	0 (FP)	28
No segmentation	3(FN)	121 (TN)	124	5 (FN)	126 (TN)	131
Total	38	121	159	33	126	159

5.1.2. Sensitivity and specificity tests for each method with the both cases (Case-1 and Case-2)

TABLE V: VALIDATION OF ACCURACY AND COMPLETENESS OF SEGMENTATION IN ALL THREE METHODS AND THREE MODES OF SEGMENTATION

Methods	Method A		Method B		Method C					
	Case1	Case2	Case1	Case2	Case1			Case2		
Modes of segmentation					Manual	Auto	Hybrid	Manual	Auto	Hybrid
Sensitivity	15.7%	9%	26.3%	15.1%	97.3%	89.5%	92.1%	90.9%	78.7%	84.8%
Specificity	78%	54.7%	89.2%	76.9%	100%	100%	100%	100%	100%	100%
Positive predictive value	18.7%	5%	43.4%	14.7%	100%	100%	100%	100%	100%	100%
Negative predictive value	74.8%	69%	79.4%	77.6%	99.1%	96.8%	97.5	97.5%	94.7%	96.1%

In this work, sensitivity is more useful than specificity because it is so important to find out the method (algorithm) that increases the sensitivity of tumor identification/extraction and reflects the probability of tumor detection. Table V demonstrated these results.

Finally, from the previous results, it was obvious that method C particularly manual mode were the best approaches for segmentation but frequency of user intervention of manual segmentation will impact on the workflow. Therefore, the hybrid mode which has highly accurate results with less user intervention would be considered as the best.

5.2. Verification of volume calculation

Volume calculation was performed in two levels: 1) by calculating the segmented tumor, and 2) by assessing the actual volume of the tumor.

5.2.1. Volume calculation of the segmented tumor by the three methods for the three modes of segmentation (manual, automatic and hybrid) of method C

The volume was calculated by determining the volume of each DICOM image read into M-3Ds. Then this calculated volume was compared against two industry standard software applications: Autodesk Inventor and MeshLab. In order to calculate the volume of 3D object that creates from mesh by Inventor, this object should be watertight. As a result, another software should be used first to convert this object into watertight [126] and this software was a MeshLab software as shown in Fig.5.1. Also, both of these programs were used in volume calculation of that object (tumor). In conclusion, three programs

were used to verifying the volume measurement and all of them demonstrated similar or closer results as displayed in Fig.5.2.and Table VI.

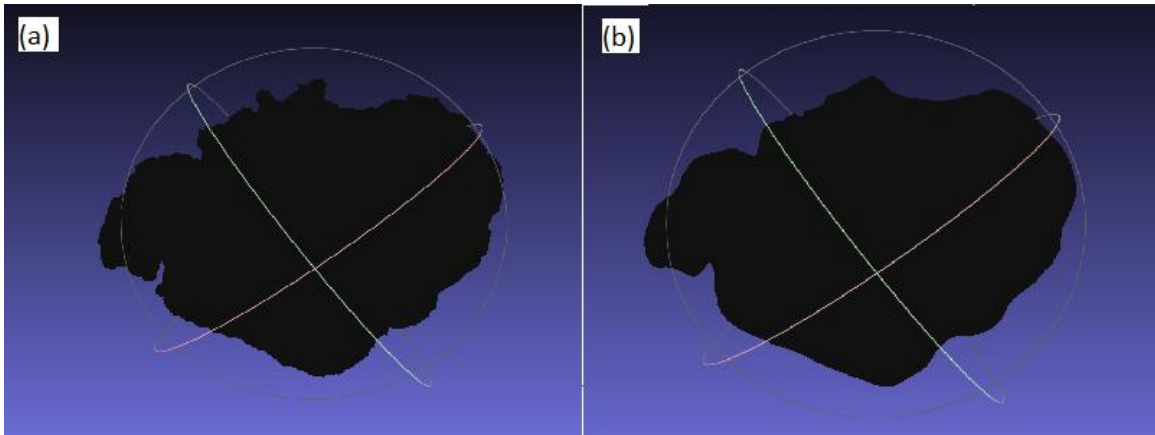


Figure 5-1 MeshLab converts non-watertight object into watertight.(a) non-watertight object, (b) watertight object.

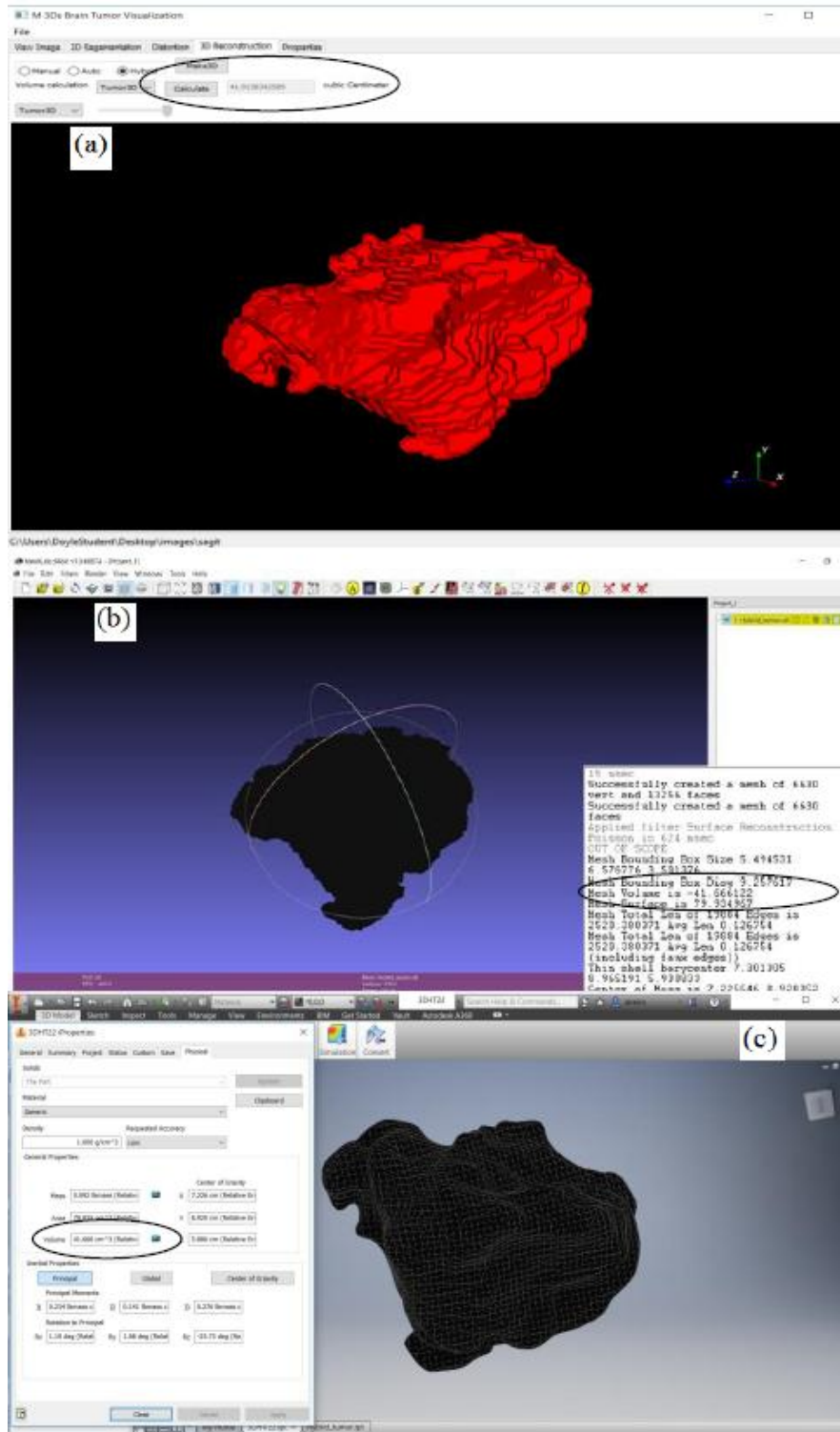


Figure 5-2 Similarity of volume measuring results of different approaches.(a) M-3Ds, (b) MeshLab and (c) Autodesk Inventor.

5.2.1.1. Python (Mathematics)

M-3Ds software provides volume measurement by integrating mathematical equation into python as shown in Fig.31. In order to create 3D reconstructed object Marching Cube algorithm was used. As described in the second chapter marching cubes is a computer graphics algorithm, for separating a polygonal mesh from an isosurface based on a three-dimensional discrete scalar field. A polygon mesh can be defined as an object which consists of a collection of vertices, edges and faces. The faces consist of triangle and in some cases a polygon mesh can contain only series of vertices in this situation it is called a point-cloud. Polygon formed of three or more points (vertices) and a number of polygons may create a surface. In turn, a number of surfaces will form an object. The volume of this object can be defined by the set of vertices in the triangulated mesh assuming all the vertices are oriented (all the set of vertices are connected by edges, where the edges have a direction associated with them) the following expression holds:

$$V(v) = \frac{1}{3} \sum_{i=1}^N v_{i,1} * n_i * A_i \dots \dots \dots 1$$

Where v is the vertices, n is the normal, A is the area and N is the total number of vertices

The above equation is the divergence formula for polyhedral. Expanding equation 1 which is the divergence formula for a polyhedral by using the fact that the cross product of the two triangle sides (a parallelogram) is a normal vector of the triangle with magnitude twice the area of the triangle [127].

$$V(v) = \frac{1}{3} \sum_{i=1}^N v_{i,1} * \frac{(v_{i,2} - v_{i,i}) * (v_{i,3} - v_{i,1})}{2} \dots \dots \dots 2$$

Expanding Equation 2 gives:

$$V(v) = \frac{1}{6} \sum_{i=1}^N v_{i,1} * (v_{1,2} * v_{i,3} - v_{i,2} * v_{i,1} - v_{i,1} v_{i,3}) \dots \dots \dots 3$$

Equation3 can be used to calculate the volume of a triangulated mesh. Equation 3 can be program using Python. A “for loop” function will be used to calculate the volume from i= 1 to N which is the total number of vertices in the 3D model. If a negative value is gotten (this happen the mesh is not watertight/solid) the absolute value of the result is taken.

5.2.1.2. Autodesk Inventor

Autodesk Inventor is a computer-aided design (CAD) application for creating 3D digital prototypes used in the design, visualization, and simulation [128].Autodesk Inventor has the tool to determine the geometric properties of a mesh which include density, surface area, weight, and volume. For this property to determine the mesh must have characteristics of been watertight or been a solid, if the mesh is not watertight, we can use the tool called “stitch” to create a surface around it and make it watertight. The volumetric properties can be check under file-> iProperties. All steps of volume measuring by Autodesk Inventor were displayed in Appendix 2.1.

In details, STL files can be imported into Inventor using the Open command. However, the imported 3D model cannot be edited in inventor. Also, it cannot be converted into

workable objects. The reasons are that when we import STL file into Inventor the edge and vertices are not active and inventor uses the edges and vertices to edit a model if this STL object cannot be edited in Inventor it is impossible to measure the volume of the STL file. In order to activate the vertices and edge a utility tool will have to be installed called “Mesh Enabler for Autodesk Inventor.” This utility tool allows the conversion of imported meshes into the base feature (that is the edge, and the vertices are activated) this conversion may take time depending on the complexity and size of the mesh. After the mesh has been converted to Inventor workable file the next step is to make the object watertight (that converts it to solid by filling every hole in the object) this can be done by using the “stitch” command. When the object is watertight we can check the volume by going to iProperties, Autodesk Inventor files have properties called iProperties which include the physical properties of the object like volume, surface area weight and so on, the volume of the object can be calculated [129].

5.2.1.3. MeshLab

MeshLab [130] is an open source mesh processing tool. Regardless of the technology used to acquire the geometry, the generation of a 3D model is a multi-step process and it is quite standard. For this reason, a tool which covers the various stages of the post-processing as mesh cleaning, data filtering, range scans alignment, surface merging and etc. is perfectly able to deal with data coming from dense stereo tools. The MeshLab Poisson reconstruction filter [131] removes part of the sampling noise and reconstructs an overall triangulated mesh from the sampled points by also closing all the small missing gaps and holes filling [132].

MeshLab provides several solutions to reconstruct the shape of an object, ranging from volumetric (Marching Cube) to implicit surfaces (Screened Poisson). MeshLab can be used to prepare 3D models for printing by creating inner shells, resampling/remeshing the 3D model to make slicing easier, closing small holes to obtain watertight meshes. A good way to do this is to Apply Poisson Reconstruction. Go to **Filters->Remeshing, Simplification and Reconstruction->Surface Reconstruction: Poisson**[126]. This uses the point and normals using the Poisson surface reconstruction approach and a watertight mesh is generated [130], [132] MeshLab includes a linear measurement tool. A tool allowing displaying the volume of a model or the surface of a selected area (with the brush) could be very useful for medical applications. To calculate the volume of segmented tumor by this tool, go to **Filter->Quality Measure and Computation->Compute Geometric Measure**. All of these steps were illustrated in Appendix 2.2.

TABLE VI: VERIFICATION BY VOLUME MEASUREMENTS OF 3D RECONSTRUCTED TUMOR OF THE THREE METHODS AND THREE MODES OF METHOD C (THE UNIT IS CUBIC CENTIMETER)

Methods	Method A		Method B		Method C					
	Case1	Case2	Case1	Case2	Case1			Case2		
Modes of segmentation					Manual	Auto	Hybrid	Manual	Auto	Hybrid
Python (Mathematics)	-	-	-	-	44.80	41.59	44.80	14.84	13.21	14.09
MeshLab (watertight)	9.76	2.76	16.27	4.6	44.95	41.27	43.67	14.45	13.56	14.10
Autodesk Inventor (watertight)	9.76	2.76	16.27	4.6	44.95	41.27	43.67	14.45	13.56	14.10

5.2.2. Volume calculation of the actual tumor

Another approach was also achieved to get the volume of the actual tumor by using 3D Slicer. In this approach, the researcher outlined the boundaries of the tumor manually for both cases 1 and 2. After that, isolation of the tumor was performed by Editing and GrowthCutEffect as shown in Fig.5.3. Next, STL file was created then imported into Inventor Autodesk to check the volume as displayed in Fig.5.4. Finally, it was found the results were close to M-3Ds software, which demonstrates the high level of accuracy of this new software. Table VII illustrates these results and Fig.5.4.

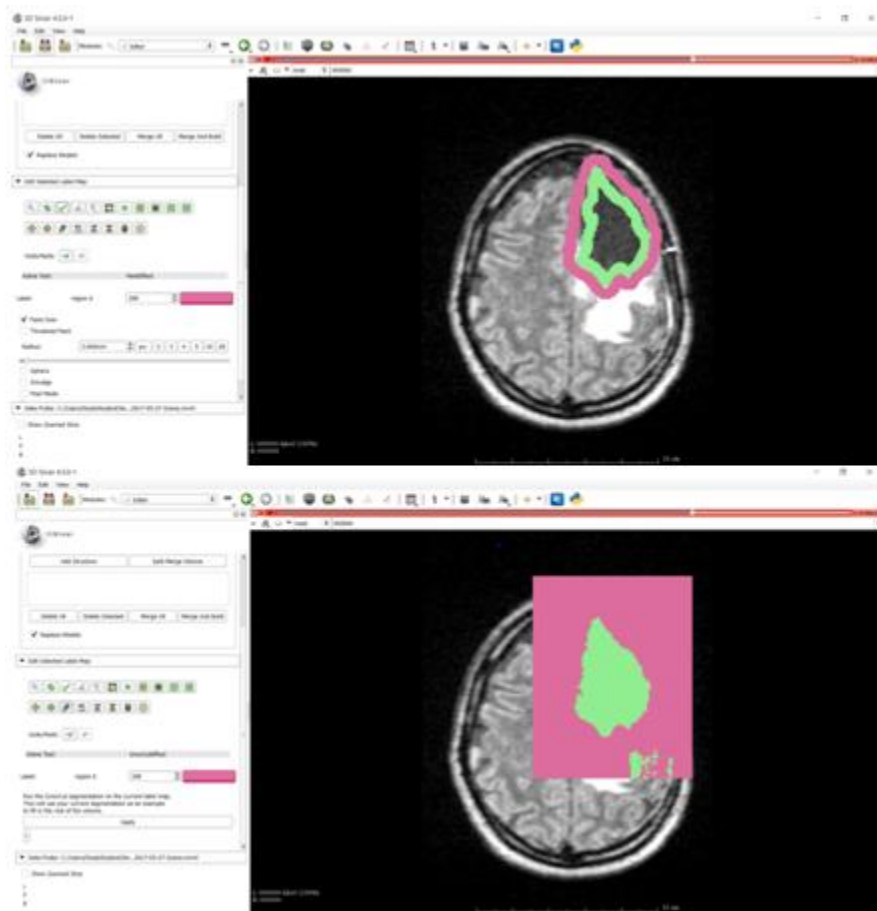


Figure 5-3 Outline and isolate the tumor by 3D Slicer through using Editing and GrowthCutEffect.

TABLE VIVII: VOLUME CALCULATION OF SEGMENTED TUMOR BY M-3Ds AND ACTUAL TUMOR BY 3D SLICER

Software	M 3Ds (Segmented tumor)	3D Slicer (Actual tumor)
Case 1	44.95 cm ³	52.74 cm ³
Case 2	14.45 cm ³	14.05 cm ³

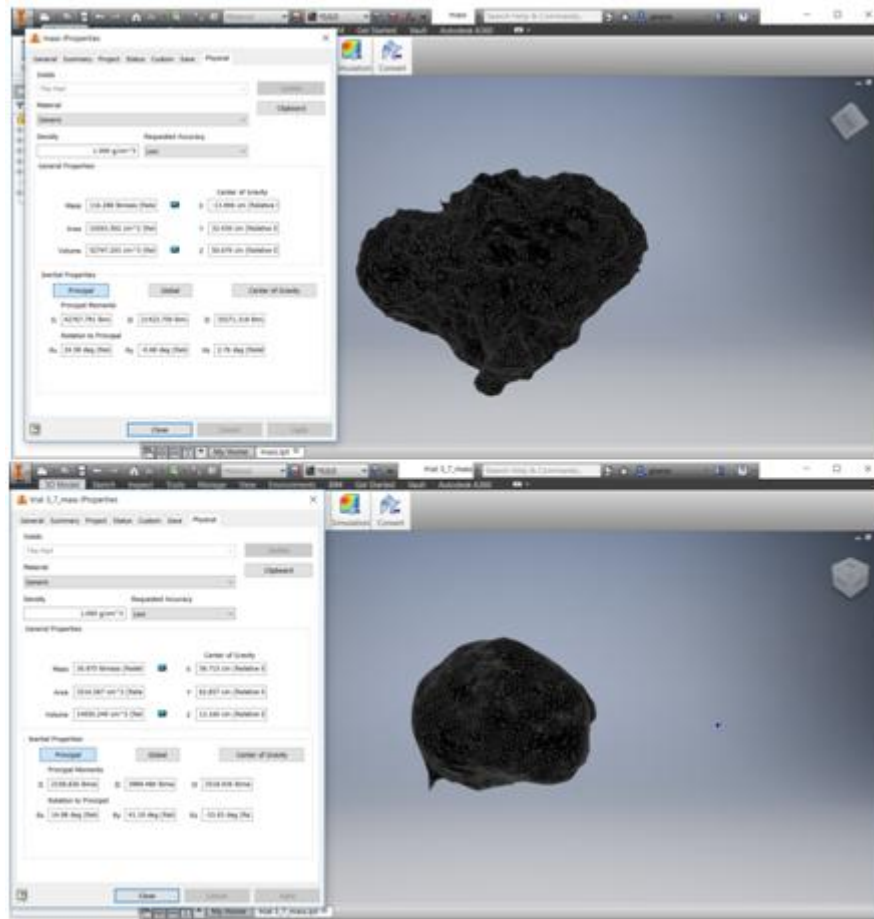


Figure 5-4 Volume calculation of the actual tumor for both cases by Inventor Autodesk

Chapter 6

6. Conclusion and future work

6.1. Limitations

This system is proposed to work on sagittal MRI of particular types of brain tumors that have the following features: hypointensity, localized, non enhanced and homogenous tumors as gliomas and meningiomas. This prototype is able to identify the brain tumor only but it is not able to classify brain tumors. FLAIR sequence was chosen to cross-check the extension of the edema and discriminate it against ventricles and other fluid-filled structures. The initial “edema” segmentation in T2 and FLAIR contained the core structures that were then relabelled in subsequent steps [104]. On the other hand, limited source of DICOM images for localized brain tumor and most of them are associated with surgical intervention that changes the shape of the tumor and the surrounding tissue.

6.2. Challenges

Challenges could be divided into two categories: challenges related to the researcher’s background and challenges during developing M3Ds software.

6.2.1. Challenges related to the researcher’s background

The key challenges in this work are related to in the background of the researcher and the approaches taken to overcome these challenges are:

1. Writing the software: the researcher had a radiological background and lacked expertise in programming. As a result, learning programming was started through online courses to get the required skills to create this piece of software.
2. Developing a model that converts 2D images into 3D reconstruction: to overcome this challenge reviewing the existing literature on current methods to create 2D segmentation and 3D reconstruction was conducted. This included reviewing different algorithms and libraries. Finally, different kinds of algorithms were experimented about which one was more applicable to this kind of software.
3. Developing full application for 3D visualization: By learning how to write a graphical user interface where it is not just a single push button, it is a whole system that would be helpful for the radiographers, students and clinicians.
4. Exploring different methodologies for 2D segmentation and 3D reconstruction: by exploring different kinds of existing open-sources software such as: 3D slicer and imageJ, and using them to understand the modes of segmentation and ways of 3D reconstruction.

6.2.2. Challenges during developing M3Ds software

Other challenges could be classified into the followings:

6.2.2.1. 2D Segmentation challenges

- Extracting the tumor

While extracting the brain tumor from the DICOM image there was challenges in the efficiency of the extraction process. The efficiency was low because of the pixel information. The pixel of soft tissue also fell within the range of the pixel of the brain tumor so when the brain tumor was extracted the soft tissue was also would be extracted. Therefore, determination of seed point was the solution to this challenge.

- Disjoining the tumor from lateral ventricle.

If the tumor is in contact with the lateral ventricle, it will also be extracted with the brain tumor thereby not given the brain tumor the right geometry, this is because the pixel of the lateral ventricle is also in the range of the brain tumor. The solution this was to use the shape of the tumor to determine if it's only tumor or is connected to lateral ventricle because the shape of the brain tumor looks like a disk shape.

- Reading the DICOM file.

In this work skimage library was used to achieve the segmentation of the brain tumor and this library only accept the processing of numpy array, the challenge was to convert the MR DICOM images to numpy array. The solution was to load the entire DICOM images from beginning to the end and convert them to a numpy array in a single matrix of M by N where M is the number of DICOM image in the directory and N is the numpy array of the converted DICOM image.

- Loading and storing the seed point of automatic mode

The hybrid and automatic modes was not achieved easily there was a problem how to know the best seed point for each image. Because the best seed point for DICOM image X may be different from DICOM image Y (x, y can represent any DICOM image with tumor). To achieve a possible solution for this problem a database storing the information of the seed point of each DICOM image was introduced (the database is in a text file which is stored in the seed folder of the directory) the database is created automatically on running the program. The storing of the seed point information is the key to effectiveness of the hybrid mode also a further research may be done on machine learning using this information.

6.2.1.2. 3D reconstruction challenges

- Thresholding

When displaying both the brain and the tumor at the same time because the two object are solid the biggest object, which is the brain will over shadow the smallest objects which is the brain tumor. The challenge was to reduce the threshold of the brain so as to see the brain tumor. This was done in a way that the brain threshold was changed on each production of the brain3D and it takes 20 minutes on each production. The solution was infeasible because its time consuming another solution was developed by introducing alpha channel of the brain (opacity), since the brain and brain tumor are different objects, so the

opacity of the brain could be controlled to allow us to see the position and location of the brain tumor without consuming time.

- Displaying both the tumor and the brain

Displaying both the brain and brain tumor on the same 3D window at the same time was also a big challenge but this challenge was prevailed by tricking the 3D window that is loading the same object twice without resetting the 3D window.

- Auto and hybrid 3D

When making 3D object from the manual mode is very simple but in auto and hybrid mode is complex because the seed point is not inputted. So successful loading of the stored seed point in the database was an effective method.

- Adherence in between the tumor and 3D tumor showing with lateral ventricle.

This was the biggest problem related to 3D visualization because the effectiveness of the 3D reconstruction is determined by how the 3D object looks like. The challenge was that there was adherence between the solid object of the tumor and gives incorrect geometrical shape of the tumor because the lateral ventricle for lesser extent was included. This was solved by effective 2D segmentation (as mentioned in chapter four).

6.3. Future directions

One of the main contributions of 3D cancer visualization software is the reduction of the cognitive demands needed by health care professionals, and the improvement of depth perception in medical augmented and virtual reality that is required in diagnosis and surgical planning. In augmented reality systems, the viewer perceives a real world simultaneously superimposed with virtual objects [133]. However, virtual reality environments provides a high level of immersion where the viewer is a part of a modeled scene and full immersion can be achieved as a CAVE system (a room with multiwall projections that used in flight simulators) [133]. Therefore, leveraging the 3D model repository would provide the resources to generate the holographic in-situ 3D visualization of brain tumor for education and treatment. Applying our model to a device like the Microsoft HoloLens [134] or the MAD Gaze X5 offers an immersive real time experience by overlaying three-dimensional holographic models in-situ within the user's field-of-view, conceptually similar to surgeon's view during the operation. From this point, M-3Ds was designed to directly provide the 3D model for the mixed reality by using Hololens as shown in Fig.6.1.

This type of support visualization leads to enhanced spatial orientation and navigation, and is meant to replace the cognitive process required of physicians [6]. All of these factors play a part in the clinician's decision of whether the patient should undergo interventional procedures (invasive) or treatment planning (non-invasive) procedures. For example, 2D planning of radiotherapy for 3D tumor leads to a large volume of irradiation

for the normal surrounding tissues. However, 3D visualization provides accurate tumor localization and maximum sparing of normal tissue, which mitigates the disadvantage of radiotherapy especially if applied with augmented reality. Further academic works were performed in different fields of 3D virtual reality as virtual surgery, virtual radiology, and virtual endoscopy. In conclusion, developing of an accurate framework for in-situ visualization and immersion application (VIA) that address 3D visualization and isolation of the tumor at the same time suitable for augmented and virtual reality should be established. According the previous results, it was found that hybrid mode offers the best solutions for tumor segmentation in term of accuracy and significant user intervention that enhances the decision making of health care professionals.

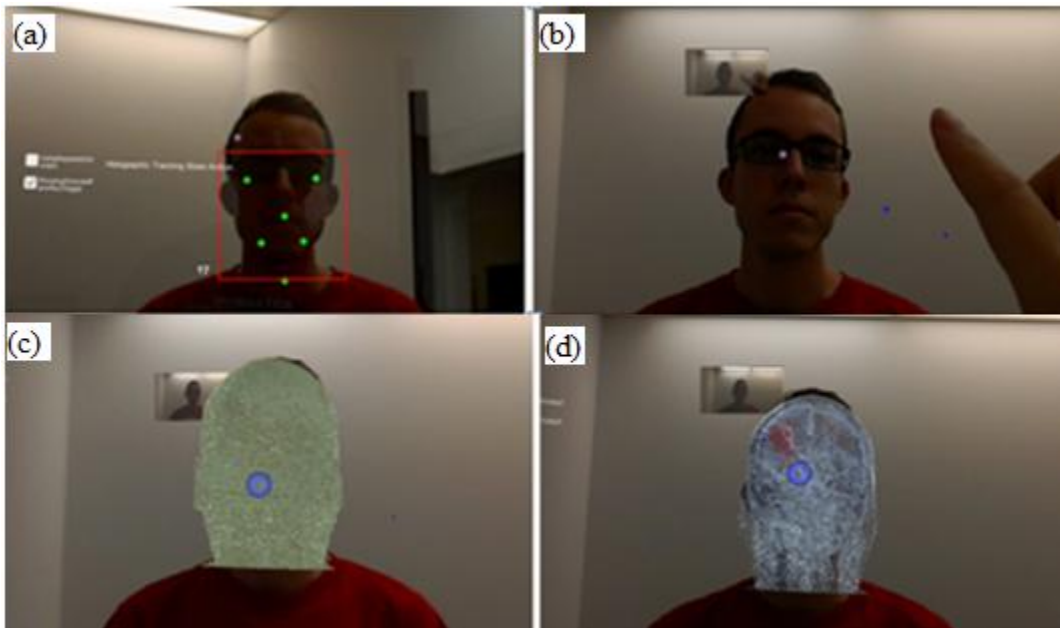


Figure 6.1: Initial work with Augmented Reality, (a) six points serve as anatomical landmarks, (b) clicking by two fingers to apply the hologram (c) 3D model is projected on the patient's head, (d) See-through technique by changing the skull transparency to localize the tumor.

It is a helpful tool and has a potential to be considered as a part of Clinical Decision Support System (CDSS) especially if machine-learning techniques are applied in future. Furthermore, this proposed software work as a mobile technology where it could be consider as a portable workstation if provided with additional functionalities that could increase the clinicians' performance. Also, as a telediagnostic imaging support system particularly if the 3D object is down sized.

Appendices

Appendix 1: Distortion

In this Tab segmentation method was based on [114], it was performed to separate the white matter from gray matter and displayed the mass effect of tumor and the surrounding edema on these structures. The main using algorithms for tumor segmentation were *region growing and connecting component algorithms*. Image processing passed through different phases; pre-processing, processing and post-processing.

Image processing

i. Pre-processing:

(a) Image acquisition:

5. Loading DICOM file: A SimpleITK use Grassroots DICOM library (GDCM) to load DICOM files that leads pesky JPEG compressed DICOM files.
6. Reading the entirety of the DICOM file series
7. Labelling white and gray matters:

High intensity of white matter = 1 Low intensity gray matter = 2

8. Image displayed in size of 220 x 255

(b) Smoothing/ denoising:

Image-smoothing is a required step for the majority of segmentation algorithms.

Smoothing the image with `CurvatureFlowImageFilter` that implements a curvature driven image denoising algorithm. The math behind this filter is based on a finite-differences algorithm and is quite convoluted.

ii. Processing:

(c) Applying segmentation algorithms:

From this step image segmentation of white and gray matters are going to be processed separately, then they are going to be recombined at the end of processing as demonstrated in the flowchart

The aim of this method is separate the white matter from gray matter by applying region growing algorithm in assistance of `ConnectedThresholdImageFilter`. This filter labels pixels that are connected to a seed and fall within a range of pixel values. This filter operates on the input image starting from a series of given 'seed points.' After that, it starts 'growing' a region around those points and keeps adding the neighbouring points of those which their values fall within given thresholds.

For gray matter: Lower threshold = 150

Upper threshold= 270

For white matter: Lower threshold = 130

Upper threshold = 190

iii. Post-processing:

(d) Rescaling image:

Denoising and image smoothing comprises pixels with float values while the results of segmentation should be on integer type. Mixing both of them will not work properly.

Therefore, rescaling the image is required by applying the `RescaleIntensityImageFilter` and its default values ranges between 0 and 255.

(e) Colour depiction:

Then overlay the image through the `SimpleITK.LabelOverlayImageFilter` which creates a nice basic-color RGB depiction of the otherwise monochrome 2nd image.

(f) Hole-Filling:

Hole-filling is a very standard procedure in image segmentation, especially when employing region-growing algorithms. Often, enough regions of the tissue exhibit pixel values outside the defined thresholds either due to excessive noise in the image or the nature of the tissue itself in the given region. SimpleITK provides as the `VotingBinaryHoleFillingImageFilter` which in a nutshell that fills in holes and cavities by applying a voting operation on each pixel. This filter checks every 'off' pixel, i.e., a pixel with a `backgroundValue`, and sets it to a `foregroundValue` if the majority of the pixels around it also have a `foregroundValue`.

(G) Combination of the two label fields:

Since the `SimpleITK.Image` class overloads and supports all binary and arithmetic operators. The two label-fields should be combined, i.e., the tumor and oedema.

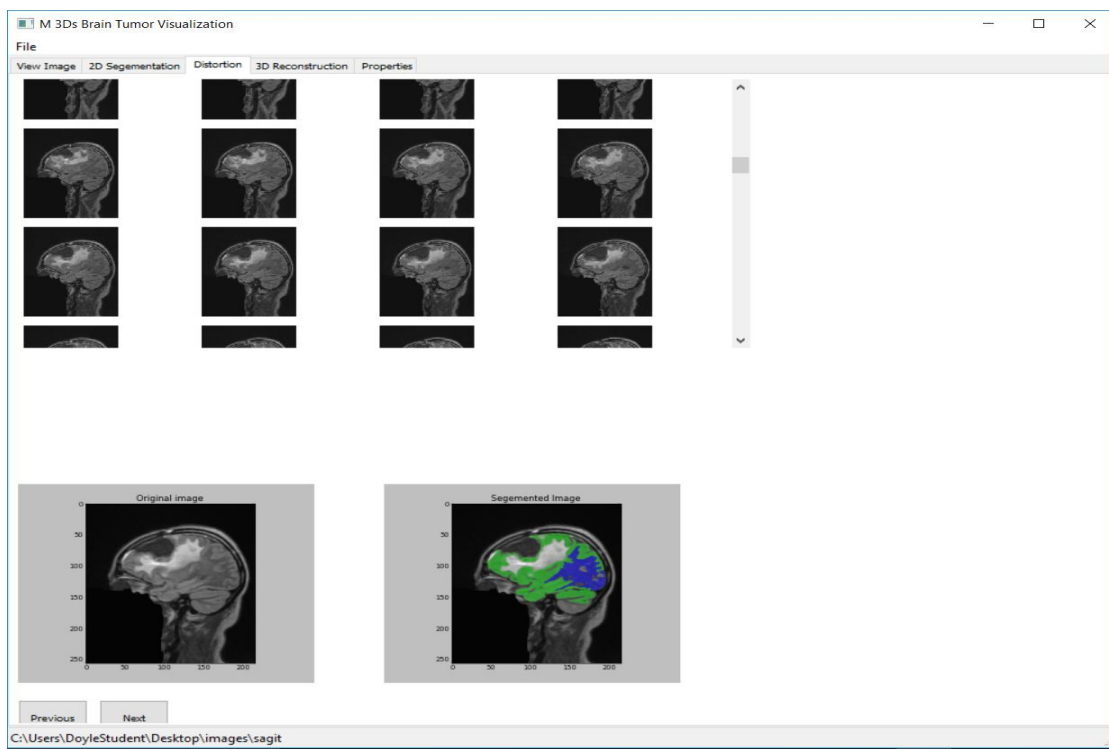


Figure 1: (Appendix 1) Distortion tab differentiates the grey and white matter (black region: tumor, white region: edema, green area: grey matter and blue area: white matter)

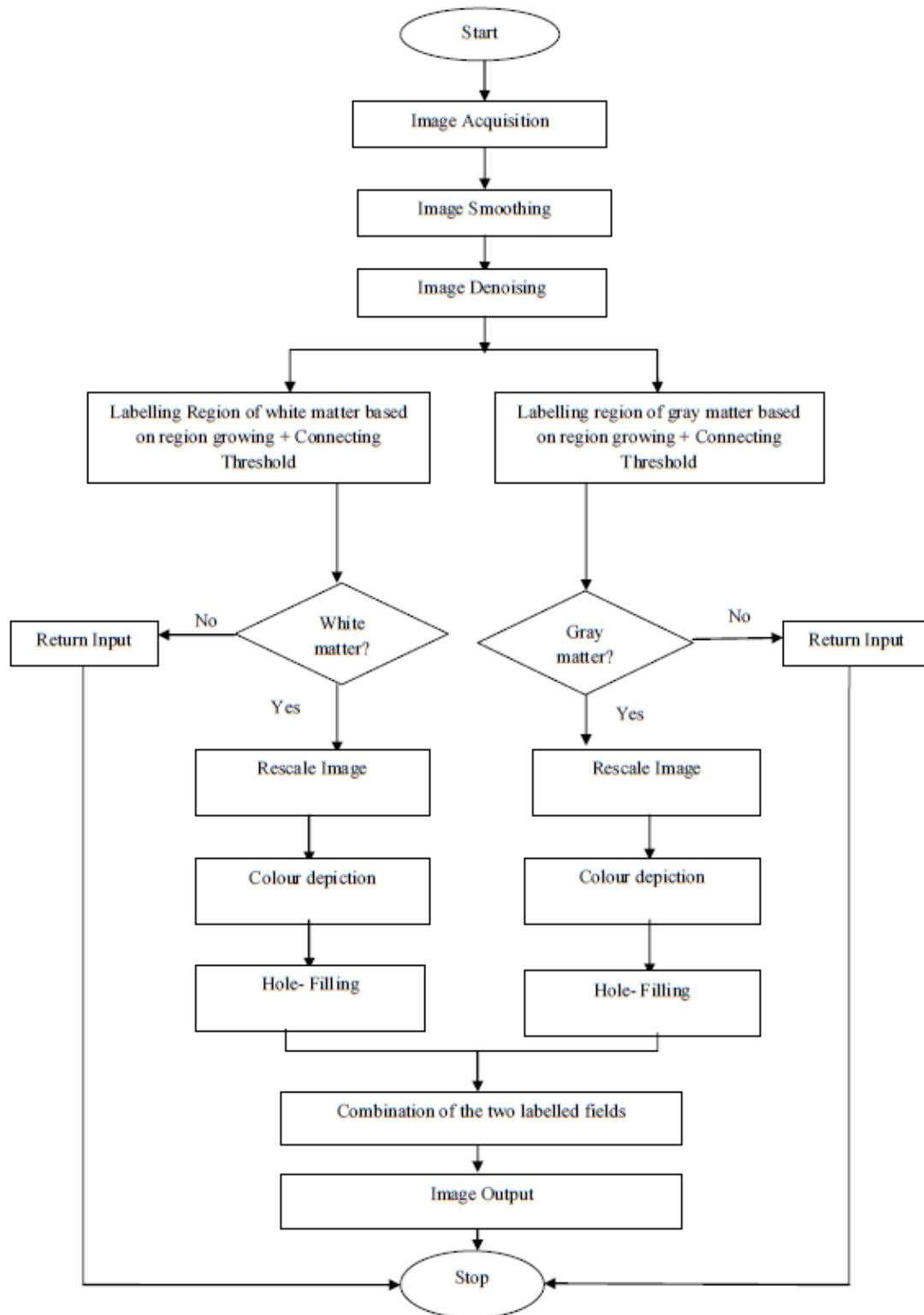


Figure 2: (Appendix1) Flowchart processing of white and grey matter distortion

Appendix 2: Volume calculation software programs

2.1. Autodesk Inventor

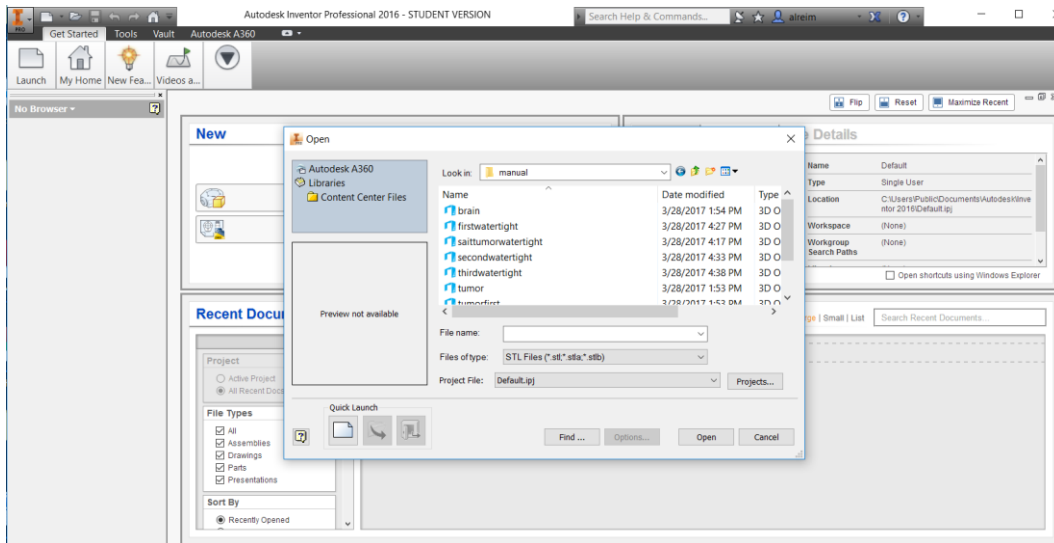


Figure 3: (Appendix 2.1) Open STL file

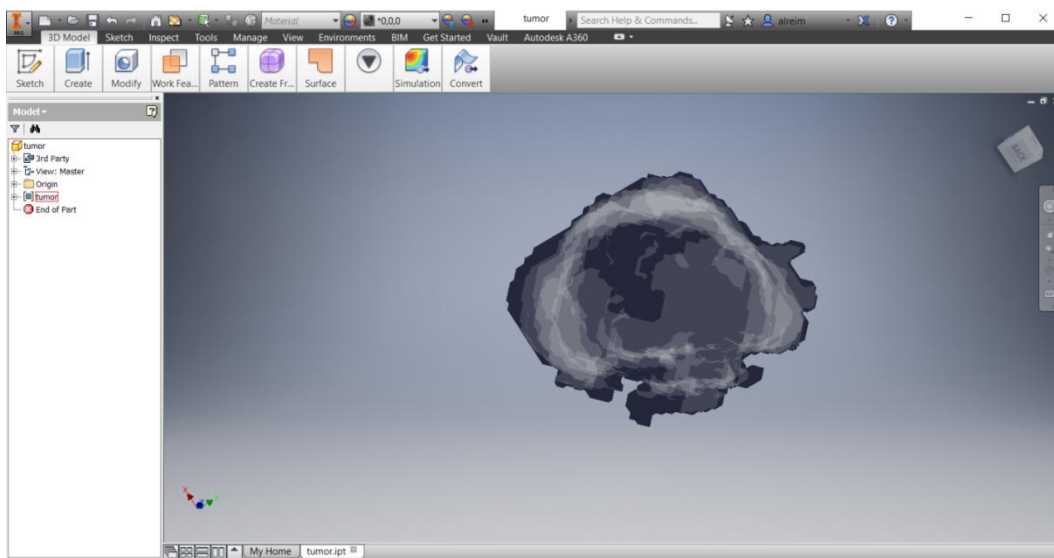


Figure 4: (Appendix 2.1) Visibility

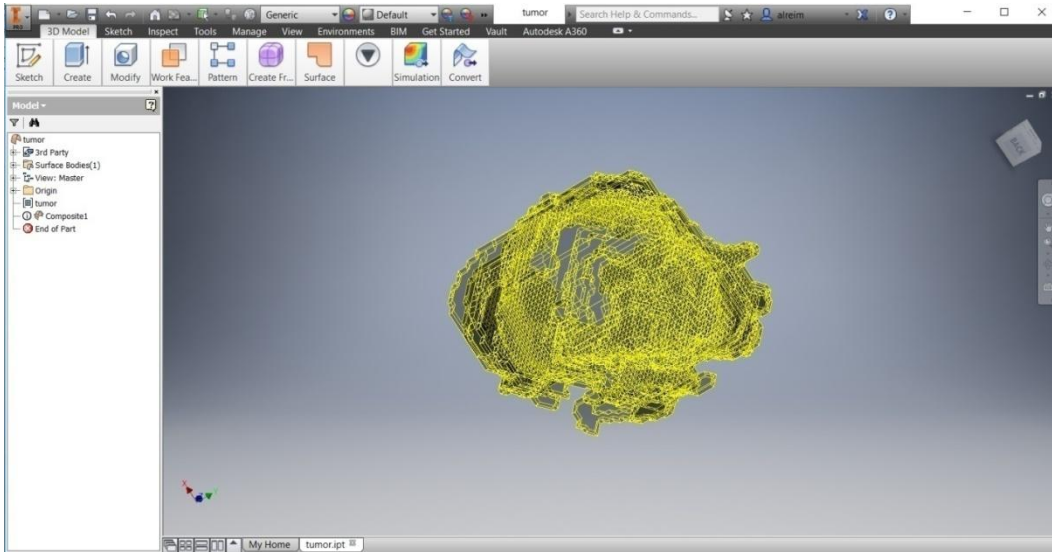


Figure 5: (Appendix 2.1) converts to base feature

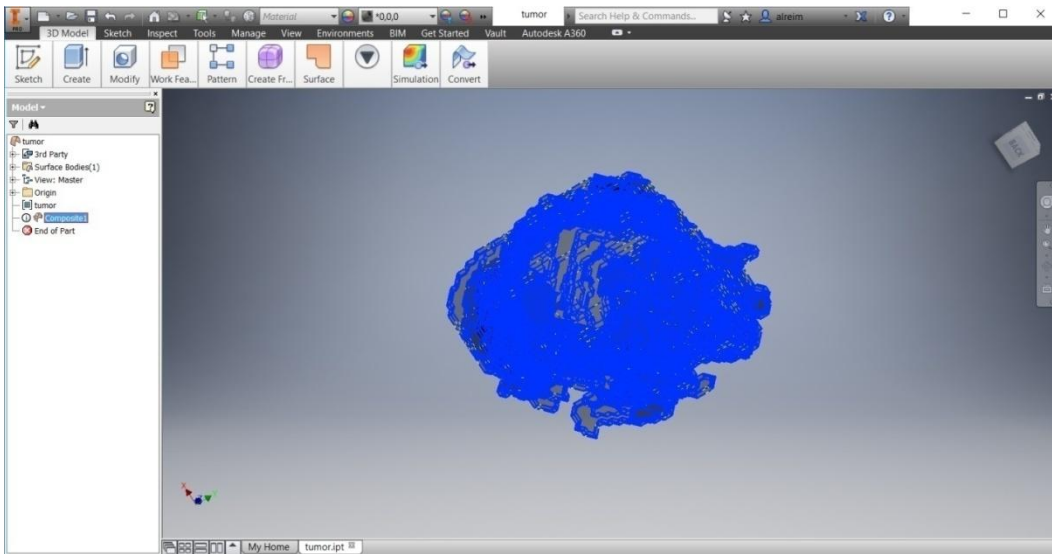


Figure 6: (Appendix 2.1) Press composite to start stitching

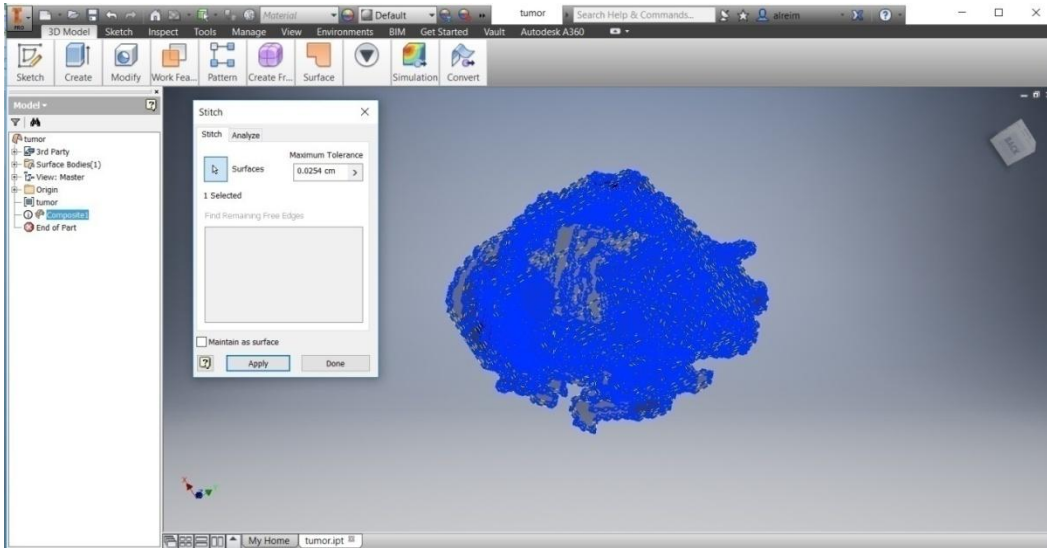


Figure 7: (Appendix 2.1) Apply stitching

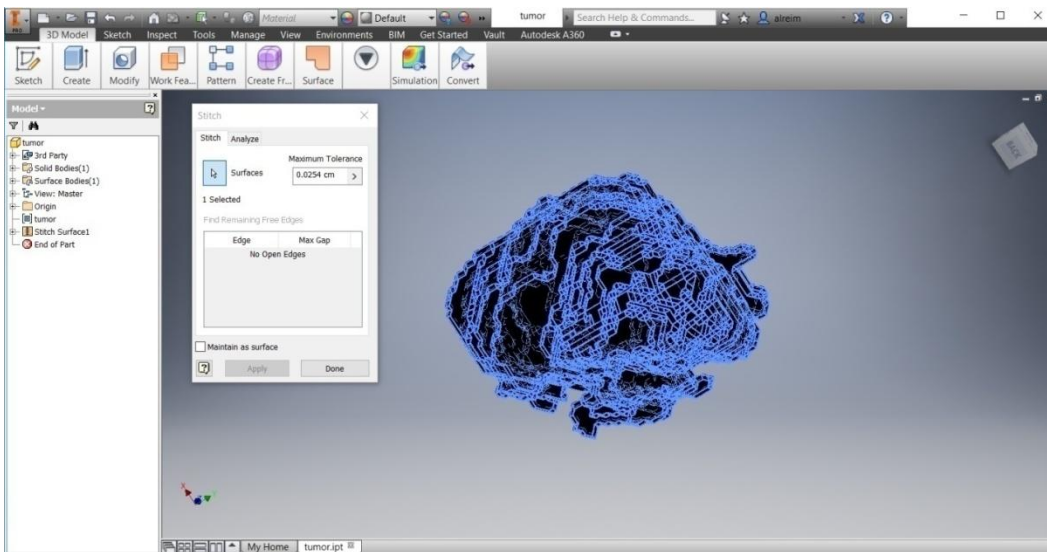


Figure 8: (Appendix 2.1) No open edges

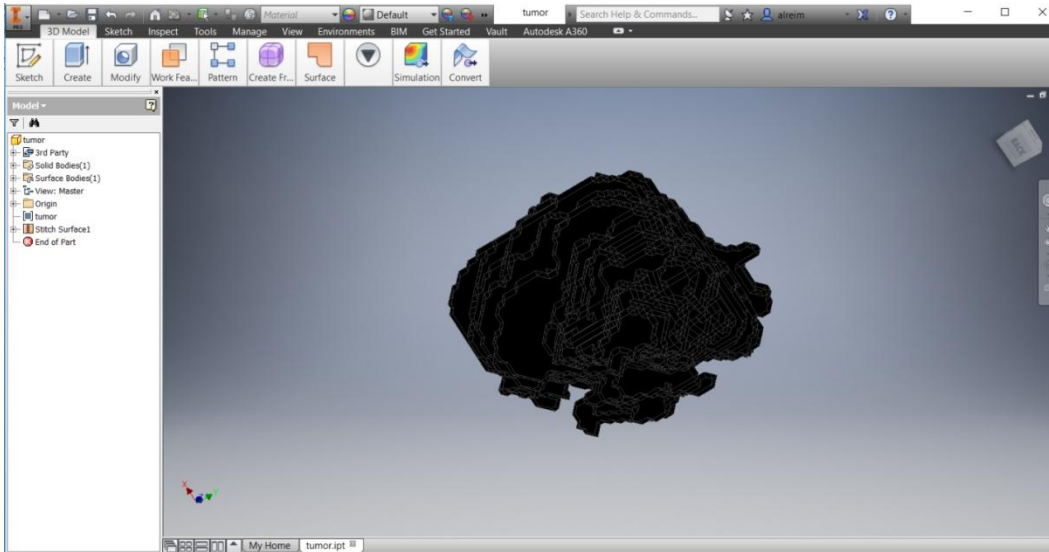


Figure 9: (Appendix 2.1) stitching is done

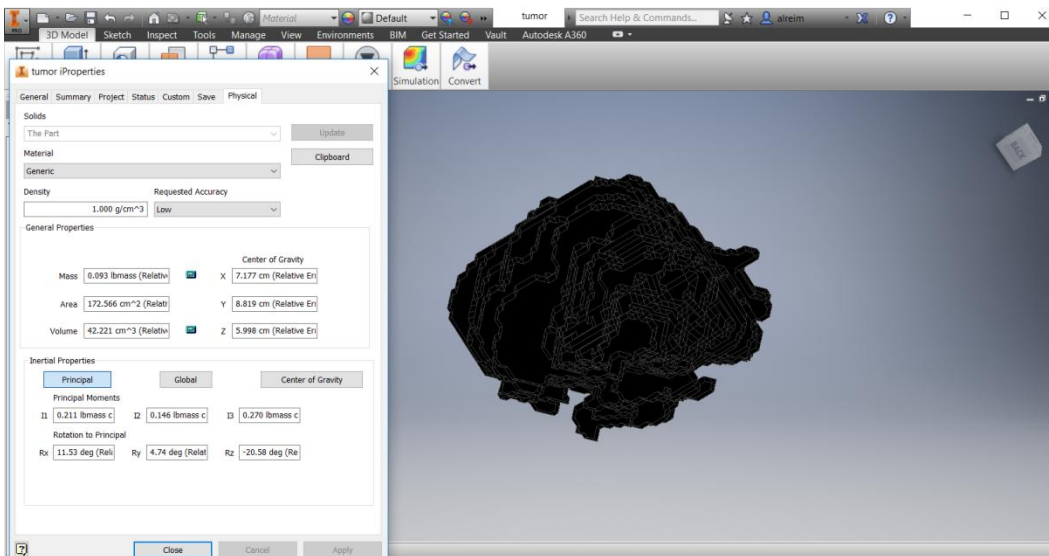


Figure 10: (Appendix 2.1) from iProperties --> Physical--> Update--> the volume is calculated

2.2.  MeshLab

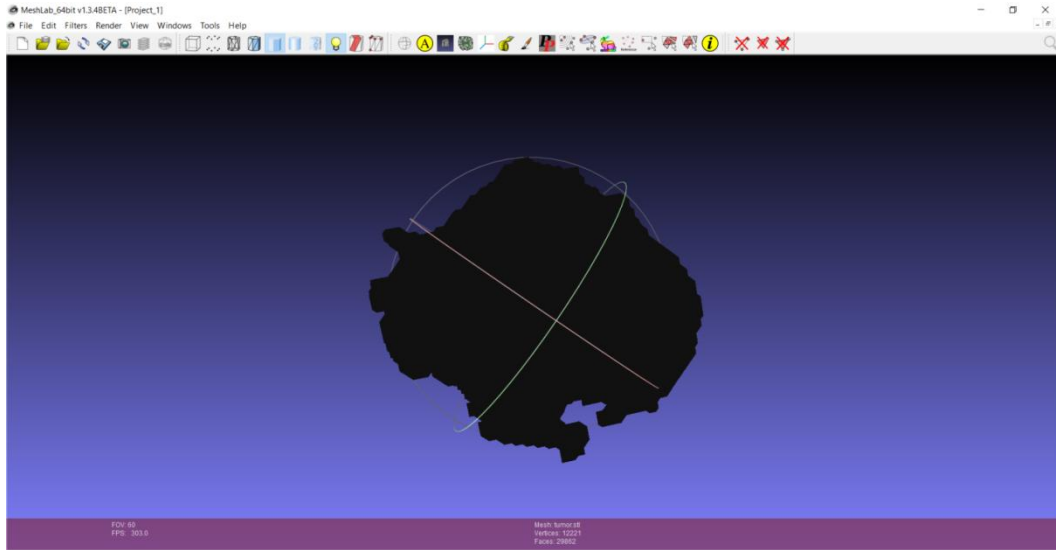


Figure 11: (Appendix 2.2) Import mesh

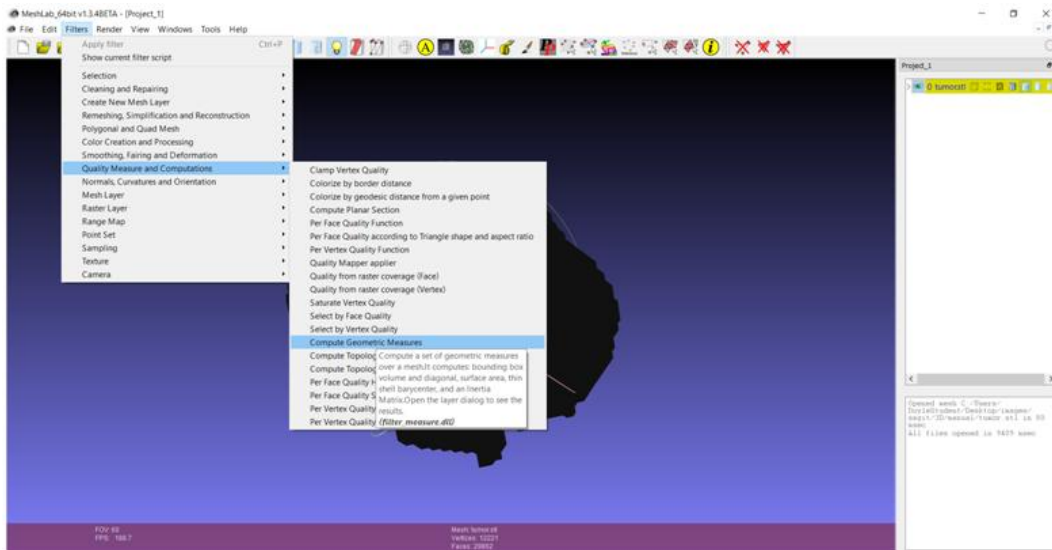


Figure 12: (Appendix 2.2) Filters--> Quality measure and computation--> Compute Geometric measures

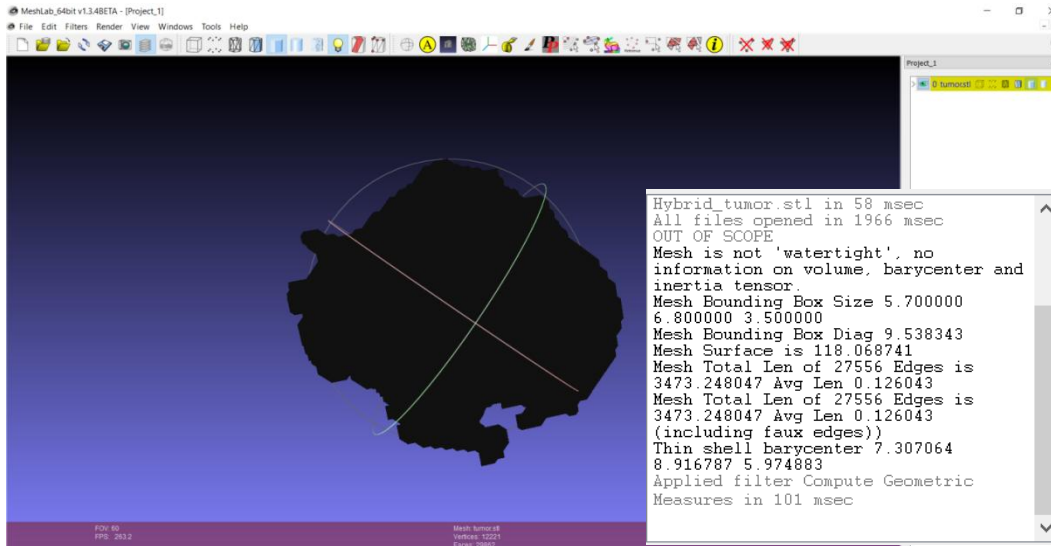


Figure 13: (Appendix 2.2) shows it is not watertight

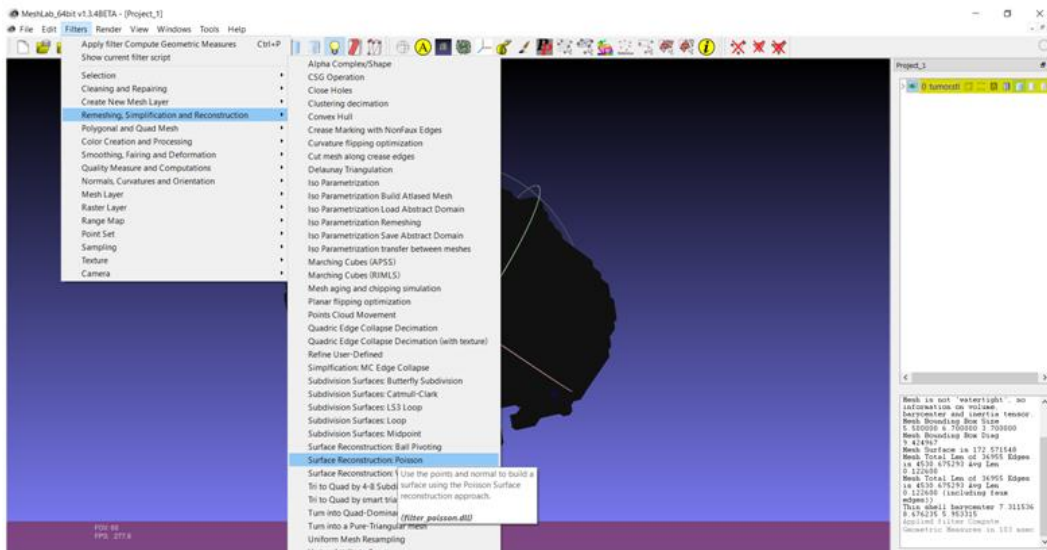


Figure 14 : (Appendix 2.2) In order to convert it into watertight: Filter-->Remeshing -->Simplification and reconstruction--> Surface Reconstruction: Poisson

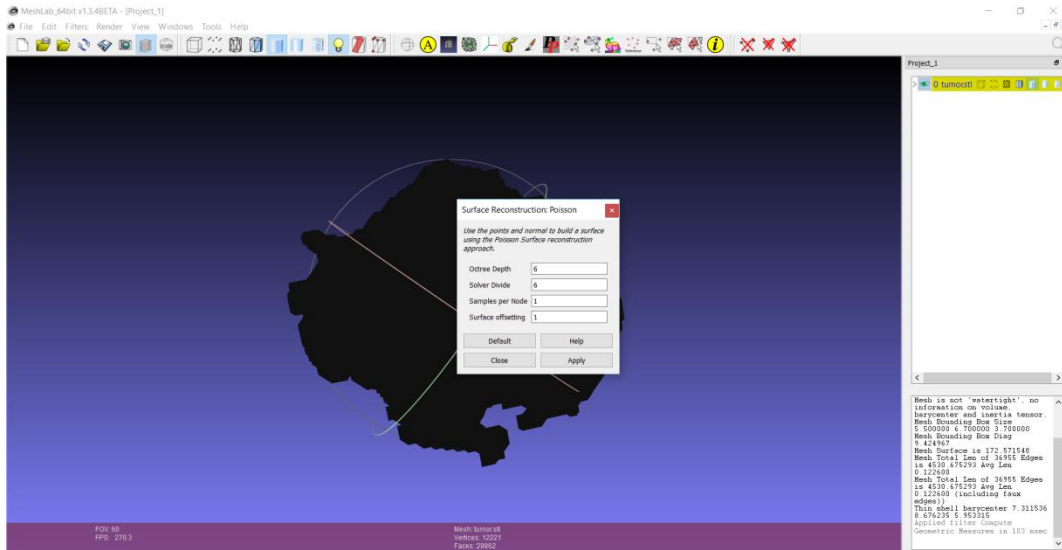


Figure 15: (Appendix 2.2) Apply

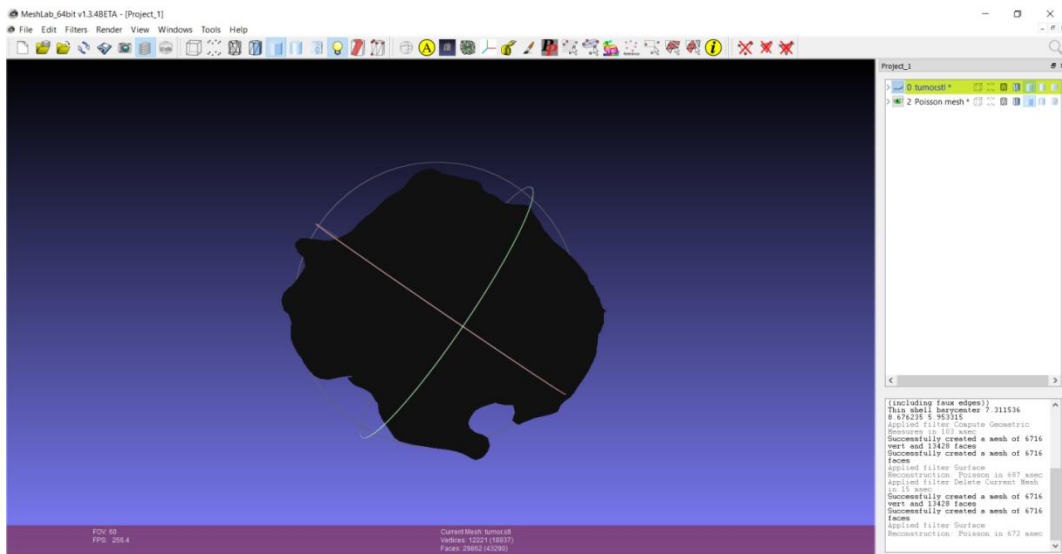


Figure 16: (Appendix 2.2) watertight object

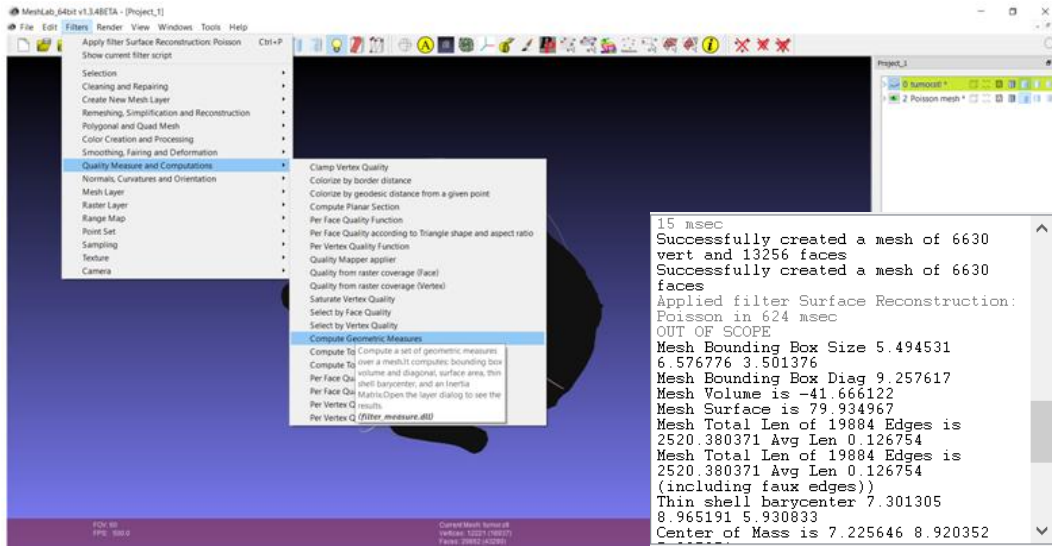


Figure 17: (Appendix 2.2) Now the tumor is watertight and it can be measured by MeshLab. Filters--> Quality measure and computation--> Compute Geometric measures.

Appendix 3: Texts file for area and perimeter of each segmentation mode

Image properties (Hybrid/semi automated)

Slice 36Area= 0 perimeter= 0
Slice 37Area= 0 perimeter= 0
Slice 38Area= 17 perimeter= 14.0710678119
Slice 39Area= 80 perimeter= 26.5985425456
Slice 40Area= 290 perimeter= 75.5979797464
Slice 41Area= 165 perimeter= 51.2842712475
Slice 42Area= 211 perimeter= 61.3553390593
Slice 43Area= 278 perimeter= 78.5979797464
Slice 44Area= 560 perimeter= 127.39696962
Slice 45Area= 839 perimeter= 149.43860018
Slice 46Area= 528 perimeter= 114.568542495
Slice 47Area= 955 perimeter= 159.09545443
Slice 48Area= 825 perimeter= 141.781745931
Slice 49Area= 870 perimeter= 131.539105243
Slice 50Area= 960 perimeter= 133.639610307
Slice 51Area= 1093 perimeter= 146.468037432
Slice 52Area= 1251 perimeter= 157.710678119
Slice 53Area= 1417 perimeter= 165.781745931
Slice 54Area= 1616 perimeter= 174.024386618
Slice 55Area= 1840 perimeter= 180.852813742
Slice 56Area= 1791 perimeter= 183.852813742

Slice 57Area= 2095 perimeter= 194.509667992

Slice 58Area= 2032 perimeter= 183.681240867

Slice 59Area= 2090 perimeter= 189.095454443

Slice 60Area= 2194 perimeter= 203.237590053

Slice 61Area= 2231 perimeter= 205.823376491

Slice 62Area= 2118 perimeter= 203.237590053

Slice 63Area= 2082 perimeter= 201.48023074

Slice 64Area= 2084 perimeter= 206.965512115

Slice 65Area= 2306 perimeter= 224.894444303

Slice 66Area= 2404 perimeter= 231.965512115

Slice 67Area= 2580 perimeter= 277.906637612

Slice 68Area= 2363 perimeter= 256.350288425

Slice 69Area= 1918 perimeter= 222.758405333

Slice 70Area= 1547 perimeter= 196.379725677

Slice 71Area= 930 perimeter= 152.367532368

Slice 72Area= 459 perimeter= 96.9116882454

Slice 73Area= 0 perimeter= 0

Slice 74Area= 0 perimeter= 0

Image properties (Manual)

Slice 34Area= 0 perimeter= 0

Slice 35Area= 0 perimeter= 0

Slice 36Area= 24 perimeter= 15.6568542495

Slice 37Area= 28 perimeter= 18.4852813742

Slice 38Area= 31 perimeter= 19.4852813742

Slice 39Area= 51 perimeter= 25.4852813742

Slice 40Area= 148 perimeter= 52.941125497

Slice 41Area= 165 perimeter= 51.2842712475

Slice 42Area= 212 perimeter= 62.3553390593

Slice 43Area= 262 perimeter= 68.7695526217

Slice 44Area= 499 perimeter= 119.74011537

Slice 45Area= 516 perimeter= 111.982756057

Slice 46Area= 534 perimeter= 116.325901808

Slice 47Area= 712 perimeter= 132.639610307

Slice 48Area= 803 perimeter= 138.367532368

Slice 49Area= 870 perimeter= 131.539105243

Slice 50Area= 960 perimeter= 133.639610307

Slice 51Area= 1093 perimeter= 146.468037432

Slice 52Area= 1248 perimeter= 157.539105243

Slice 53Area= 1416 perimeter= 166.610173055

Slice 54Area= 1609 perimeter= 173.43860018

Slice 55Area= 1828 perimeter= 181.681240867

Slice 56Area= 1795 perimeter= 183.43860018

Slice 57Area= 1917 perimeter= 199.752308679

Slice 58Area= 1921 perimeter= 183.681240867

Slice 59Area= 2016 perimeter= 190.409162928

Slice 60Area= 2182 perimeter= 204.066017178

Slice 61Area= 2198 perimeter= 206.651803616

Slice 62Area= 2104 perimeter= 203.48023074

Slice 63Area= 2055 perimeter= 202.208152802

Slice 64Area= 2101 perimeter= 207.379725677

Slice 65Area= 2088 perimeter= 209.894444303

Slice 66Area= 2152 perimeter= 218.13708499

Slice 67Area= 2256 perimeter= 231.622366364

Slice 68Area= 2101 perimeter= 234.279220614

Slice 69Area= 1784 perimeter= 213.030483272

Slice 70Area= 1365 perimeter= 180.308657865

Slice 71Area= 919 perimeter= 150.953318806

Slice 72Area= 78 perimeter= 33.8994949366

Slice 73Area= 0 perimeter= 0

Slice 74Area= 0 perimeter= 0

Image properties (Auto)

Slice 37Area= 0 perimeter= 0

Slice 38Area= 0 perimeter= 0

Slice 39Area= 94 perimeter= 38.4203102168

Slice 40Area= 154 perimeter= 53.941125497

Slice 41Area= 165 perimeter= 51.2842712475

Slice 42Area= 212 perimeter= 62.3553390593

Slice 43Area= 278 perimeter= 78.5979797464

Slice 44Area= 403 perimeter= 103.497474683

Slice 45Area= 506 perimeter= 111.154328933

Slice 46Area= 527 perimeter= 115.154328933

Slice 47Area= 675 perimeter= 128.639610307

Slice 48Area= 785 perimeter= 133.539105243

Slice 49Area= 861 perimeter= 129.882250994

Slice 50Area= 953 perimeter= 136.26093065

Slice 51Area= 1093 perimeter= 149.539105243

Slice 52Area= 1222 perimeter= 155.539105243

Slice 53Area= 1343 perimeter= 160.024386618

Slice 54Area= 1362 perimeter= 161.781745931

Slice 55Area= 1494 perimeter= 169.43860018

Slice 56Area= 1497 perimeter= 173.09545443

Slice 57Area= 1603 perimeter= 182.509667992

Slice 58Area= 1717 perimeter= 173.43860018

Slice 59Area= 1820 perimeter= 180.994949366

Slice 60Area= 1954 perimeter= 189.722871427

Slice 61Area= 1932 perimeter= 192.066017178

Slice 62Area= 1885 perimeter= 192.651803616

Slice 63Area= 1849 perimeter= 188.308657865

Slice 64Area= 1827 perimeter= 189.722871427

Slice 65Area= 1796 perimeter= 193.793939239

Slice 66Area= 1731 perimeter= 199.823376491

Slice 67Area= 1708 perimeter= 197.379725677

Slice 68Area= 1627 perimeter= 193.823376491

Slice 69Area= 1387 perimeter= 176.509667992

Slice 70Area= 877 perimeter= 142.267027305

Slice 71Area= 621 perimeter= 109.497474683

Slice 72Area= 78 perimeter= 33.8994949366

Slice 73Area= 0 perimeter= 0

Slice 74Area= 0 perimeter= 0

Bibliography

- [1] K. U. Barthel, “Interactive 3D Surface Plot (ImageJ),” *Internationale Medieninformatik, Berlin, Germany*. [Online]. Available: <https://imagej.nih.gov/ij/plugins/surface-plot-3d.html>. [Accessed: 08-Aug-2017].
- [2] 3D-DOCTOR, “3D-DOCTOR converts CT/MRI images to 3D mesh models,” 1998. [Online]. Available: <http://ablesw.com/3d-doctor/brochure.pdf>. [Accessed: 19-Mar-2017].
- [3] A. Rosset, L. Spadola, and O. Ratib, “OsiriX: An open-source software for navigating in multidimensional DICOM images,” *J. Digit. Imaging*, vol. 17, no. 3, pp. 205–216, 2004.
- [4] Z. Li, J. Sun, and J. Zhang, “A new approach of building 3D visualization framework for multimodal medical images display and computed assisted diagnosis,” in *SPIE Medical Imaging, International Society for Optics and Photonics*, 2012, p. 831911.
- [5] H. Dong, L. Xia, J. Zhang, and A. Cai, “Medical Image Reconstruction Based on ITK and VTK,” in *Computer Sciences and Applications (CSA) International Conference*, 2013, pp. 642–645.
- [6] H. M. Moftah, A. Ella Hassanien, and M. Shoman, “3D brain tumor segmentation scheme using K-mean clustering and connected component labeling algorithms,” in *Proceedings of the 2010 10th International Conference on Intelligent Systems Design and Applications, ISDA '10*, 2010, pp. 320–324.
- [7] K. Bandyopadhyay, S, “BrainTumor Boundary Detection in MR Image by Homogeneity Enhancement Process,” *Int. J. Comput. Sci. Inf. Technol.*, pp. 0975–9646.
- [8] C. Hansen, J. Wieferrich, F. Ritter, C. Rieder, and H. O. Peitgen, “Illustrative visualization of 3D planning models for augmented reality in liver surgery,” *Int. J. Comput. Assist. Radiol. Surg.*, vol. 5, no. 2, pp. 133–141, 2010.
- [9] D. A. Dahab, S. S. A. Ghoniemy, and G. M. Selim, “Automated Brain Tumor Detection and Identification Using Image Processing and Probabilistic Neural Network Techniques,” *Int. J. Image Process. Vis. Commun.*, vol. 1, no. 2, pp. 2319–1724, 2012.
- [10] S. E. Mahmoudi *et al.*, “Web-based interactive 2D/3D medical image processing and visualization software,” *Comput. Methods Programs Biomed.*, vol. 98, no. 2, pp. 172–182, 2010.
- [11] G. Iliadis *et al.*, “The Importance of Tumor Volume in the Prognosis of Patients

with Glioblastoma Comparison of Computerized Volumetry and Geometric Models,” *Strahlenther Onkol*, vol. 185, no. 11, pp. 743–50, 2009.

- [12] F. Masulli and A. Schenone, “A fuzzy clustering based segmentation system as support to diagnosis in medical imaging,” *Artif. Intell. Med.*, vol. 16, no. 2, pp. 129–147, 1999.
- [13] S. Bauer, R. Wiest, L.-P. Nolte, and M. Reyes, “A survey of MRI-based medical image analysis for brain tumor studies,” *Phys. Med. Biol.*, vol. 58, no. 13, p. R97, 2013.
- [14] J. J. Caban, A. Joshi, and P. Nagy, “Rapid development of medical imaging tools with open-source libraries,” *J. Digit. Imaging*, vol. 20, no. 1, pp. 83–93, 2007.
- [15] A. Fedorov *et al.*, “3D Slicer as an image computing platform for the Quantitative Imaging Network,” *Magn. Reson. Imaging*, vol. 30, no. 9, pp. 1323–1341, 2012.
- [16] 3D Slicer, “A multi-platform, free and open source software package for visualization and medical image computing,” *Slicer 4.6 released*, 2017. [Online]. Available: <https://www.slicer.org/>. [Accessed: 15-Mar-2017].
- [17] E. Rios Velazquez *et al.*, “Volumetric CT-based segmentation of NSCLC using 3D-Slicer,” *Sci. repoert*, vol. 3, p. 3529, 2013.
- [18] U. Ayachit *et al.*, “The ParaView Guide,” 2015. [Online]. Available: <https://www.paraview.org/paraview-guide/>. [Accessed: 15-Mar-2017].
- [19] J. Hennessey, M. Bowers, A. Kolasny, T. Brown, T. Ratnanather, and M. Miller, “Computational Anatomy Works (CAWorks): Enhancing Paraview for Medical Imaging Computational Anatomy Works (CAWorks): Enhancing Paraview for Medical Imaging Cardiovascular Research Grid,” *Annu. Rev. Biomed. Eng.*, vol. 43, no. 2, pp. 375–405, 2002.
- [20] I. Kitware, *VTK User’s Guide Version 5*. Columbia, USA: Kitware, Inc, 2010.
- [21] T. Kapur *et al.*, “The National Alliance for Medical Image Computing, a roadmap initiative to build a free and open source software infrastructure for translational research in medical image analysis,” *J. Am. Med. Informatics Assoc.*, vol. 19, no. 2, pp. 176–180, 2012.
- [22] L.-D. Chiorean, T. Szasz, M.-F. Vaida, and A. Voina, “3D RECONSTRUCTION AND VOLUME COMPUTING IN MEDICAL IMAGING,” *Acta Tech. Napocensis*, vol. 52, no. 3, p. 18, 2011.
- [23] MIDAS, “Welcome to MIDAS!,” *Kitware Inc.*, 2010. [Online]. Available: <http://www.insight-journal.org/midas/>. [Accessed: 01-May-2017].
- [24] J. Jomier, A. Bailly, M. Le Gall, and R. Avila, “An Open - Source Digital

- Archiving System for Medical and Scientific Research,” *Open Repos.*, 2010.
- [25] P. A. Uday, N. Digvijay, and J. B. Jeeva, “PRE-OPERATIVE BRAIN TUMOR SEGMENTATION USING SLICER-3D,” in *Green Computing Communication and Electrical Engineering (ICGCCCE) International Conference*, 2014, pp. 1–4.
- [26] ImageJ, “Image Processing and Analysis in Java,” *NIH*, 2004. [Online]. Available: <https://imagej.nih.gov/ij/index.html>. [Accessed: 16-Mar-2017].
- [27] M. D. Abràmoff, P. J. Magalhães, and S. J. Ram, “Image processing with imageJ,” *Biophotonics Int.*, vol. 11, no. 7, pp. 36–42, 2004.
- [28] K. P. Kumara, “Reconstructing Solid Model from 2D Scanned Images of Biological Organs for Finite Element Simulation,” *My Google Knols*, 2011. [Online]. Available: <https://knolskiranakumarap.wordpress.com/2011/07/03/reconstructing-solid-model-from-2d-3rc2kfwq179j2-5/>. [Accessed: 18-Mar-2017].
- [29] J. Schindelin *et al.*, “Fiji: an open-source platform for biological-image analysis.,” *Nat. Methods*, vol. 9, no. 7, pp. 676–682, 2012.
- [30] D. Prodanov and K. Verstreken, “Automated Segmentation and Morphometry of Cell and Tissue Structures. Selected Algorithms in ImageJ,” *Mol. imaging, InTech*, pp. 183–208, 2012.
- [31] SYNAPSE 3D, “Discover the power of SYNAPSE 3D,” *FUJIFILM*, 2017. [Online]. Available: <http://3dimaging.fujimed.com/>. [Accessed: 19-Mar-2017].
- [32] Osirix, “Osirix User Manual,” 2017. [Online]. Available: <http://pixmeo.pixmeo.com/documents/OsiriXUserManualExtract.pdf>. [Accessed: 18-Mar-2017].
- [33] Osirix, “The World Famous DICOM Veiwew,” 2017. [Online]. Available: <http://www.osirix-viewer.com/>. [Accessed: 18-Mar-2017].
- [34] H.-S. Shin, S.-W. Yoon, J.-Y. Kim, and M.-H. Lee, “Down-Scaled 3D Object for Telediagnostic Imaging Support System,” *J. Biomed. Eng. Res.*, vol. 26, no. 4, pp. 185–191, 2005.
- [35] Y. Abe *et al.*, “Computer assisted surgery, preoperative planning and navigation for pancreatic cancer,” *J. Hepatobiliary. Pancreat. Sci.*, vol. 21, no. 4, pp. 251–255, 2014.
- [36] Y. Sharma and P. Kaur, “Detection and Extraction of Brain Tumor from MRI Images Using K-Means Clustering and Watershed Algorithms,” *Int. J. Comput. Sci. Trends Technol.*, vol. 3, no. 2, pp. 32–8, 2013.
- [37] D. N. Louis *et al.*, “The 2016 World Health Organization Classification of Tumors

- of the Central Nervous System: a summary,” *Acta Neuropathol.*, vol. 131, no. 6, pp. 803–820, 2016.
- [38] S. Bauer, A. Mauricio Reyes, and C.-A. Gábor Székely, “Medical Image Analysis and Image-based Modeling for Brain Tumor Studies PhD in Biomedical Engineering,” University of Bern, 2013.
- [39] D. Paulei, F. Floeth, L. Tellmann, and et al, “Comparison of O-(2-18F-Fluoroethyl)-L-Tyrosine PET and 3-123I-Iodo- α -Methyl-L-Tyrosine SPECT in Brain Tumors,” *J. Nucl. Med.*, vol. 45, no. 3, pp. 374–381, 2004.
- [40] A. Drevelegas and N. Papanikolaou, “Imaging modalities in brain tumors,” in *Imaging of Brain Tumors with Histological Correlations*, 2011.
- [41] J. W. Scuffham, M. D. Wilson, P. Seller, and et al, “A CdTe detector for hyperspectral SPECT imaging,” *J. Instrum.*, vol. 7, no. 8, p. P08027, 2012.
- [42] K. A. Follett, M. A. Nathan, J. G. Piper, M. Madsen, and P. T. Kirchner, “Diagnosis of Recurrent Brain Tumor: Value of 201Tl SPECT vs 8F-fluorodeoxyglucose PET,” *Am. J. Roentgenol.*, vol. 163, no. 6, pp. 1459–1465, 1994.
- [43] B. Leonard and H. Abdei Dayem, “The Clinical Role of SPECT in Patients with Brain Tumors,” *J. Neuroimaging*, vol. 5, no. s1, pp. s34–s39.
- [44] K. L. Black, R. A. Hawkins, K. T. Kim, D. P. Becker, C. Lerner, and D. Marciano, “Use of thallium-201 SPECT to quantitate malignancy grade of gliomas,” *J Neurosurg*, vol. 71, no. 3, pp. 342–346, 1989.
- [45] G. A. Alexiou, A. D. Fotopoulos, A. Papadopoulos, A. P. Kyritsis, K. S. Polyzoidis, and S. Tsiouris, “Evaluation of brain tumor recurrence by 99mTc-tetrofosmin SPECT: A prospective pilot study,” *Ann. Nucl. Med.*, vol. 21, no. 5, p. 293, 2007.
- [46] G. Mariani *et al.*, “A review on the clinical uses of SPECT/CT,” *Eur. J. Nucl. Med. Mol. Imaging*, vol. 37, no. 10, pp. 1959–1985, 2010.
- [47] A. P. Apurva, M. P. Bipin, and M. P. Kirti, “Role of PET scan in Clinical Practice,” *Gurata Med. J.*, vol. 8, no. 12, pp. 19–22, 2013.
- [48] J. Menendez, A. Nanda, and R. S. Polin, *PET SCAN FOR BRAIN TUMORS*, vol. 11, no. 3. 333 Seventh Avenue, New York, NY 10001, USA.: Thieme Medical Publishers, Inc., 2000.
- [49] S. T. Chao, J. H. Suh, S. Raja, S. Y. Lee, and G. Barnett, “The sensitivity and specificity of FDG PET in distinguishing recurrent brain tumor from radionecrosis in patients treated with stereotactic radiosurgery,” *Int. J. Cancer*, vol. 96, no. 3, pp.

191–197, 2001.

- [50] S. Kamdi and R. K. Krishna, “Image Segmentation and Region Growing Algorithm,” *Int. J. Comput. Technol. Electron. Eng.*, vol. 2, no. 1, pp. 2249–6343, 2012.
- [51] Y.-L. Huang, D.-R. Chen, and S.-C. Chang, “Three-Dimensional Region-Based Segmentation for Breast Tumors on Sonography,” *Multidiscip. Med. ultrasound J.*, vol. 32, no. 5, pp. 835–846, 2012.
- [52] R. Adams and L. Bischof, “Seeded Region Growing,” *IEEE Trans. Pattern Anal. Mach. Intell.*, vol. 16, no. 6, pp. 641–647, 1994.
- [53] J. Fan, G. Zeng, M. Body, and M. S. Hacid, “Seeded region growing: An extensive and comparative study,” *Pattern Recognit. Lett.*, vol. 26, no. 8, pp. 1139–1156, 2005.
- [54] P. K. Sahoo, S. Soltani, and A. K. C. Wong, “A survey of thresholding techniques,” *Comput. Vision, Graph. Image Process.*, vol. 41, no. 2, pp. 233–260, 1988.
- [55] G. Leedham, C. Yan, K. Takru, J. H. N. Tan, and L. Mian, “Comparison of some thresholding algorithms for text/background segmentation in difficult document images,” *Proc. Int. Conf. Doc. Anal. Recognition, ICDAR*, vol. 2, pp. 859–864, 2003.
- [56] S. U. Lee, S. Yoon Chung, and R. H. Park, “A comparative performance study of several global thresholding techniques for segmentation,” *Comput. Vision, Graph. Image Process.*, vol. 52, no. 2, pp. 171–190, 1990.
- [57] C. A. Glasbey, “An Analysis of Histogram-Based Thresholding Algorithms,” *CVGIP Graph. Model. Image Process.*, vol. 55, no. 6, pp. 532–537, 1993.
- [58] B. Sankur, “Survey over image thresholding techniques and quantitative performance evaluation,” *J. Electron. Imaging*, vol. 13, no. 1, pp. 146–168, 2004.
- [59] J. Lázaro, J. L. Martin, J. Arias, A. Astarloa, and C. Cuadrado, “Neuro semantic thresholding using OCR software for high precision OCR applications,” *Image Vis. Comput.*, vol. 28, no. 4, pp. 571–578, 2010.
- [60] G. C. Anagnostopoulos, “SVM-based target recognition from synthetic aperture radar images using target region outline descriptors,” *Nonlinear Anal. Theory, Methods Appl.*, vol. 71, no. 12, pp. e2934–e2939, 2009.
- [61] Y. T. Hsiao, C. L. Chuang, Y. L. Lu, and J. A. Jiang, “Robust multiple objects tracking using image segmentation and trajectory estimation scheme in video frames,” *Image Vis. Comput.*, vol. 24, no. 10, pp. 1123–1136, 2006.

- [62] M. T. Doelken *et al.*, “1H-MRS profile in MRI positive- versus MRI negative patients with temporal lobe epilepsy,” *Seizure*, vol. 17, no. 6, pp. 490–497, 2008.
- [63] S. D. Salman and A. A. Bahrani, “Segmentation of tumor tissue in gray medical images using watershed transformation method,” *Int. J. Adv. Comput. Technol.*, vol. 2, no. 4, 2010.
- [64] A. Mustaqeem, A. Javed, and T. Fatima, “An Efficient Brain Tumor Detection Algorithm Using Watershed & Thresholding Based Segmentation,” *Int. J. Image, Graph. Signal Process.*, vol. 4, no. 10, p. 34, 2012.
- [65] R. G. Selkar and M. N. Thakare Assistant Professor Sr Gr, “BRAIN TUMOR DETECTION AND SEGMENTATION BY USING THRESHOLDING AND WATERSHED ALGORITHM,” *ISSN*, vol. 1, no. 3, pp. 2348–9928, 2014.
- [66] J. B. T. M. Roerdink and A. Meijster, “The Watershed Transform: Definitions, Algorithms and Parallelization Strategies,” *Fundam. Informaticae*, vol. 41, no. 1,2, pp. 187–228, 2001.
- [67] M. Shafry *et al.*, “Connected Component Labeling Using Components Neighbors-Scan Labeling Approach,” *J. Comput. Sci.*, vol. 6, no. 10, pp. 1099–1107, 2010.
- [68] P. Bourke, “Polygonising a scalar field,” 1994. [Online]. Available: <http://paulbourke.net/geometry/polygonise/>. [Accessed: 22-Jun-2016].
- [69] A. Som, “Surface Extraction: Creating a mesh from pixel-data using Python and VTK,” *PyScience*, 2014. [Online]. Available: <https://pyscience.wordpress.com/2014/09/11/surface-extraction-creating-a-mesh-from-pixel-data-using-python-and-vtk/>. [Accessed: 19-Jun-2016].
- [70] W. E. Lorensen and H. E. Cline, “Marching cubes: A high resolution 3D surface construction algorithm,” *Comput. Graph. (ACM)*, vol. 21, no. 4, pp. 163–169, 1987.
- [71] M. Segal and K. Akeley, *The OpenGL R Graphics System: A Specification (Version 4.4 (Core Profile) - March 19, 2014)*, Version 4.4. 2006-2014 The Khronos Group Inc, 2014.
- [72] S. Tariq, “D3D11 Tessellation,” *In Game Developers Conference, Session: Advanced Visual Effects with Direct3D for PC*, 2009. [Online]. Available: http://developer.download.nvidia.com/presentations/2009/GDC/GDC09_D3D11Tessellation.pdf. [Accessed: 09-Jun-2016].
- [73] DAGRA, “Linear Interpolation with Excel,” *Blue Leaf Software*, 2016. [Online]. Available: <http://www.datadigitization.com/dagra-in-action/linear-interpolation-with-excel/>. [Accessed: 10-Jun-2016].

- [74] B. Guo, “A Multiscale Model for Structure-Based Volume Rendering,” *IEEE Trans. Vis. Comput. Graph.*, vol. 1, no. 4, pp. 291–301, 1995.
- [75] D. Laur and P. Hanrahan, “Hierarchical Splatting: A Progressive Refinement Algorithm for Volume Rendering,” *ACM SIGGRAPH Comput. Graph.*, vol. 25, no. 4, pp. 285–288, 1991.
- [76] J. Kniss, G. Kindlmann, and C. Hansen, “Interactive Volume Rendering Using Multi-Dimensional Transfer Functions and Direct Manipulation Widgets,” in *Proceeding VIS '01 Proceedings of the conference on Visualization '01*, 2001, pp. 255–262.
- [77] Scientific Visualization Tutorials, “Volume rendering techniques.” [Online]. Available: <http://www.cc.gatech.edu/scivis/tutorial/linked/volrend.html>. [Accessed: 05-Jul-2016].
- [78] R. A. Drebin, L. Carpenter, and P. Hanrahan Pixar San Rafael, “Volume Rendering,” *ACM SIGGRAPH Comput. Graph.*, vol. 22, no. 4, pp. 65–74, 1988.
- [79] P. G. Lacroute, “FAST VOLUME RENDERING USING A SHEAR-WARP FACTORIZATION OF THE VIEWING TRANSFORMATION,” in *Proceedings of the 21st annual conference on Computer graphics and interactive techniques*, 1995, pp. 451–458.
- [80] M. R. Kaus, S. K. Warfield, A. Nabav, P. M. Black, and et al, “Automated segmentation of MRI images of brain tumors,” *Radiology*, vol. 218, no. 2, pp. 586–591, 2001.
- [81] E. Varga and A. Freudenthal, “User interface prototyping to understand radiology thinking,” *Image-Guidance Multimodal Dose Plan. Radiat. Ther.*, p. 121, 2012.
- [82] E. Varga, P. M. T. Pattynama, and A. Freudenthal, “Manipulation of mental models of anatomy in interventional radiology and its consequences for design of human-computer interaction,” *Cogn. Technol. Work*, vol. 15, no. 4, 2013.
- [83] B. M. Hemminger *et al.*, “Assessment of real-time 3D visualization for cardiothoracic diagnostic evaluation and surgery planning,” *J. Digit. Imaging*, vol. 18, no. 2, pp. 145–153, 2005.
- [84] M. Tory and T. Mö, “Human Factors in Visualization Research,” *IEEE Trans. Vis. Comput. Graph.*, vol. 10, no. 1, pp. 72–84, 2004.
- [85] J. Vuchkova, T. S. Maybury, C. S. Farah, and V. is Lecturer, “Testing the Educational Potential of 3D Visualization Software in Oral Radiographic Interpretation,” *J. Dent. Educ.*, vol. 75, no. 11, pp. 1417–1425, 2011.
- [86] J. Molka-Danielsen, A. Steed, M. Fominykh NTNU, and L. M. Hokstad,

- “Teaching Threshold Concepts in Virtual Reality: Exploring the Conceptual Requirements for Systems Design,” *Stavanger*, pp. 18–20, 2013.
- [87] R. Land, J. Rattray, and P. Vivian, “Learning in the liminal space: A semiotic approach to threshold concepts,” *High. Educ.*, vol. 67, no. 2, pp. 199–217, 2014.
- [88] J. Molka-Danielsen, M. Fominykh, D. Swapp, and A. Steed, “Designing a demonstrator virtual learning environment to teach the threshold concept of space syntax: Seeing from the user’s perspective,” in *IFIP Advances in Information and Communication Technology*, 2015, pp. 180–191.
- [89] S. Mengmeng and W. Shuicai, “A software development of DICOM image processing based on QT, VTK and ITK,” in *Medical Imaging Physics and Engineering (ICMIPE), 2013 IEEE International Conference*, 2013, pp. 231–235.
- [90] N. N. Gopal and Karnanm M, “Diagnose brain tumor through MRI using image processing clustering algorithms such as Fuzzy C Means along with intelligent optimization techniques,” in *Computational Intelligence and Computing Research (ICCIC), 2010 IEEE International Conference*, 2012, pp. 1–4.
- [91] D. M. Joshi, N. K. Rana, and V. M. Misra, “Classification of brain cancer using artificial neural network,” in *Electronic Computer Technology (ICECT), 2010 International Conference*, 2010, pp. 112–116.
- [92] M.-N. Wu, C.-C. Lin, and C.-C. Chang, “Brain Tumor Detection Using Color - Based K - Means Clustering Segmentation,” in *Intelligent Information Hiding and Multimedia Signal Processing, 2007.IIHMSp 2007. Third International Conference*, 2007, pp. 245–250.
- [93] P. Vasuda and S. Satheesh, “Improved Fuzzy C-Means Algorithm for MR Brain Image Segmentation,” *Int. J. Comput. Sci. Eng.*, vol. 2, no. 5, pp. 1713–1715, 2010.
- [94] P. G. Cavalcanti, S. Shirani, D. Koff, and et al, “Lung nodule segmentation in chest computed tomography using a novel background estimation method,” *Quant. Imaging Med. Surg.*, vol. 6, no. 1, p. 16, 2016.
- [95] J. Liu, M. Li, J. Wang, F. Wu, T. Liu, and Y. Pan, “A Survey of MRI-Based Brain Tumor Segmentation Methods,” *Tsinghua Sci. Technol.*, vol. 19, no. 6, pp. 578–595, 2014.
- [96] D. L. Pham, C. Xu, and J. L. Prince, “Current methods in medical images segmentation,” *Annu. Rev. Biomed. Eng.*, vol. 2, no. 1, pp. 315–337, 2000.
- [97] N. Idrissi and F. E. Ajmi, “A hybrid segmentation approach for brain tumor extraction and detection,” in *International Conference on Multimedia Computing and Systems -Proceedings*, 2014, pp. 235–240.

- [98] A. Devos, L. Lukas, A. W. Simonetti, and et al, “Does the combination of magnetic resonance imaging and spectroscopic imaging improve the classification of brain tumours?,” in *Engineering in Medicine and Biology Society, 2004. IEMBS '04. 26th Annual International Conference* , 2004, pp. 407–410.
- [99] A. Mikheev, G. Nevsky, S. Govindan, R. Grossman, and H. Rusinek, “Fully automatic segmentation of the brain from T1-weighted MRI using Bridge Burner algorithm,” *J. Magn. Reson. Imaging*, vol. 27, no. 6, pp. 1235–1241, 2008.
- [100] B. Fischl *et al.*, “Whole brain segmentation: Automated labeling of neuroanatomical structures in the human brain,” *Neuron*, vol. 33, no. 3, pp. 341–355, 2002.
- [101] S. J. Taka and S. Srinivasan, “NIRViz: 3D visualization software for multimodality optical imaging using visualization toolkit (VTK) and insight segmentation toolkit (ITK),” *J. Digit. Imaging*, vol. 24, no. 6, pp. 1103–1111, 2011.
- [102] J.-M. Yu, M.-C. Pan, Y.-F. Hsu, and et al, “Design and implementation of threedimensional ring-scanning equipment for optimized measurements of nearinfrared diffuse optical breast imaging,” *Opt. Eng.*, vol. 54, no. 7, pp. 073107–073107, 2015.
- [103] S. Reza and K. M. Iftkharuddin, “Multi - fractal Texture Features For Brain Tumor and Edema Segmentation,” in *SPIE Medical Imaging, International Society for Optics and Photonics*, 2014, pp. 903503–903503.
- [104] B. H. Menze *et al.*, “The Multimodal Brain Tumor Image Segmentation Benchmark (BRATS),” *IEEE Trans. Med. Imaging*, vol. 34, no. 10, pp. 1993–2024, 2015.
- [105] B. Preim, C. Tietjen, W. Spindler, and H.-O. Peitgen, “Integration of Measurement Tools in Medical 3d Visualizations,” in *in Proceedings of the conference on Visualization '02, IEEE Computer Society* , 2002, pp. 21–28.
- [106] D. Xue and R. E. Albright, “Preoperative Anaplastic Glioma Tumor Volume Effects on Patient Survival,” *J. Surg. Oncol*, vol. 72, no. 4, pp. 199–205, 1999.
- [107] R. O.duda, P. E. Hart, and D. G.Strok, *Pattern classification*, Second. California: John Wiley & Sons, 2102.
- [108] C. M. Bishop, *Pattern Recognition And Machine Learning*. 233 Spring Street, New York, NY 10013, USA: Springer , 2006.
- [109] H. Tek and B. B. Kimia, “Shock-Based Reaction-Diusion Bubbles for Image Segmentation,” *Comput. Vision, Virtual Real. Robot. Med.*, pp. 434–438, 1995.
- [110] B. N. Saha, N. Ray, R. Greiner, A. Murtha, and H. Zhang, “Quick detection of

- brain tumors and edemas: A bounding box method using symmetry,” *Comput. Med. Imaging Graph.*, vol. 36, no. 2, pp. 95–107, 2012.
- [111] Cancer Image Archive, “TCIA Collections,” 2014. [Online]. Available: <http://www.cancerimagingarchive.net/>. [Accessed: 23-Jul-2016].
- [112] K. Clark *et al.*, “The cancer imaging archive (TCIA): Maintaining and operating a public information repository,” *J. Digit. Imaging*, vol. 26, no. 6, pp. 1045–1057, 2013.
- [113] F. W. Prior *et al.*, “TCIA: An information resource to enable open science,” in *Engineering in Medicine and Biology Society (EMBC), 2013 35th Annual International Conference*, 2013, pp. 1282–1285.
- [114] A. Som, “Image Segmentation with Python and SimpleITK,” *PyScience*, 2014. [Online]. Available: <https://pyscience.wordpress.com/2014/10/19/image-segmentation-with-python-and-simpleitk/#more-126>. [Accessed: 27-Jun-2016].
- [115] S. Z. Oo and A. S. Khaing, “BRAIN TUMOR DETECTION AND SEGMENTATION USING WATERSHED SEGMENTATION AND MORPHOLOGICAL OPERATION,” *IJRET Int. J. Res. Eng. Technol*, vol. 3, no. 3, pp. 367–374, 2014, 2014.
- [116] N. Otus, “A Threshold Selection Method from Gray-Level Histograms,” *IEEE Trans. Syst. Man. Cybern.*, vol. 9, no. 1, pp. 62–66, 1979.
- [117] S. Beucher and C. Lantuéjoul, “Use of watersheds in contour detection,” in *International workshop on image processing: Real-time edge and motion detection/estimation*, 1979.
- [118] A. B. Ayoub, “The eccentricity of a conic section,” *Coll. Math. J.*, vol. 34, no. 2, p. 116, 2003.
- [119] R. H. Chan, C. W. Ho, and M. Nikolova, “Salt-and-pepper noise removal by median-type noise detectors and detail-preserving regularization,” *IEEE Trans. Image Process.*, vol. 14, no. 10, pp. 1479–1485, 2005.
- [120] M. Nikolova, R. H. Chan, and J.-F. Cai, “Two-phase approach for deblurring images corrupted by impulse plus gaussian noise,” *Inverse Probl. Imaging*, vol. 2, no. 2, pp. 187–204, 2008.
- [121] J. A. Sethian, *Level set methods and fast marching methods: evolving interfaces in computational geometry, fluid mechanics, computer vision, and materials science*, Second. USA: Cambridge University Press, 2002.
- [122] J. Peiró, L. Formaggia, M. Gazzola, A. Radaelli, and V. Rigamonti, “Shape reconstruction from medical images and quality mesh generation via implicit

- surfaces,” *Int. J. Numer. Methods Fluids*, vol. 53, no. 8, pp. 1339–1360, 2007.
- [123] P. Kalavathi and P. Sowdeeswari, “Edge Enhanced Anisodiffusion Filter for Denoising Gaussian Noise in Medical Images,” *Int. J. Control Theory Appl.*, vol. 9, no. 27, pp. 203–210, 2016.
- [124] S. Torbert, *Applied computer science*. Fairfax, Virginia, USA: Springer, 2012.
- [125] V. P. Gladis, P. Rathi, and S. Palani, “A novel approach for feature and selection on MRI images for brain tumor classification,” in *International Conference Computing Science Engineering Applications*, 2012, pp. 225–234.
- [126] B. Ducke, D. Score, and J. Reeves, “Multiview 3D reconstruction of the archaeological site at Weymouth from image series,” *Comput. Graph.*, vol. 35, no. 2, pp. 375–382, 2011.
- [127] stack overflow, “How do I calculate the volume of an object stored in STL files?,” *Stack Exchange Inc*, 2017. [Online]. Available: <http://stackoverflow.com/questions/6518404/how-do-i-calculate-the-volume-of-an-object-stored-in-stl-files>. [Accessed: 13-Mar-2017].
- [128] C. Waguespack, *Mastering Autodesk Inventor 2014 and Autodesk Inventor LT 2014: Autodesk Official Press*. New York: John Wiley & Sons, 2013.
- [129] Autodesk Inventor, “iProperties for Inventor files,” *AUTODESK KNOWLEDGE NETWORK*, 2016. [Online]. Available: <https://knowledge.autodesk.com/support/inventor-products/learn-explore/caas/CloudHelp/cloudhelp/2016/ENU/Inventor-Help/files/GUID-DB4F5723-939F-4034-857C-6D54429ED024-htm.html>. [Accessed: 15-Apr-2017].
- [130] M. Dellepiane, N. Dell’Unto, M. Callieri, S. Lindgren, and R. Scopigno, “Archeological excavation monitoring using dense stereo matching techniques,” *J. Cult. Herit.*, vol. 14, no. 3, pp. 201–210, 2013.
- [131] P. Cignoni, M. Callieri, M. Corsini, M. Dellepiane, F. Ganovelli, and G. Ranzuglia, “MeshLab: an Open-Source Mesh Processing Tool,” in *Eurographics Italian Chapter Conference*, 2008, pp. 129–136.
- [132] T. Rashid, S. Sultana, and M. A. Audette, “Watertight and 2-manifold Surface Meshes Using Dual Contouring with Tetrahedral Decomposition of Grid Cubes,” *Procedia Eng.*, vol. 163, pp. 136–148, 2016.
- [133] G. Glombitza, H. Evers, S. Hassfeld, U. Engelmann, and H.-P. Meinzer, “Virtual Surgery in a (Tele-)Radiology Framework,” *IEEE Trans. Inf. Technol. Biomed.*, vol. 3, no. 3, pp. 186–196, 1999.

- [134] HoloLens, “Mixed reality: Your world is the canvas,” 2017. [Online]. Available: <https://www.microsoft.com/en-us/hololens>. [Accessed: 06-Jul-2017].